NTNU
Norwegian University of
Science and Technology

Estimation of multiple frequencies in pathological hand tremor for a semi-active 2DOF dynamic vibration absorber designed for tremor suppression

Bjarte Mehus Sunde

Master of Science in Cybernetics and Robotics
Submission date: June 2018
Supervisor: Geir Mathisen, ITK

Norwegian University of Science and Technology
Department of Engineering Cybernetics

Dedicated to my beloved parents and family

Abstract

Pathological tremor is the most prevalent movement disorder in the world, where $\sim$14.5% of people aged 50-89 years suffer from it. The most common types of tremor are by far essential tremors (ET) and Parkinson Disease (PD). Many people experience the shaking as embarrassing, and Social Anxiety Disorder is a common occurrence among people with ET. Today's treatments for tremors consists mainly of medication or neurosurgery, but unfortunately, tremor is not adequately managed in $\sim$25% off all patients.

Our end goal is to reduce tremors in the upper limb with a mechanical solution in a non-embarrassing way. In cooperation with Estenstad [1] a design for a vibration absorber for reducing pathological hand tremor was developed. The system is semi-active, and the design consists of a dual parallel vibration absorber that can tune into two frequencies in the hand tremor. For the system to be able to work in real time, an estimator that can track these frequencies is needed. This thesis presents the development and validation of a frequency estimator for tracking multiple frequencies in pathological hand tremor for real-time applications; the Band-limited Multiple Weighted Fourier Linear Combiner (BMWFLC). Multiple tests with real and simulated tremor data was carried out to validate its performance. Using a simulated signal of a rest tremor modulated by two frequencies, the filter had two stable estimates in under 3 seconds with an error under 0.053 Hz for both. The filter showed good performance when tested on real data from both action and rest tremor. The algorithm was also implemented on an 8-bit microcontroller and tested on a 1DOF test rig that simulates pathological hand tremor with flexion-extension movement. The algorithm ran in real-time, but not with the ideal resolution or frequency window size, and only tracked one frequency. An upgrade of the microcontroller is suggested to increase the performance.

To the authors' knowledge, this is the only frequency estimator for pathological tremor estimation that can estimate frequencies that are close in the frequency domain and the first with the capability to estimate over two frequencies simultaneously.

Sammendrag

Patologisk tremor er den mest utbredte bevegelsesforstyrrelsen i verden, hvor $\sim$14.5% av folk i alderen 50-89 år lider av det. De vanligste typene tremor er Essensiell Tremor (ET) og Parkinsons Sykdom (PS). Mange opplever skjelvingene som pinlig, og sosial angst er vanlig blant personer med ET. Dagens behandlinger for tremor består hovedsakelig av medisinering eller nevrokirurgi, men dessverre får ikke $\sim$25% av pasientene tilstrekkelig behandeling.

Vårt mål er å redusere rystelser i øvre lem med en mekanisk løsning på en ikke-sjenerende måte. I samarbeid med Estenstad [1] ble det utviklet et design for en vibrasjonsdemper for å redusere patologisk hånd tremor. Systemet er semi-aktivt, og designet består av en dobbel parallell vibrasjonsdemper som kan justere seg til to frekvenser i hånd tremoren. For at systemet skal kunne fungere i sanntid, er det nødvendig med en estimator som kan estimere disse frekvensene. Denne oppgaven presenterer utvikling og validering av en frekvensestimator for å estimere flere frekvenser i patologisk hånd tremor for sanntidsapplikasjoner; en Band-limited Multiple Weighted Fourier Linear Combiner (BMWFLC). Flere tester med ekte og simulert tremor data ble utført for å validere ytelsen til estimatoren. Ved hjelp av et simulert signal av hvile tremor modulert av to frekvenser hadde filteret to stabile estimater på under 3 sekunder med en feil under 0,053 Hz for begge. Filteret viste god ytelse når den ble testet på ekte data fra både handling og hvile tremor. Algoritmen ble også implementert på en 8-bits mikrokontroller og testet på en testrigg med en som simulerer patologisk håndskjelving med fleksjon-utvidelse bevegelse. Algoritmen kjørte i sanntid, men ikke med den ideelle oppløsningen eller frekvensvinduestørrelsen, og bare en frekvens ble estimert. En oppgradering av mikrokontroller foreslås for å øke ytelsen.

Til forfatterens kunnskaper er dette den eneste frekvens estimatoren for patologisk tremor som kan estimere frekvenser som ligger nært i frekvensdomenet og den første med evnen til å estimere over to frekvenser samtidig.

Preface

This master thesis presents the development process of a wearable device for upper limb tremor suppression. The problem was first addressed in the course Experts in team at NTNU in the spring of 2017. When the course ended, the team was eager to continue the development, as we had faith in the idea, and were eager to solve the problem. Hence, the team kept working on the problem, and during this spring the development has been the basis of this master project. The work done previous to the master was mainly focused on finding competitors on the market, through market analysis, and not so much on the technology behind our envisioned product. This master thesis is focused on the software part of the device. However, the device has been developed in partnership with Ida Estenstad who has written a master thesis from a mechanical point of view, which is focused on the mechanical and hardware parts of the device.

Both students had completely different specialization projects the previous semester, so the work on this master has only spanned one semester. Some parts of the thesis have been written in collaboration with Ida Estenstad since they overlap between our thesis, and is approved by our supervisors. The parts are: chapter 1, section 2.1, section 2.2 and the introduction for chapter 3.

The linear actuator from chapter 8 was lent to us by Stefano Brevik Bertelli from the Department of Engineering Cybernetics. Help was provided to find and old project report that had used the actuator, but it contained no useful information on how to use it. The setup was done solely by the students and took us over two weeks to get it to do what we wanted. The microcontroller from chapter 8 is my own, and the two sensors were bought with money we have won from pitching our idea in competitions.

Geir Mathisen has been my supervisor and has helped me get a structure for my thesis, given me deadlines and guided me to the right people to discuss my thesis. Jan Tommy Gravdahl has been my technical supervisor, the one I have discussed and presented my Ideas too, and he has given me feedback on them.

The development tremor suppression concept has been in collaboration with Ida Estenstad. I have solely developed all of the algorithms presented as new in this thesis, and new knowledge has mostly been gained from reading research papers and from books on the relevant topics.

Acknowledgements

I would like to give many thanks to everyone at Inalto: **Ida Estenstad, Simen Liberg Tronsaune**, **Shahrukh Khxn** and **Anja Wollan**. This thesis would never have existed without you, and your passion for wanting to help people. And a special thanks to Ida for our collaboration on this project, it has been a pleasure working with you. The whole team is amazing, and I wish everyone the best of luck in your future endeavors. I would also like to thanks **Bendik Fon** who has been a great mentor for us, and for pushing us out of our comfort zones to realize our ideas.

Innhold

Abstract i

Sammendrag iii

Preface v

Acknowledgements vii

List of Tables xiii

List of Figures xix

Abbreviations xx

1 Introduction 1
- 1.1 Background and motivation . . . 1
- 1.2 Problem description . . . 2
- 1.3 Project scope . . . 3
  - 1.3.1 Thesis structure . . . 4

2 Basic Theory 5
- 2.1 Tremor theory . . . 5
  - 2.1.1 Essential tremor . . . 5
  - 2.1.2 Parkinson Disease . . . 6
  - 2.1.3 Tremor stability . . . 7
  - 2.1.4 Harmonics and fundamental frequencies . . . 7
  - 2.1.5 Comparison of tremor diseases . . . 9
- 2.2 Vibration damping . . . 10
- 2.3 Adaptive filter . . . 11
  - 2.3.1 Adaptive linear combiner . . . 11
  - 2.3.2 Performance surface . . . 12
  - 2.3.3 LMS algorithm . . . 13

2.4 Fourier Series . . . 15
2.4.1 Trigonometric Fourier Series . . . 15
2.4.2 Magnitude spectrum . . . 15

3 Existing technology **19**
3.1 Active . . . 19
3.1.1 Exoskeletons . . . 19
3.1.2 Electrical stimulation . . . 20
3.1.3 Utensils . . . 20
3.1.4 Vibration . . . 21
3.2 Semi-active . . . 21
3.3 Passive solutions . . . 23
3.3.1 Dynamic Vibration Absorber . . . 23
3.3.2 Limb weights . . . 24
3.3.3 Gyroscope . . . 24
3.4 Conclusion . . . 25

4 Vibration absorber design **27**

5 Tremor estimation **29**
5.1 Tremor estimators . . . 30
5.1.1 Estimators . . . 30
5.1.2 FLC . . . 32
5.1.3 WFLC . . . 33
5.1.4 BMFLC . . . 34
5.1.5 E-BMFLC . . . 36
5.2 BMWFLC . . . 38
5.2.1 Core equations . . . 38
5.2.2 Adaptive learning rate . . . 40
5.2.3 Magnitude spectrum - extracting frequencies . . . 41
5.2.4 Flowchart for BMWFLC algorithm . . . 45

6 Tremor data **47**
6.1 Real dataset . . . 47
6.2 Simulated data . . . 48
6.2.1 Involuntary movement . . . 48
6.2.2 Voluntary movement . . . 48
6.2.3 Noise . . . 49

7 Time-Frequency analysis **51**
7.1 Power Spectral Density . . . 51
7.2 Spectrogram . . . 52

8 Test rig setup **53**

9 Results **55**
9.1 Simulated tremor data - Tuned filter . . . 55
9.1.1 Initial filter settings . . . 55
9.1.2 Simulated signal settings . . . 55
9.1.3 Simulated signal 1 - Rest tremor . . . 57
9.1.4 Simulated signal 2 - Rest tremor . . . 59
9.1.5 Simulated signal 3 - Action tremor . . . 61
9.1.6 Simulated signal 4 - Varying amplitude . . . 63
9.1.7 Simulated signal 5 - Varying frequency . . . 65
9.1.8 Simulated signal 6 - Multiple frequencies . . . 67
9.2 Testing different filter settings . . . 69
9.2.1 Simulated signal 2 with $\boldsymbol{\mu}_k = 0$ . . . 69
9.2.2 Simulated signal 4 with μ_k and $\boldsymbol{\mu}_k$ constant . . . 71
9.3 Real tremor data - Tuned filter . . . 73
9.3.1 Recording 1 - Rest tremor . . . 73
9.3.2 Recording 6 - Rest tremor . . . 75
9.3.3 Recording 12 - Postural tremor . . . 77
9.3.4 Recording 15 - Action tremor . . . 79
9.4 Real-time test with DVA system . . . 81
9.5 Summary . . . 84
9.5.1 Rest tremor . . . 84
9.5.2 Action tremor . . . 84
9.5.3 Postural tremor . . . 85
9.5.4 Stress tests . . . 85
9.5.5 Real-time test with DVA system . . . 85

10 Discussion and conclusion **87**

11 Further work **89**

Bibliography **90**

Appendices **103**

A Schematic for Arduino and LSM6DS3 **105**

B Real tremor data - Tuned filter **107**
B.1 Recording 2 - Rest tremor . . . 108
B.2 Recording 3 - Rest tremor . . . 109
B.3 Recording 4 - Rest tremor . . . 110
B.4 Recording 5 - Rest tremor . . . 111
B.5 Recording 7 - Rest tremor . . . 112
B.6 Recording 8 - Voluntary movement . . . 113
B.7 Recording 9 - Rest tremor . . . 114
B.8 Recording 10 - Voluntary movement . . . 115
B.9 Recording 11 - Rest tremor . . . 116

B.10 Recording 13 - Postural tremor 117
B.11 Recording 14 - Action tremor 118

Tabeller

1.1 Project Overview 3

2.1 Different tremor syndromes and their corresponding frequencies [2] . . . 6
2.2 Comparison of Enhanced physiological tremor, essential tremor and parkinson disease [2] 9

6.1 Real dataset 48

Figurer

2.1 Flexion (left) and extension (right) movement of the wrist. 6
2.2 Pronation (left) and supination (right) movement of the wrist. 7
2.3 Vibration absorber types 10
2.4 Adaptive linear combiner with desired response and error signal. 12
2.5 Adaptive linear combiner with performance feedback 12
2.6 Surface of two-dimensional quadratic performance surface. The optimum weight vector is located at bottom of the surface, for this example $\mathbf{w}^* = (1.1, 1.5)$ and the minimum MSE is 0.0. 13
2.7 Adaptive linear combiner with the LMS algorithm 14
2.8 Magnitude spectrum for first five harmonics 16
2.9 Combined plot of the three first harmonics from the Fourier series for a square wave 17

3.1 (a) WOTAS, (b) Voluntary-Driven Elbow Orthosis with Speed-Controlled Tremor Suppression, (c) An integrated wearable robot for tremor suppression with context aware sensing, (d) Real-Time Pathological Tremor Identification and Suppression in Human Arm via Active Orthotic Devices . . 20
3.2 (A) Components of Tremor's glove, including an adjustable glove, control box, and smart phone. (B) Patient wearing Tremor's glove (C) Patient wearing sham glove 21
3.3 Liftware Steady™[3] with spoon attachment 21
3.4 (a) Emma Watch (b) ARC Pen 22
3.5 Tremor suppression with shape memory alloy vibration absorber 22
3.6 Vib-bracelet 23
3.7 (a) Model of a single absorber connected to the forearm of the hand [4] (b) 2 DOF parallel absorber 24
3.8 Readi-Steadi® Anti-Tremor Orthotic Glove System [5] 25
3.9 The GyroGlove ™ [6] 25

4.1 (a) Dual parallel absorber (b) semi-active dual parallel absorber with variable spring constants 27

5.1 FLC architecture 33
5.2 WFLC architecture 34
5.3 BMFLC architecture 35
5.4 BMFLC frequency distribution 35
5.5 Complete frequency distribution of hand motion 38
5.6 BMWFLC 40
5.7 BWMFLC frequency distribution with two dominant frequency, ω_4 and ω_7. 43
5.8 (a) Magnitude of BMWFLC after 10 seconds running on simulated signal. (b) Heatmap of magnitude spectrum from the BMWFLC 44
5.9 Flowchart for BMWFLC algorithm 45

6.1 Recording number 1 from Table 6.1 49
6.2 Simulated signal. $m_{k-i} = 128\sin(2\pi \cdot 4.6 \cdot t) + 153\cos(2\pi \cdot 5.2 \cdot t) + n_k$, with $\sigma_{n_k} = 10$ 49

7.1 PSD with (a) linear and (b) logarithmic scaling of recording 1 52
7.2 Spectrogram of recording 9 with Hanning window with length 20% of the sample data, and a overlap of 99%. Estimated frequencies by the BMWFLC are plotted with black and red markers for most and second most power respectively 52

8.1 Wiring diagram for the Arduino Uno and the two LSM6DS3 sensors . . . 53
8.2 (a) Test rig (b) Test rig with DVA attached 54
8.3 Application for controlling the actuator 54

9.1 Simulated signal 2: Simulation of rest tremor 57
9.2 Estimated frequencies from simulated signal 1 using the BMWFLC filter . 57
9.3 (a) PSD with linear scaling. (b) Heatmap of magnitude spectrum from the BMWFLC filter. (Simulated signal 1) 57
9.4 Error between real frequency and estimated frequency. (Simulated signal 1) 58
9.5 Simulated signal 2: Simulation of rest tremor 59
9.6 Estimated frequencies from simulated signal 2 using the BMWFLC filter . 59
9.7 (a) PSD with linear scaling. (b) Heatmap of magnitude spectrum from the BMWFLC filter. (Simulated signal 2) 59
9.8 Error between real frequency and estimated frequency. (Simulated signal 2) 60
9.9 Magnitude spectrum at (a) 4 seconds and (b) 4.5 seconds 60
9.10 Simulated signal 3: Simulation of action tremor 61
9.11 Estimated frequencies from simulated signal 3 using the BMWFLC filter . 61
9.12 (a) PSD with linear scaling. (b) Heatmap of magnitude spectrum from the BMWFLC filter. (Simulated signal 3) 61
9.13 Error between real frequency and estimated frequency. (Simulated signal 3) 62
9.14 Simulated signal 4: Simulation of tremor with varying amplitude 63
9.15 Estimated frequencies from simulated signal 4 using the BMWFLC filter . 63

9.16 (a) PSD with linear scaling. (b) Heatmap of magnitude spectrum from the BMWFLC filter. (Simulated signal 4) 63
9.17 Error between real frequency and estimated frequency. (Simulated signal 4) 64
9.18 Simulated signal 5: Simulation of tremor with varying frequencies 65
9.19 Estimated frequencies from simulated signal 5 using the BMWFLC filter . 65
9.20 (a) PSD with linear scaling. (b) Heatmap of magnitude spectrum from the BMWFLC filter. (Simulated signal 5) 65
9.21 Error between real frequency and estimated frequency. (Simulated signal 5) 66
9.22 Simulated signal 6: Simulation of tremor with 6 frequencies 67
9.23 Estimated frequencies from simulated signal 6 using the BMWFLC filter . 67
9.24 (a) PSD with linear scaling. (b) Heatmap of magnitude spectrum from the BMWFLC filter. (Simulated signal 6) 67
9.25 Error between real frequency and estimated frequency. (Simulated signal 6) 68
9.26 Estimated frequencies from simulated signal 2 using the BMWFLC filter with $\boldsymbol{\mu}_k = 0$ 69
9.27 (a) PSD with linear scaling. (b) Heatmap of magnitude spectrum from the BMWFLC filter. (Simulated signal 2). With $\boldsymbol{\mu}_k = 0$ 69
9.28 Error between real frequency and estimated frequency. (Simulated signal 2) 70
9.29 Estimated frequencies from simulated signal 4 using the BMWFLC filter with μ_k and $\boldsymbol{\mu}_k$ constant 71
9.30 (a) PSD with linear scaling. (b) Heatmap of magnitude spectrum from the BMWFLC filter. (Simulated signal 4). With μ_k and $\boldsymbol{\mu}_k$ constant 71
9.31 Error between real frequency and estimated frequency. (Simulated signal 4) 72
9.32 Recording 1 from session 1. Orientation: P+/S. Placement: RH 73
9.33 PSD with (a) linear and (b) logarithmic scaling. (Recording 1) 73
9.34 (a) Spectrogram of signal with estimated frequencies and (b) Heatmap of the magnitude spectrum from the BMWFLC filter. (Recording 1) 73
9.35 Estimated frequencies from recording 1. f_1 and f_2 are also estimates in this figure 74
9.36 Recording 6 from session 4. Orientation: P/S+. Placement: LH 75
9.37 PSD with (a) linear and (b) logarithmic scaling. (Recording 6) 75
9.38 (a) Spectrogram of signal with estimated frequencies and (b) Heatmap of the magnitude spectrum from the BMWFLC filter. (Recording 6) 75
9.39 Spectrogram of signal 6 with $ftt = 3$ 76
9.40 Recording 12 from session 6. Orientation: F+/E. Placement: RH 77
9.41 PSD with (a) linear and (b) logarithmic scaling. (Recording 12) 77
9.42 (a) Spectrogram of signal with estimated frequencies and (b) Heatmap of the magnitude spectrum from the BMWFLC filter. (Recording 12) 77
9.43 Recording 15 from session 7. Orientation: P+/S. Placement: LH 79
9.44 PSD with (a) linear and (b) logarithmic scaling. (Recording 15) 79
9.45 (a) Spectrogram of signal with estimated frequencies and (b) Heatmap of the magnitude spectrum from the BMWFLC filter. (Recording 15) 79
9.46 Recording from test rig 30 seconds 81
9.47 Recording from test rig zoomed in 81

9.48 (a) Linear PSD of simulated tremor from test rig. Plots of the arm with nothing, weight and DVA attached; blue, green and red line repectivly. (b) Logarithmic plot of tremor with nothing attached 81

A.1 Connection between the two LSM6DS3 and the Arduino Uno 105

B.1 Recording 2 from session 2. Orientation: P+/S. Placement: RH 108
B.2 PSD with (a) linear and (b) logarithmic scaling. (Recording 2) 108
B.3 (a) Spectrogram of signal with estimated frequencies and (b) Heatmap of the magnitude spectrum from the BMWFLC filter. (Recording 2) 108
B.4 Recording 3 from session 2. Orientation: P+/S. Placement: LH 109
B.5 PSD with (a) linear and (b) logarithmic scaling. (Recording 3) 109
B.6 (a) Spectrogram of signal with estimated frequencies and (b) Heatmap of the magnitude spectrum from the BMWFLC filter. (Recording 3) 109
B.7 Recording 4 from session 3. Orientation: P+/S. Placement: RH 110
B.8 PSD with (a) linear and (b) logarithmic scaling. (Recording 4) 110
B.9 (a) Spectrogram of signal with estimated frequencies and (b) Heatmap of the magnitude spectrum from the BMWFLC filter. (Recording 4) 110
B.10 Recording 5 from session 3. Orientation: F+/E. Placement: RH 111
B.11 PSD with (a) linear and (b) logarithmic scaling. (Recording 5) 111
B.12 (a) Spectrogram of signal with estimated frequencies and (b) Heatmap of the magnitude spectrum from the BMWFLC filter. (Recording 5) 111
B.13 Recording 7 from session 4. Orientation: P+/S. Placement: RH 112
B.14 PSD with (a) linear and (b) logarithmic scaling. (Recording 7) 112
B.15 (a) Spectrogram of signal with estimated frequencies and (b) Heatmap of the magnitude spectrum from the BMWFLC filter. (Recording 7) 112
B.16 Recording 8 from session 5. Orientation: P+/S. Placement: RH 113
B.17 PSD with (a) linear and (b) logarithmic scaling. (Recording 8) 113
B.18 (a) Spectrogram of signal with estimated frequencies and (b) Heatmap of the magnitude spectrum from the BMWFLC filter. (Recording 8) 113
B.19 Recording 9 from session 5. Orientation: P+/S. Placement: LH 114
B.20 PSD with (a) linear and (b) logarithmic scaling. (Recording 9) 114
B.21 (a) Spectrogram of signal with estimated frequencies and (b) Heatmap of the magnitude spectrum from the BMWFLC filter. (Recording 9) 114
B.22 Recording 10 from session 5. Orientation: F+/E. Placement: RH 115
B.23 PSD with (a) linear and (b) logarithmic scaling. (Recording 10) 115
B.24 (a) Spectrogram of signal with estimated frequencies and (b) Heatmap of the magnitude spectrum from the BMWFLC filter. (Recording 10) 115
B.25 Recording 11 from session 5. Orientation: F/E+. Placement: LH 116
B.26 PSD with (a) linear and (b) logarithmic scaling. (Recording 11) 116
B.27 (a) Spectrogram of signal with estimated frequencies and (b) Heatmap of the magnitude spectrum from the BMWFLC filter. (Recording 11) 116
B.28 Recording 13 from session 6. Orientation: F/E+. Placement: LH 117
B.29 PSD with (a) linear and (b) logarithmic scaling. (Recording 13) 117
B.30 (a) Spectrogram of signal with estimated frequencies and (b) Heatmap of the magnitude spectrum from the BMWFLC filter. (Recording 13) 117

B.31 Recording 14 from session 7. Orientation: P+/S. Placement: RH 118
B.32 PSD with (a) linear and (b) logarithmic scaling. (Recording 14) 118
B.33 (a) Spectrogram of signal with estimated frequencies and (b) Heatmap of the magnitude spectrum from the BMWFLC filter. (Recording 14) 118

Abbreviations

2D	=	Two-dimensional
3D	=	Three-dimensional
1DOF	=	One degrees of freedoml
ALC	=	Adaptive Linear Combiner
BMFLC	=	Band-limited Multiple FLC
DOF	=	Degree of freedom
DVA	=	Dynamic vibration absorber
E-BMFLC	=	Enhanced-BMFLC
EEG	=	Electroencephalography
EMG	=	Electromyography
ET	=	Essential Tremor
FLC	=	Fourier Linear Combiner
PD	=	Parkinson's Disease
TVA	=	Tuned vibration absorber
WFLC	=	Weighted-frequency FLC

Kapittel 1

Introduction

1.1 Background and motivation

Tremor is the most prevalent movement disorder in the world, where $\sim$14.5% of people aged 50-89 years suffer from it [7]. The most common types of tremor are by far essential tremors (ET) and Parkinson Disease (PD) [8]. It is estimated that about 26000 people suffer from ET [9], and 8000 from PD [10] in Norway today; worldwide the numbers are over 300 and 10 million respectively [11, 12]. The tremors affect people differently. Among others, they can make it challenging to perform basic, daily tasks such as drinking coffee or brushing teeth, or profession specific precision work such as painting and surgery. Many people experience the shaking as embarrassing [13], and Social Anxiety Disorder is a common occurrence among people with ET [14].

Today's treatments for tremors consists mainly of medication or neurosurgery, the most common method for the latter is Deep Brain Stimulation (DBS), which is a neurological procedure and involves the implementation of a medical device deep inside the brain [15]. Although DBS has proven to be an effective treatment for tremors caused by PD, patients in Norway are only considered for the operation when symptoms cannot be treated adequately by medication, and they reduce the patient's life quality [16]. The DBS does not work optimal for everyone [17], the effect can decrease over time [18], and it can lead to some severe side effects, like cognitive decline - processing speed and work memory [19]. When it comes to medication, side effects are common, and many patients abandon their treatment because of this [20, 21]. The effectiveness of drugs also decreases over time [22]. As a result, many patients are left without any treatment for their tremor, and tremor is not effectively managed in up to 25% of all patients according to some estimates [23]. A good option for them may be too suppress the tremor mechanically.

1.2 Problem description

The presented problem forms the basis of this project, and this thesis is built around the following problem:

How to reduce tremors in the upper limb with a mechanical solution in a non-embarrassing way?

The aim of this project is to design a system that suppresses tremors in the hand by a mechanical solution. The system will consist of a wearable device worn on the wrist or arm, that suppresses the tremors actively or passively. The assignment will consist of a literature study of tremors from PD and ET to find out what frequency, amplitude and force they have, and get a better understanding of how tremors work on the body in general. Using the knowledge gained from the study, one or more actuators or dampers will be designed/chosen. After this, the development of the device itself will start, where one or several prototypes should be made and evaluated. The prototype should have all the necessary sensors to measure the tremors.

1.3 Project scope

Scope

Design a system that suppresses the tremors in the hand in one dimension by a mechanical solution

Objectives

Mechanical engineering:	Cybernetics and robotics:
• Execute a literature study of existing solutions and relevant technology. • Choose one or more concepts to test. • Build a test rig that simulates a shaking arm. • Develop and build a prototype for testing • Conduct experimental tests of concept(s) • Measure the amount of suppression when the concept is applied to the test rig. • Investigate how the concept can be implemented in a wearable design worn on the wrist.	• Execute a literature study of existing solutions and tremor estimation methods. • Choose one or more estimation methods to implement. • Develop a tremor estimation algorithm to estimate two frequencies for real-time applications.. • Test and validate developed algorithm with real and simulated tremor data. • Test the developed algorithm for real-time applications on the test rig.

Out of Scope

- Build a prototype of the concept implemented in a wearable device.
- Test of concept when the frequency is not stationary.
- Test the concept in several dimensions.

Tabell 1.1: Project Overview

1.3.1 Thesis structure

The background and motivation from this chapter describe the problem that forms the basis of the following work. Chapter 2 presents the basic theory about tremors, relevant technology, and relevant concepts. Chapter 3 presents literature of existing technology, both on the marked and concepts in the research phase. In chapter 4 the concept design for our vibration absorber is presented, and an outline of what parts of the absorber will be in focus in this thesis is given. In chapter 5 existing tremor estimators are reviewed, and a new design for a frequency estimator is presented. In chapter 6 the real dataset and the methods for generating the simulated dataset are shown. Chapter 7 presents time-frequency analysis methods, the necessary tools used to analyze tremor data. In chapter 8 the setup of the test rig used for testing vibration absorbers presented. In chapter, 9 the results from the new filters performance on real and simulated data, and when it is running in real time on the test rig are presented. In chapter 10 the results are then discussed. In chapter 11 possible future work is presented

Kapittel 2

Basic Theory

2.1 Tremor theory

Tremor is a rhytmic, oscillatory movement produced by alternating or synchronous contractions of antagonist muscles.[24] Everyone can experience tremors in their hands when doing precision work. This kind of tremor is called *Physiological tremor* and is considered to be normal. Physiological tremor is normally not of inconvenience for people, except for, for example, eye surgeons. *Pathological tremor* on the other hand, impairs a patient's function and is visible to the naked eye [25]. Tremor is often categorised as *Rest tremors*, *Postural tremors* or *Kinetic tremors*. Rest tremor is prevalent when the affected body part is in complete rest, supported against gravity. Often the tremors disappears or are reduced when the body part is activated [2]. Postural tremor is prevalent when the affected body part is maintaining a posture against gravity, while Kinetic tremor is prevalent when the body part is performing a voluntary activity [2]. Both postural tremor and kinetic tremor are forms of *Active tremors*, and will disappear when the affected body part is at rest [2].

Several diagnosis' and conditions will cause tremors. The frequency range of the tremor is different depending on the syndrome. In table 2.1 different syndromes are listed together with the frequency range normal for the syndrome.

2.1.1 Essential tremor

The prevalence of ET is uncertain, as the diagnostic criteria varies and as many people with ET do not seek medical attention [26]. However, it has been estimated that about 0.4-6% of the population suffer from ET [9]. The prevalence increases with age, and it has been estimated that about 6-9% of the population over the age of 60 experience tremor due to ET [2]. The prevalence of ET is uncertain, as the diagnostic criteria varies and as many people with ET do not seek medical attention [26]. However, it has been estimated that about 0.4-6% of the population suffer from ET [9]. The prevalence increases with age, and it has been estimated that about 6-9% of the population over the age of 60 experience

Tremor syndrome	Frequency [Hz]
Enhanced physiological tremor	10-14
Essential tremor syndrome	4-12
Primary orthostatic tremor	14-18
Task spesific tremor	4-8
Holmes tremor	3-5
Tremor of Parkinson disease	3-7
Cerebellar tremor	5-7
Palatal tremor	2-6
Dystonic tremor	5-7
Alcoholic tremor	3-4
Toxic and drug induced tremor	5-10
Psychogenic tremor	Variable

Tabell 2.1: Different tremor syndromes and their corresponding frequencies [2]

tremor due to ET [2]. The tremor frequency of ET is in the range of 4-12 Hz (table 2.1). However, the most common is a frequency in the range of 7-10 Hz [2]. The frequency has been shown to decrease by 0.06-0.08 Hz each year. The decrease in frequency is shown to correlate with an increase in amplitude [27].

ET normally gives a movement in the wrist of the characteristic flexion extension (figur 2.1), and might also give an abduction movement of the fingers (figure) [2].

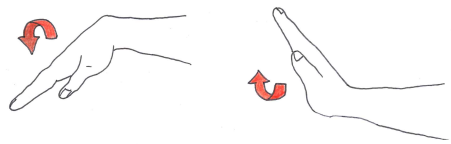

Figur 2.1: Flexion (left) and extension (right) movement of the wrist.

2.1.2 Parkinson Disease

Parkinsonism is a syndrome manifested by a combination of the following six features: tremor-at-rest, rigidity, bradykinesia, loss of postural reflexes, flexed posture and freezing. The most common form of parkinsonism is Parkinsons Disease (PD), first recognized by James Parkinson in 1817. [24]. About 100 years after Parkinson published *An Essay on the Shaking Palsy*, the lack of dopamine-containing cells in the brain was recognized. Levadopa is now a commonly used treatment to reduce symptoms in relation to PD. The prevalence of Parkinson is increasing as life expectancy increases. This is estimated to double the prevalence of Parkinson to 9 million people (on a world basis) by the year of 2030 [25]. The prevalence is about 1% in the age group 50-70 year and somewhat higher among people older than 70 years [10]. Rest tremor is, as already mentioned, a

characteristic feature of Parkinson Disease. The tremor frequency of Parkinson's disease is in the range of 3-7 Hz (table 2.1), and the tremor is often most prominent in the distal part of an extremity. Parkinson's normally gives a movement in the wrist characterized by pronation supination (figure 2.2).

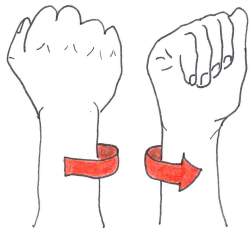

Figur 2.2: Pronation (left) and supination (right) movement of the wrist.

The prevalence of Parkinson is increasing as life expectancy increases. This is estimated to double the prevalence of Parkinson (on a world basis) by the year of 2030 [25].

2.1.3 Tremor stability

Tremors are spatially complex movements. Pathological hand tremors are generally composed of concurrent rotations of more than one axis of the wrist: pronation–supination, combined with wrist flexion-extension and/or ulnar flexion and extension. In general, tremors are best approached as nonstationary processes, tremors with a recording time ten seconds or less, the frequency may appear to be stable, but even on the timescale of 1 min, tremors are generally highly labile. Even if the tremor persists as one continuous record, its component frequencies shift, split into sidebands, exhibit harmonics, and have variable power [28].

2.1.4 Harmonics and fundamental frequencies

Spectral analysis of a tremor signal might show a spectrum consisting of multiple components of significant amplitude. It can be hard to distinguish between peaks that shows the existence of separate tremor mechanisms and peaks that are consequences of fluctuations in the frequency (harmonics). [29] If a signal is periodic with frequency f, the only frequencies composing the signal are integer multiples off f. These multiples of the frequency are named harmonics, while the frequency f is named the fundamental frequency. [30] Even though the harmonics often are found in spectral analysis of tremors, there are no studies that have discovered the reason for their presence, as which muscle groups responsible for tremor that participate in the production of harmonic components. [31]. In [32] 18 PD patients hand and finger tremors where studied in the time and frequency domain. Results showed that the second harmonic makes a large contribution to the tremor, and they concluded that it should not neglected in the designing of tremor suppression devices.

A component of significant amplitude might also be present due to the existence of a separate tremor mechanism, giving two fundamental frequencies. The presence of two peaks in the tremor spectrum has been used as an argument for the existence of two present tremor mechanisms. However, since multiple peaks can be caused by variations in frequency and amplitude, the spectrum alone cannot conclude on the existence of two tremor mechanisms. [29] Gebai et. al. did recently investigate this matter by developing a model of the human arm that describes the flexion motion at shoulder, elbow and wrist joint. [33] They tested three scenarios: One where a DVA was tuned to the wrist joint's response, due to shoulder muscle activation (first natural frequency). One where a DVA was tuned to the wrist joint's response, due to elbow muscle activation (second natural frequency). In the last scenario they tested with both DVA's, to suppress both natural frequencies. The damping were close to 100% when using two DVA's and showed significant increase in damping from using only one DVA. This is an indication of that the tremors might consist of two fundamental frequencies.

2.1.5 Comparison of tremor diseases

	Enhanced physiological tremor	**Essential tremor**	**Parkinson disease**
Common body parts affected	Hands	Hands, head, voice	Hands or arms, legs, chin
Accompanying symptoms	None or symptoms of anxiety state	None	Rigidity, bradykinesia and postural instability
Frequency	10-14 Hz	Mainly 7-10 Hz (but may range from 4 to 12 Hz)	3-6 Hz
Positional component	Posture>Kinetic	Kinetic>Posture, may have a slight resting component if severe	Resting (may have a postural/kinetic or re-emergent component in severe cases)
Symmetry	Bilateral, symmetric	Bilateral, can be mildly asymmetrical	Initially unilateral, bilateral and asymmetrical in advanced stage
Course	Usually none progressive	Progressive	Progressive
Response to alcohol	Minimal or none	Responds significantly	None
Effect of caffeine, stress, stimulants	Increases	Increases	Increases
Inheritance	None	Autosomal dominant with variable penetrance	Sporadic or related to genetics of Parkinson disease

Tabell 2.2: Comparison of Enhanced physiological tremor, essential tremor and parkinson disease [2]

2.2 Vibration damping

To reduce tremors, methods used in other application areas where suppression of vibrations are necessary has been investigated. There are examples of applications where vibrations are useful, but most often this motion is not desired, and several methods have been used to avoid it. Stiffening, damping and isolation are all methods to avoid vibrations. However, in the application of suppressing tremors, damping is the most relevant method. *Damping* consists of reducing the resonance peaks by dissipating the vibration energy. [34]

Damping can be done either passively, actively or semi-actively. With passive damping the kinetic energy is usually transformed into heat. An option is to use a transducers as an energy converter, to transform vibration energy into electrical energy. With semi-active damping a passive damper is used but there is a possibility of controlling one or several properties. The active damping is done with an actuator actively suppressing the vibrations, working in the opposite phase of the undesired vibration.

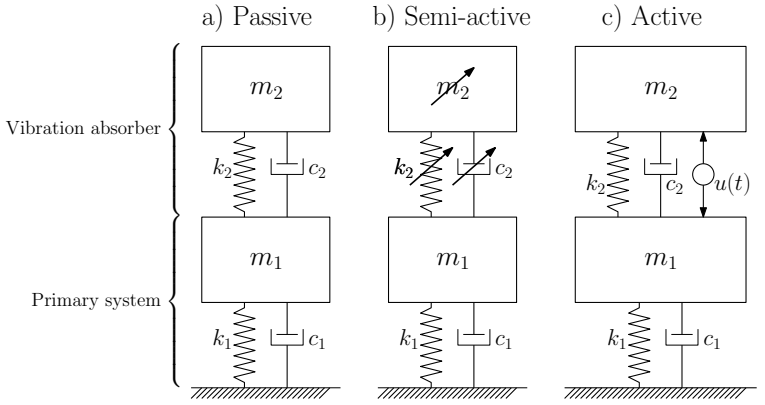

Figur 2.3: Vibration absorber types

In Figure 2.3 we see the three different absorbers [35], they are

- **Passive** - Mass, stiffness and damping are decided at the design stage
- **Semi-active** - Stiffness, damping and/or mass properties can be changed to minimise the response
- **Active** - A dynamic force is applied to the system to minimize the response

2.3 Adaptive filter

This section will present the basic principles of an adaptive filter needed to understand the tremor estimation algorithms reviewed in section 5.1.1. Signal processing and adaptive filters are a well established field, and the following theory is excerpts from the book Adaptive Signal Processing [36] by Widrow and S.D. Stearns. Bernard Widrow.

2.3.1 Adaptive linear combiner

An adaptive linear combiner (ALC) is is also called a non-recursive adaptive filter. A diagram of a multiple-input linear combiner with desired response and error signal is shown in figure 2.4. There also exists a single-input linear combiner, but we will only look at the multiple-input type, since this is the relevant one for us. The ALC consists of a signal input vector $\mathbf{x}_{Nk}$, an adjustable weight vector $\mathbf{w}_{Nk}$, a summing unit, and a single output signal y_k. The procedure for adjusting the weights is often called *weight adjustment*. The combiner is called *linear* because the output is a linear combination of the input components, when the weights have a fixed setting. The input vector $\mathbf{x}_k$ can be seen as simultaneous inputs from $N + 1$ different input sources, the k stands for stands for the sampling time. In some multiple-input systems, a *bias weight* is required, which basically adds a variable bias into the sum, y_k. This can be accomplished by setting the first input element , x_{0k}, equal to 1, then the weight w_{0k} becomes the bias weight.

The signal input vector

$$\mathbf{x}_k = \begin{bmatrix} x_{0k} & x_{1k} & \dots & x_{Nk} \end{bmatrix}^T \tag{2.1}$$

The weight vector

$$\mathbf{w}_k = \begin{bmatrix} w_{0k} & w_{1k} & \dots & w_{Nk} \end{bmatrix}^T \tag{2.2}$$

The input-output relationship

$$y_k = \sum_{n}^{N} w_{nk} x_{nk} \tag{2.3}$$

The input-output relationship using vector notation

$$y_k = \mathbf{x}_k^T \mathbf{w}_k = \mathbf{w}_k^T \mathbf{x}_k \tag{2.4}$$

In an ALC with performance feedback, like in figure 2.5, the weight vector $\mathbf{w}_k$ is adjusted to make the output y_k resemble the desired signal d_k as closely as possible. This is done by comparing the output with the desired signal to obtain the error signal ε_k, and then adjusting the weight vector to minimize the error.

The error signal

$$\varepsilon_k = d_k - y_k \tag{2.5}$$

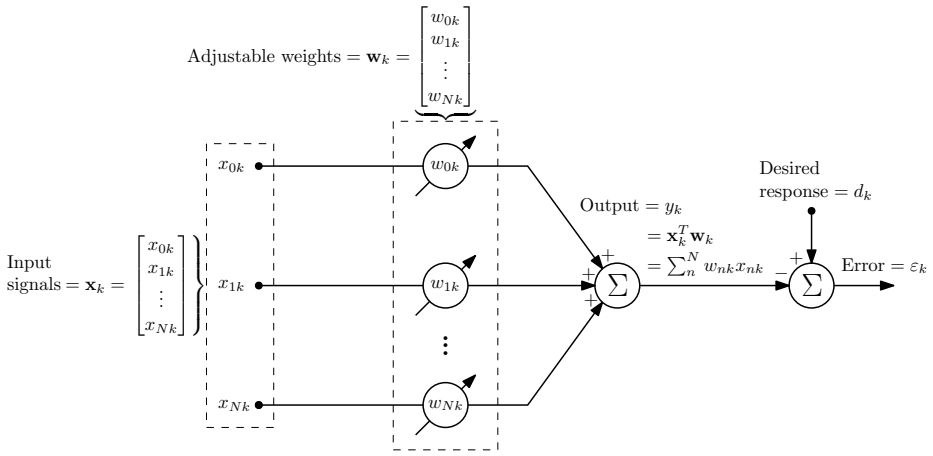

Figur 2.4: Adaptive linear combiner with desired response and error signal.

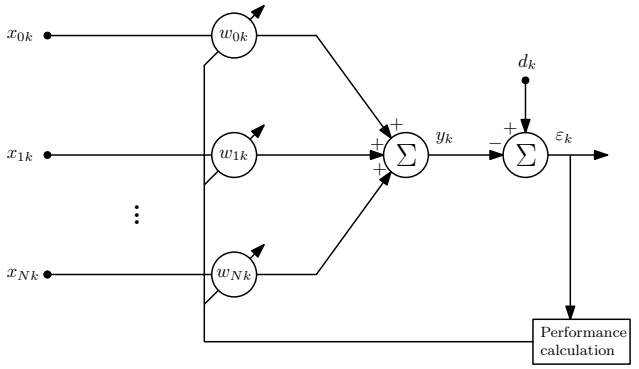

Figur 2.5: Adaptive linear combiner with performance feedback

2.3.2 Performance surface

The mean-square-error (MSE) performance surface for the adaptive linear combiner is a quadratic function of weights when the input signal and the desired response are statistically stationary. The error signal with index k from figure 2.4 is

$$\varepsilon_k = d_k - y_k \tag{2.6}$$

Substituting (2.4) into the error signal gives us

$$\varepsilon_k = d_k - \mathbf{x}_k^T \mathbf{w} \tag{2.7}$$

Now we take the square of (2.7), dropping the subscript k for convenience, since we don't want to adjust the weights for this discussion.

$$\varepsilon_k^2 = d_k - \mathbf{w}^T \mathbf{x}_k \mathbf{x}_k^T \mathbf{w} - 2 d_k \mathbf{x}_k^T \mathbf{w} \tag{2.8}$$

Then we take the expexted value of (2.8) which will give us the MSE, and will be designated by ξ

$$\text{MSE} \triangleq \xi = E\left[d_k^2\right] + \mathbf{w}^T E\left[\mathbf{x}_k \mathbf{x}_k^T\right] \mathbf{w} - 2E\left[d_k \mathbf{x}_k^T\right] \mathbf{w} \tag{2.9}$$

A portion of a typical two-dimensional mean-square error function for is shown in figure 2.6. The z axis represents the mean-square error, and the x and y axis represents the weights w_1 and w_0 respectively. The function plotted is called the *performance surface*, and has a parabolic shape or a hyperparaboloid if there are more than two weights. The optimal weight vector it is $\mathbf{w}^*$ is the point of minimum-square error and is located at the lowest point on the performance surface. With a quadratic performance function there is only a single global optimum and no local minimum exist.

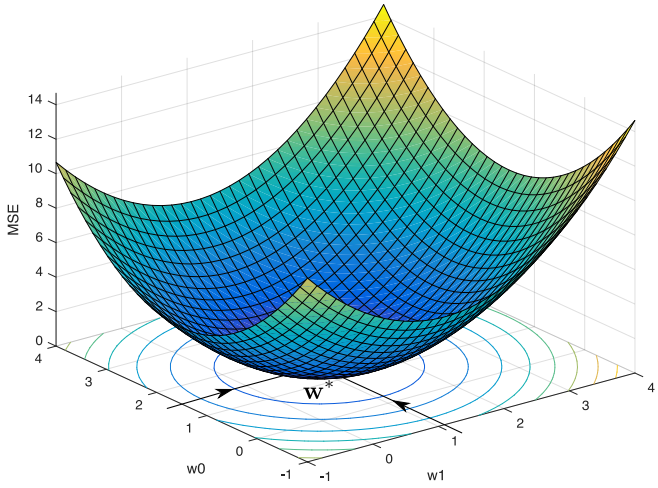

Figur 2.6: Surface of two-dimensional quadratic performance surface. The optimum weight vector is located at bottom of the surface, for this example $\mathbf{w}^* = (1.1, 1.5)$ and the minimum MSE is 0.0.

2.3.3 LMS algorithm

The least-mean-square (LSM) algorithm is designed to descend the performance surface, and minimize the MSE. To accomplish this it uses a gradient descent (sometimes called steepest descent) type of algorithm (2.11), this is the LMS algorithm. Here $\hat{\nabla}_k$ (2.10) is an estimate of the gradient to $\xi = E[\varepsilon_k^2]$. To find this estimate, ε_k^2 is used as an estimate of ξ. In (2.11) μ is the gain constant, it regulates the speed and stability of the adaptation. From equation (2.11) we can see that the LMS algorithm can be implemented without squaring, averaging, or differentiation, making it simple and efficient. This makes it a good choice for use in real-time systems.

$$\hat{\nabla}_k = \begin{bmatrix} \frac{\partial \varepsilon_k^2}{\partial w_0} \\ \vdots \\ \frac{\partial \varepsilon_k^2}{\partial w_0} \end{bmatrix} = 2\varepsilon_k \begin{bmatrix} \frac{\partial \varepsilon_k}{\partial w_0} \\ \vdots \\ \frac{\partial \varepsilon_k}{\partial w_N} \end{bmatrix} = -2\varepsilon_k \mathbf{x}_k \tag{2.10}$$

$$\begin{aligned} \mathbf{w}_{k+1} &= \mathbf{w}_k - \mu \hat{\nabla}_k \\ &= \mathbf{w}_k + 2\mu \varepsilon_k \mathbf{x}_k \end{aligned} \tag{2.11}$$

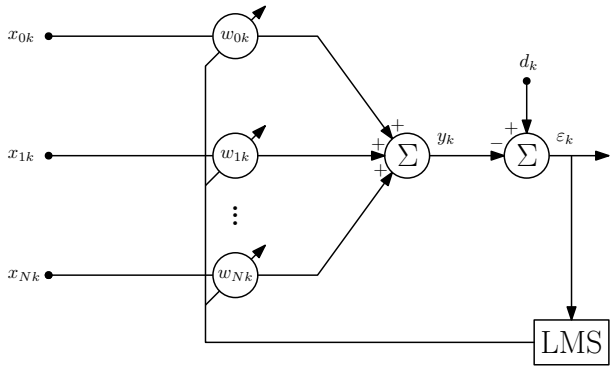

Figur 2.7: Adaptive linear combiner with the LMS algorithm

2.4 Fourier Series

2.4.1 Trigonometric Fourier Series

Any arbitrary periodic function can be expressed as an infinite sum of weighted sinusoids, this is called a *Fourier series*. The Fourier series can be expressed in three different forms, *exponential, amplitude-phase* and *trigonometric*, we will only use the latter. The trigonometric Fourier series of a periodic function $f(t)$ is given by

$$f(t) = a_0 + \sum_{n=1}^{\infty} \left[a_n \cos\left(2\pi n f_0 t\right) + b_n \sin\left(2\pi n f_0 t\right)\right] \tag{2.12}$$

The relationship between angular frequency, $\omega\ [rad/s]$, and the linear frequency, $f\ [Hz]$ is shown by the following equation

$$\omega = 2\pi f \tag{2.13}$$

Equation (2.12) can therefor also be written as

$$f(t) = a_0 + \sum_{n=1}^{\infty} \left[a_n \cos\left(n\omega_0 t\right) + b_n \sin\left(n\omega_0 t\right)\right]$$

The Fourier component a_0 is the dc component (the time average) of function $f(t)$. The Fourier components a_n and b_n are the amplitudes of the cosinusoids and sinusoids, respectively. The frequency f_0 is the **fundemental frequency** and the frequency of every trem is an integer multiple of f_0, the resulting waves are called **harmonics**. So the first wave of the Fourier series, $n = 1$, is the fundamental wave (1st harmonic), the next wave , $n = 2$, is called the 2nd harmonic and has the frequency $2f_0$. The frequencies of the harmonics are strictly integer multiples of the fundamental frequency: $f_0,\ 2f_0,\ 3f_0,\ \ldots\ nf_0$.[37, 38]

2.4.2 Magnitude spectrum

To draw the magnitude spectrum for a trigonometric Fourier series we need to consider both a_n and b_n. To find the magnitudes to the harmonics of the two coefficients we take the root-sum-square (RSS) [39]

$$M_n = \sqrt{a_n^2 + b_n^2} \tag{2.14}$$

The distinction between amplitude and magnitude can be somewhat confusing, and often these two terms are used interchangeably. Lets try to make the destination as clear as possible how these will be used when we talk about Fourier series. The Fourier components a_n and b_n are the amplitudes of the cosinusoids and sinusoids, respectively, they can have both positive and negative values. When we take the RSS of these two we get the magnitude, which is always positive. The amplitude and magnitude can have the same value in some cases [40]. The magnitude spectrum for the Fourier series can now be drawn, where the y-axis magnitude and the x-axis is frequency.

To make a small example we can take the Fourier series of a square wave with the fundamental frequency $f_0 = 1$ Hz

$$\text{Square}(t) = \sin 2\pi t + \frac{\sin 3 \cdot 2\pi t}{3} + \frac{\sin 5 \cdot 2\pi t}{5} + \ldots = \sum_{n=1}^{\infty} \frac{\sin{(2n-1)2\pi t}}{2n-1} \tag{2.15}$$

This is an odd function, meaning that it is symmetric about the origin. It contains only sinusoids, not cosinusoids, so $a_n = 0$. The magnitudes become $Mn = \sqrt{a_n^2 + b_n^2} = \sqrt{b_n^2}$. For this Fourier series, the amplitudes b_n of the sinusoids will be the same as the magnitude Mn, since all the values of b_n are positive. The magnitudes spectrum of the first 5 harmonics can be seen in Figure 2.8.

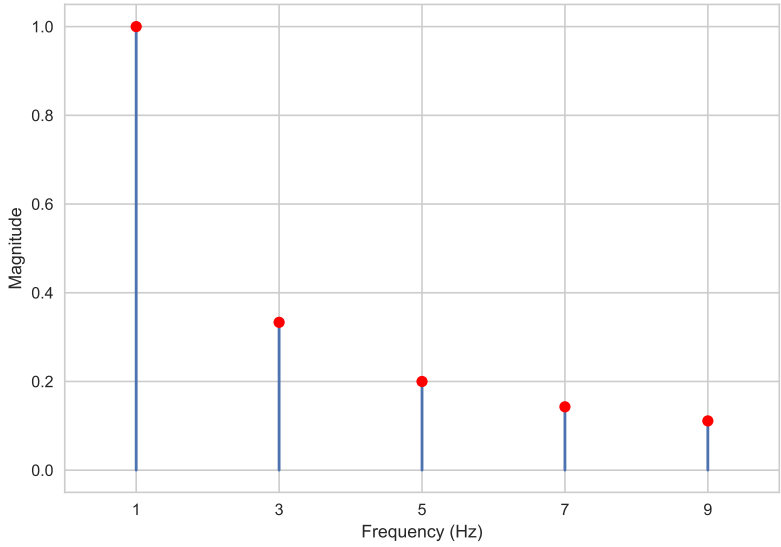

Figur 2.8: Magnitude spectrum for first five harmonics

In Figure 2.9 the magnitude spectrum and the time series of the signal in the same plot. We call the three first harmonics for h_1, h_2 and h_3, with the magnitudes $M_1 = 1$, $M_2 = \frac{1}{3}$ and $M_3 = \frac{1}{5}$, and linear frequencies, $f_1 = f_0 = 1$, $f_2 = 3f_0 = 3$ and $f_3 = 5f_0 = 5$, respectively.

$$h_1 = \underset{\downarrow M_1}{1} \cdot \sin 2\pi \cdot \underset{\downarrow f_1}{1} \cdot x, \quad h_2 = \underset{\downarrow M_2}{\frac{1}{3}} \sin 2\pi \cdot \underset{\downarrow f_2}{3} \cdot x, \quad h_3 = \underset{\downarrow M_3}{\frac{1}{5}} \sin 2\pi \cdot \underset{\downarrow f_3}{5} \cdot x$$

Taking the sum of h_1, h_2 and h_3 gives us the signal in the blue field, we see that the square wave starts to take form, the more harmonics we add the better the approximation gets. The magnitude spectrum is plotted in the red field.

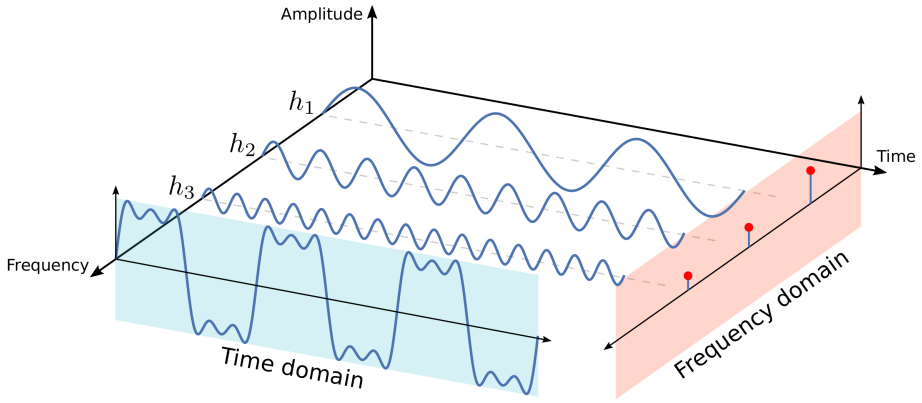

Figur 2.9: Combined plot of the three first harmonics from the Fourier series for a square wave

Kapittel 3

Existing technology

The work done previous to the master was mainly focused on finding competitors on the market, through market analysis, and not so much on the technology behind our envisioned product. This review aimed to get an overview of what solutions that already exist and on research done in the field; to get inspiration and technical insight before choosing our final concept. This review is divided into three parts: active, semi-active and passive vibration absorbers. See definition of the absorber types in section 2.2.

3.1 Active

3.1.1 Exoskeletons

Exoskeletons are a widely researched technology for rehabilitation, assistive robotics, and human power argumentation [41]. Some research has also been done in the subcategory of upper limb tremor suppression.

The WOTAS (Wearable Orthosis for Tremor Assessment and Suppression) [42, 43] which is a 3DOF upper-limb exoskeleton robot, using three flat brushless DC motors + pancake gears, designed for monitor and diagnosis. They develop two control strategies for tremor suppression, one active and the other passive. 1) Tremor reduction through impedance control, which modifies the stiffness, dampening and mass properties of the upper limb to suppress the tremor. 2) Notch filtering at tremor frequency, a strategy that implements an active noise filter at the tremor frequency. The WOTAS was tested on six patients suffering from essential tremor, achieving a tremor suppression of roughly 80%. The patients considered that the use of such a device could cause social exclusion because of its size.

Other exoskeletons that has been developed for tremor suppression is a 1DOF elbow orthosis using a DC motor [44] (Figure 3.1b), a 2DOF exoskeleton using DC motors [45] 3.1c) and a 1DOF exoskeleton using pneumatic actuators [46] (Figure 3.1d). Showing 99.8%, 77% and 96.93% tremor suppression respectively. These results are from simulations, not real patients like in the WOTAS study.

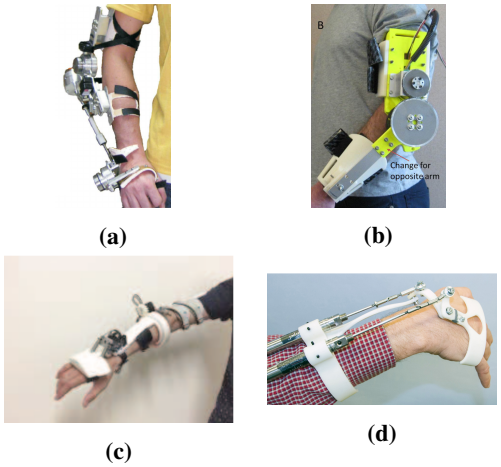

Figur 3.1: (a) WOTAS, (b) Voluntary-Driven Elbow Orthosis with Speed-Controlled Tremor Suppression, (c) An integrated wearable robot for tremor suppression with context aware sensing, (d) Real-Time Pathological Tremor Identification and Suppression in Human Arm via Active Orthotic Devices

3.1.2 Electrical stimulation

A range of research has been done on electrical stimulation for pathological tremor suppression; electrical muscle stimulation (EMS) [47–54], Functional electrical stimulation (FES) [55–62] and Transcutaneous electrical nerve stimulation (TENS) [63]. One of the most recent contributions is the Tremor's glove [54], a medical device that incorporates tremor detection module and EMS to detect an suppress resting hand tremor. The glove is shown to be effective in suppressing resting hand tremor among PD patients in a randomized sham-controlled trial. The patients were asked to score the pain felt by the glove using a visual analog scale (VAS), and the score was significantly higher in the Tremor's glove group compared to the sham group. The Tremor's glove and the sham glove can be seen in Figure 3.2.

3.1.3 Utensils

Liftware [64] is a collection of products of self-stabilizing and leveling handles and attachments designed to help people with hand tremor limited hand and arm mobility. One of their products is the Liftware Steady^{TM}[3], which is an electronic stabilizing handle with a selection of different attachments. In Figure 3.3 we can see the handle with a spoon attachment. The handle contains motion sensors to detect the tremor, and two DC motors are used to stabilize the attachment.

Figur 3.2: (A) Components of Tremor's glove, including an adjustable glove, control box, and smart phone. (B) Patient wearing Tremor's glove (C) Patient wearing sham glove

Figur 3.3: Liftware Steady^{TM}[3] with spoon attachment

3.1.4 Vibration

Twenty patients with upper limb tremor due to multiple sclerosis (MS) had vibration applied to the tendons of the wrist extensor muscles by a commercially available vibration probe. Patients used a motion tracking device to move a cursor on a computer screen, doing a memory-guided slow wrist step-tracking task. The accuracy of tracking was used to determine damping of the tremor by tendon vibration. There was a reduction in tremor amplitude of 28% as measured by the motion tracking system [65]. Project Emma is an ongoing research project at Microsoft [66]; they are developing a device they called Emma Watch (Figure 3.4a), a watch-like device that introduces a rhythmic vibration effect through small motors around the wrist. Another device in development by different company is the ARC pen [67] (Figure 3.4b). The ARC pen uses high-frequency, low amplitude vibration, which stimulates the muscles in the hand. Both the ARC pen and Emma Watch are in the research stage, and reliable data on their tremor suppression capabilities are hard to find.

3.2 Semi-active

In [68] they develop DVA system with the ability to change its stiffens, and tune it for specific tremor frequencies. The device formes a rectangular spring mass damper system, on each side, weight is suspended by two springs made out of shape memory alloy (SMA) (Figure 3.5). The SMA alloy springs can change the stiffens when different amounts of current run through it. When testing the system experimentally at 3 Hz, a reduction in the

(a) **(b)**

Figur 3.4: (a) Emma Watch (b) ARC Pen

acceleration of 40% was archived.

A self-tunable DVA system designed for PD tremor suppression [69]. By using piezoelectric micro-pumps, pumping water in and out of a tank, they vary the mass of the system; tuning the absorbers resonant frequency. The prototype they designed was big, but they argue that it is possible to build it small enough for a human arm by choosing the correct components. An experimental setup showed a reduction of 57% for simulated PD tremor.

Figur 3.5: Tremor suppression with shape memory alloy vibration absorber

3.3 Passive solutions

3.3.1 Dynamic Vibration Absorber

The Vib-bracelet is a passive absorber device for dampening pronation/supination tremor [70]. It is based on the principles of dynamic vibration absorption, tuned to the frequency of the hand tremor. The Vib-bracelet consists of two co-centric rigid rings: an inner open ring attached to the wrist and an outer ring connected with springs to the inner ring. An image of the bracelet is seen in Figure 3.6. Experiments and simulations on a 1DOF system showed that the device damped tremors in the 4-6 Hz range, with a maximum amplitude damping of 83%.

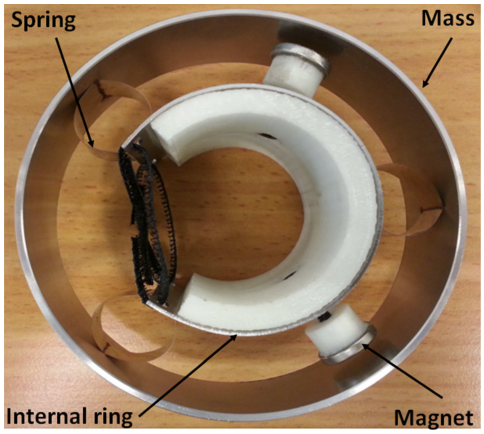

Figur 3.6: Vib-bracelet

In recent years a large number of papers have been published from The International University of Beirut in Lebanon on passive vibration absorbers for reduction of hand tremor for PD patients [4, 71–76]. In their research, they have tested many passive vibration absorbers connected to the wrist. They have run simulations on a 3DOF model of the human arm, modeled in the horizontal plane to describe the flexion-extension motion at the shoulder, elbow and wrist joints, to find how much different absorbers reduce tremor in the respective joints. They find that the dual parallel absorber and dual series elastic-viscous damper absorber are the two most effective configurations.

In their latest paper [4] they check the performance of the dual parallel passive absorber in reducing the tremor. They make a model of the absorber, Figure 3.7b, and attach it to the 3DOF hand model in Figure 3.7a, obtaining a 5 DOF system. The 2DOF absorber is formed of two single DVA's 'absorber 1' and 'absorber 2'. The two absorbers are directly connected to the forearm in parallel. The tremor is modeled as a sinusoidal function containing two resonant frequencies with white noise added. In their simulations the absorber was able to reduce 77.98-80.62%, 60.34-69.95% and 54.39-69.81% of tremor amplitude at the shoulder, elbow and wrist joints, respectively. The study shows that the 2 DOF DVA tuned at both resonance frequencies was very effective in reducing the tremor's amplitude, which suggests that design a mechanical system like this could be useful in helping

pathological tremor patients.

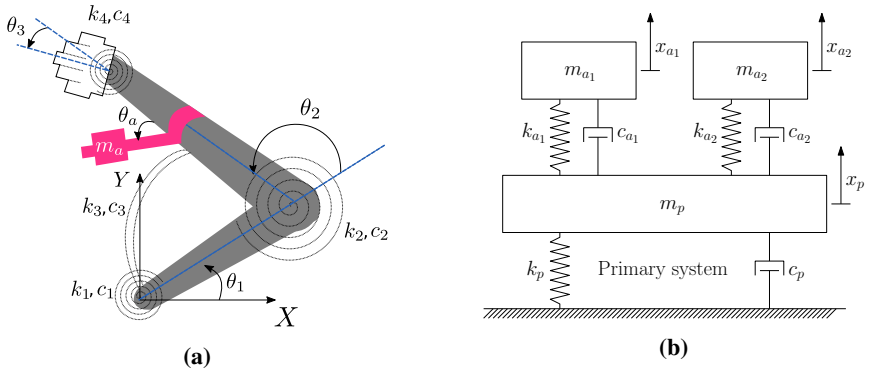

Figur 3.7: (a) Model of a single absorber connected to the forearm of the hand [4] (b) 2 DOF parallel absorber

3.3.2 Limb weights

Applying a weight is one of the most established treatments for pathological hand tremor [77]. Weighted cuff where provided 50 patients with tremor due to a range of neurological conditions [78]. Different methods were used to find the optimal weight for each patient. A combination of clinical, photographic and accelerometer recordings to asses the weighted cuffs effect. 29 patients had an objective reduction in their tremor, 18 of these felt like the reduction was useful for performing everyday tasks. 12 patients used the cuffs over six months and continued to report improvements. Patients with tremor due to multiple sclerosis and non-progressive lesions in the cerebellum benefited most, while patients with Parkinson's disease did not see any benefit.

An example of a system that uses weights to reduce pathological hand tremors is the Readi-Steadi® Anti-Tremor Orthotic Glove System [5], which is a product already on the market today. The glove is custom fitted to each patient, where multiple weights are added to the glove. It was designed to reduce resting and action tremor for people of all ages suffering from mild to severe hand tremors.

3.3.3 Gyroscope

The GyroGlove™ uses a gyroscope, which is a spinning disc, attached to the back of the hand to reduce hand tremors [6] (Figure 3.9). With the self-calibrating properties of the gyroscope, the glove can reduce tremors up to 90%. Tester has reported that using the glove feels like moving your hand through thick syrup: The motion is free and slower [79].

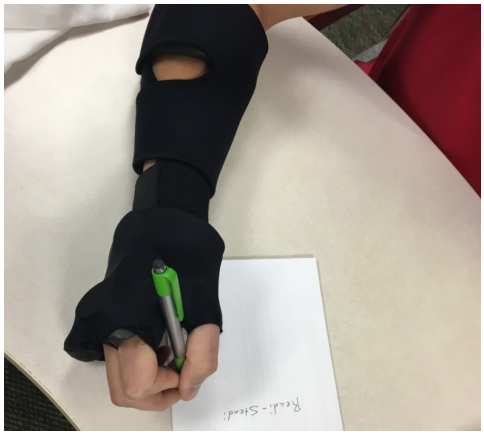

Figur 3.8: Readi-Steadi® Anti-Tremor Orthotic Glove System [5]

Figur 3.9: The GyroGlove ™ [6]

3.4 Conclusion

The tremor suppressor should be formed as a bracelet and be small enough so people will wear it without being embarrassed. It should also minimize any kind of discomfort, like heavy weight or pain.

Active solutions need some kind of power source to drive the actuators, and often need a lot of power. The WOTAS exoskeleton. It achieved a tremor suppression of roughly 80% on ET patients. The clear downside to this suppressor is its sheer size, the patients considered that the use of such a device could cause social exclusion. The solutions that use vibrators don't need as much power, because they draw small amounts of current, and can therefore be made smaller. There is little research on the effect of vibrators for tremor suppression; in one study with patients with upper limb tremor due to MS, tendon vibration on the wrist only showed a 28% reduction in tremor amplitude. Electrical stimu-

lation makes the patients feel discomfort as the study with the Tremor's glove showed, and therefore not a technology we want to use.

Passive solutions needs little or no power to work and can therefore work for long periods of time and don't need any large battery pack or power source. The GyroGlove^{TM}is a passive solution who actually needs power. There is little information about this technology but they claim the glove can reduce tremors up to 90%. Tester has reported that using the glove feels like moving your hand through thick syrup: The motion is free and slower. We will not go for this technology because of its negative effect; it doesn't just damp tremor, but all movement. Limb weights is one of the most established treatments for pathological hand tremor, but a study showed that patients with PD did not see any benefit of wearing weighted cuffs. One solution that uses DVA is the Vib-bracelet. This shows good results in experiments, but is only tested experimentally on a 1DOF system. The device damped tremor with a maximum amplitude damping of 83%. The design is nice, and could possible made so people wouldn't be embarrassed when wearing it . The International University of Beirut in Lebanon vibration absorbers for reduction of hand tremor for PD patients has in recent years published many papers on passive DVA for tremor suppersion. They us a 3DOF model of the human arm to test different absorbers, and their numbers should threfore be a bit more realstic the for the Vib-braclet that used a 1DOF model. In their latest paper [4] they check the performance of the dual parallel passive absorber in reducing the tremor. In their simulations the absorber was able to reduce 77.98-80.62%, 60.34-69.95% and 54.39-69.81% of tremor amplitude at the shoulder, elbow and wrist joints, respectively.

There is done little research on semi Semi-active solutions for tremor suppression and the two papers presented got 40% and 57% reduction respectively. The used a both used a 1DOF DVA for their suppressor. The advantages semi-active solutions are clear, they have the benefits of being small and use little power, like the passive solution, and the advantage that it can be tuned in real time to the tremor frequency.

Based on our findings form the review, the system want to design will be based on the passive dual parallel absorber [4], which show great results for dampening pathological hand tremor in simulations, and make it into a semi-active tremor suppressor; by using SMA alloy springs in the absorber and change the stiffens by running different amounts of current through it.

Kapittel 4

Vibration absorber design

From our review of existing technologies we gained enough knowledge to come up with a concept for our tremor suppressor. The design will be based on the passive 2DOF parallel absorber (Figure 4.1a) that has shown great results for dampening pathological hand tremor in simulations [4]. In the original paper this is a passive absorber, and the absorber had to be tuned to specific tremor frequency. Since tremor change over time (section 2.1.3) we want to make a semi-active solution so the system can adapt in real time to changes in tremor frequency. This can be achieved by making the spring constants in the damper variable, by using springs made out of shape memory alloy (SMA) (Figure 4.1b). We call this system the semi-active dual parallel absorber. In the original paper the two 1DOF absorbers in the 2DOF parralel absorber where tuned to two different frequencies in the tremor. A design for a vibration absorber is presented called semi-active dual parallel absorber. The

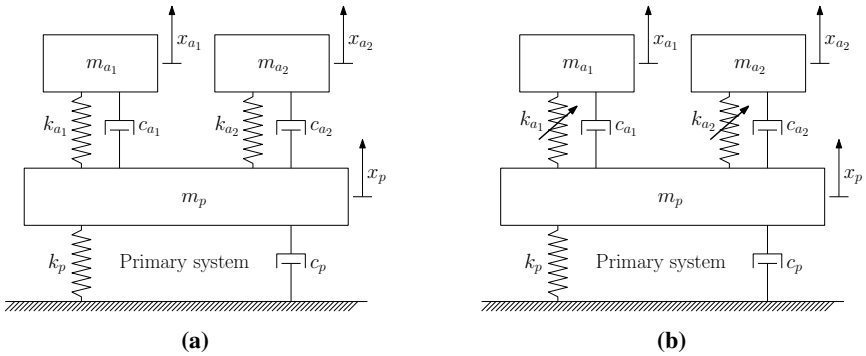

Figur 4.1: (a) Dual parallel absorber (b) semi-active dual parallel absorber with variable spring constants

In section 2.1.4 we write about harmonics and fundamental frequencies in pathological hand tremor. We want our system to be able to adapt to the two frequencies in the tremor

with the most power. This can be a fundamental frequency with a strong 2nd harmonic, or it can be two fundamental, which both have larger amplitude than their harmonics. To tune the spring constants in the dual parallel absorber we need to know what two frequencies are most dominant in the signal. For this we need a estimator that is able to estimate the these frequencies in real time. The general system for our tremor absorber can be seen in Figure 4.2a. The main focus for this thesis is outlined in Figure 4.2b. I will find or develop an algorithm that can estimate multiple frequencies in real time. Test the algorithm on real and simulated tremor data, and finally implement i onto hardware to see if its capable of running in rel time. As mentioned in the introduction, there are two students working together on this problem. The second thesis will focus on the mechanical part of the problem, which is the design and optimization of the dual parallel vibration absorber [1]. The final system design we end up with in the end can be seen in Figure 4.2d.

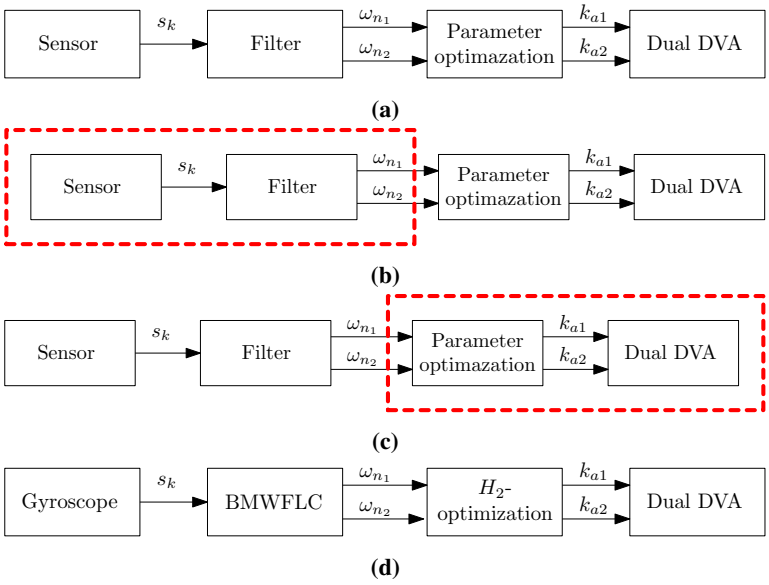

Figur 4.2: (a) The general system design of the tremor absorber (b) Focus of this thesis (c) Focus of the mechanical thesis (d) The final system design

The focus of this paper is not on the design process for the concept of the tremor absorber; this is explained in more detail in Estenstad [1].

Kapittel 5

Tremor estimation

The relationship between angular frequency, ω $[rad/s]$, and the linear frequency, f $[Hz]$ is shown by the following equation.

$$\omega = 2\pi f \tag{5.1}$$

ω and f will be used interchangeably throughout the text. For clarity to the reader, e.g. when a tremor has a frequency of $6Hz$ this is the linear frequency, f, in this case the angular frequency would be $\omega = 2\pi \times 6Hz \approx 37.7\, rad/s$.

5.1 Tremor estimators

For our proposed system, an estimator that can estimate multiple frequencies in the hand is needed. It should be able to estimate the two frequencies with the most power. If there is only one fundamental frequency in the tremor, this would be the 1st and 2nd harmonics. In some tremors there may be two fundamental frequency, and in that case the estimator should estimate those.

Section 5.1.1 presents a review of currently available frequency estimators. The conclusion from the review is; there does not exist an estimator that can fulfill our requirements. The decision is made to design an estimator for this purpose, the final filter is called the Band-limited Multiple Weighted Fourier Linear Combiner (BMWFLC). The filters that the BMWFLC is based upon are presented in the following sections: section 5.1.2 the FLC filter is presented, in section 5.1.3 the WFLC filter is presented, in section 5.1.4 the BMFLC filter is presented and in section 5.1.5 the E-BMFLC filter is presented. Finally the BMWFLC filter is presented in section 5.2, a filter designed for tracking multiple frequencies in pathological hand tremor.

5.1.1 Estimators

In recent years there seems to be an increasing interest in the development of algorithms that can accurately estimate pathological tremors [80–91]. Some of the most used filters for tremor estimation are based on the Fourier Linear Combiner (FLC) [92] filter; the Weighted Fourier Linear Combiner (WFLC) [93], the Band-limited Multiple Fourier Linear Combiner (BMFLC) [94] and the Enhanced Band-limited Multiple Fourier Linear Combiner (E-BMFLC) [86]. Especially the BMFLC and the recently developed E-BMFLC have shown high precision for extracting pathological tremor from the complete motion signal of the human hand. The estimation accuracy of the BMFLC has been shown to be 96-98% [95], and the E-BMFLC have statistically significant improvement of both accuracy and consistency in extracting pathological hand tremor for patients with PD and ET compared with the BMFLC [86].

Although the BMFLC wasn't initially intended for frequency estimation, a formula was developed that can estimate the frequency of the input signal. By weighting the contribution of each FLC, an estimate of the frequency is obtained [91]. For a first-order Fourier series, it is expressed as:

$$\omega_k = \sum_{r=0}^{n} \frac{\left(a_r^2 + b_r^2\right)\omega_r}{\sum_n^{r=0}\left(a_r^2 + b_r^2\right)} \tag{5.2}$$

The frequency estimation of the BMFLC was compared to an iteration of the WFLC filter, the KF-WFLC filter; a cascade filter consisting of a WFLC for frequency tracking, feeding it into a Kalman filter (KF) for estimating the tremor amplitude. The comparison showed that both filters provided accurate frequency estimation, though the KF-WFLC results were smother. For overall tremor tracking, the BMFLC performance was slightly worse than that of the KF-WFLC, mainly because of the improved amplitude tracking for the latter. In [84] they develop a new algorithm, based on the fast Fourier transform (FFT),

called sliding fast Fourier transform (SFFT). It's an algorithm that estimates the instantaneous tremor parameters such as the time-varying dominant frequency and amplitude. The algorithms frequency estimation was compared to the WLFC and the ABPF. It was faster to adapt when the frequency in the signal made sudden changes than the WFLC, and the estimated frequency of SFFT was more stable with small changes compared with ABPSF. This algorithm was not tested for real-time applications; they say they will carry out experiments in the future to test the feasibility of this out.

In [82] they make a filter they call the high-order WFLC-based Kalman filter. When the measured signal first enters the filter, it gets decomposed into two parts using two 1st order band-pass Butterworth filters. The two band-passed signals are then fed int each their filter, WFLC 1 and WFLC 2, where filter 1 obtains the 1st harmonic and filter 2 obtains the combination of higher harmonics. Finally, the KF adopts the estimated harmonic frequencies and the filtered harmonic signal from both channels to create the estimated tremor. The KF was added for better amplitude estimation. Their results show that the high-order WFLC-based KF performs better than the WFLC.

The WFLC algorithm adapts to a single frequency present in the tremor signal, but for tremor signals modulated by two or more frequencies close in the spectral domain, the performance of the WFLC will be degraded [94]. The BMFLC filter was designed to overcome this exact weakens; adapting to a signal with multiple dominant frequencies.

All the methods for frequency estimation mentioned above, except for [82], estimates only one frequency from the signal. Although the filter in [82] can estimate two frequencies, it is based on the WFLC algorithm which has shown to be inferior to the BMFLC when a signal modulated by two or more frequencies close in the spectral domain [94]. This filter does not take into account the possibility that multiple fundamental frequencies might be present in the signal, and can't estimate two fundamental frequencies if they are close in the frequency domain.

In early stages of the project, the filters FLC, WFLC, BMFLC and E-BMFLC where implemented and tested to get a better understanding of how they work. During this period an idea for a new filter was envisioned, a filter that could estimate multiple frequencies in the tremor signal, regardless of their placement in the frequency domain. The filter builds on the BMFLC (E-BMFLC) filter, which has shown to significantly outperform the WFLC filter when estimating a signal modulated by two or more frequencies [94]. A decision was made to pursue the development of the new filter. The new filter is called the band-limited multiple-WFLC (BMWFLC) and is presented in section 5.2.

5.1.2 FLC

The FLC is designed for modeling and estimating a quasiperiodic signal of known frequency by adapting the amplitude and phase of a reference signal, in real-time with zero phase shift [92]. The reference signal is generated artificially by a dynamic truncated Fourier series

$$y_k = \sum_{r=1}^{n} a_{rk} \sin(r\omega_0 k) + b_{rk} \cos(r\omega_0 k) \tag{5.3}$$

where k is the sampling instance, y_k the is estimated signal, n is the number of harmonics in the model, μ is the adaptive gain parameter, and the Fourier coefficients a_{rk} and b_{rk} are the adaptive weights for their respective harmonic frequency $r\omega_0$. Then $\mathbf{x}_k$ and $\mathbf{w}_k$ are defined

$$\mathbf{x}_k = \begin{bmatrix} [\sin(\omega_0 k) & \sin(2\omega_0 k) & \cdots & \sin(n\omega_0 k)]^T \\ [\cos(\omega_0 k) & \cos(2\omega_0 k) & \cdots & \cos(n\omega_0 k)]^T \end{bmatrix} \tag{5.4}$$

$$\mathbf{w}_k = \begin{bmatrix} [a_{1k} & a_{2k} & \cdots & a_{nk}]^T \\ [b_{1k} & b_{2k} & \cdots & b_{nk}]^T \end{bmatrix} \tag{5.5}$$

Using (5.4) and (5.5) the linear combiner can be written as

$$y_k = \mathbf{w}_k^T \mathbf{x}_k \tag{5.6}$$

The error between the input signal s_k and the estimated signal, y_k is

$$\varepsilon_k = s_k - y_k = s_k - \mathbf{w}_k^T \mathbf{x}_k \tag{5.7}$$

and the recursive LMS algorithm used to update the weights of $\mathbf{w}_k$

$$\mathbf{w}_{k+1} = \mathbf{w}_k + 2\mu \mathbf{x}_k \epsilon_k \tag{5.8}$$

The FLC architecture can be seen in Figure 5.1.

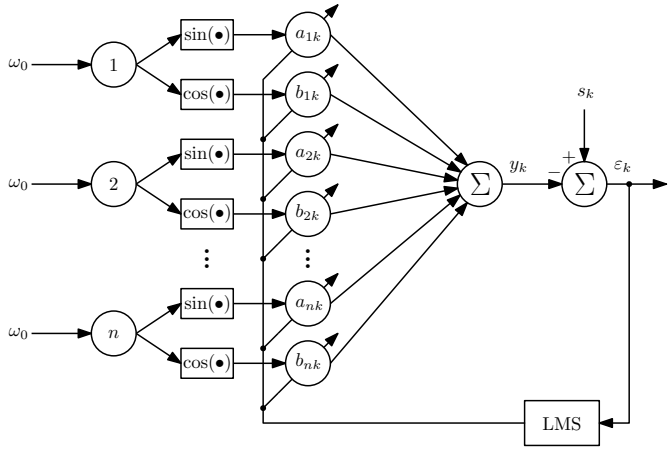

Figur 5.1: FLC architecture

5.1.3 WFLC

The WFLC is an extension of the FLC algorithm first presented in [93], and like the FLC it models the tremor input as a dynamic truncated Fourier series. Where the FLC works on a preset fixed frequency, the WFLC can adapt the frequency of the model as well as its Fourier coefficients. The WFLC can, therefore, compensate for approximately periodic disturbance of unknown frequency and amplitude. The WFLC does not filter away the voluntary movement when used for estimating a tremor signal, and in [93], a bandpass prefilter with passband 7-13 Hz was used before the WFLC to filter away voluntary motion. The bandpass filter has a small phase lag, so the estimated frequency from the WFLC is sent to an FLC with no prefiltering to get a zero-phase tremor estimation.

The equations for the WFLC filter are as follows

$$y_k = \sum_{r=0}^{n} a_{rk} \sin(r\omega_{0_k} k) + b_{rk} \cos(r\omega_{0_k} k) \tag{5.9}$$

$$\mathbf{x}_k = \begin{bmatrix} [\sin(\omega_{0_k} k) & \sin(2\omega_{0_k} k) & \cdots & \sin(n\omega_{0_k} k)]^T \\ [\cos(\omega_{0_k} k) & \cos(2\omega_{0_k} k) & \cdots & \cos(n\omega_{0_k} k)]^T \end{bmatrix} \tag{5.10}$$

$$\mathbf{w}_k = \begin{bmatrix} [a_{1k} & a_{2k} & \cdots & a_{nk}]^T \\ [b_{1k} & b_{2k} & \cdots & b_{nk}]^T \end{bmatrix} \tag{5.11}$$

$$y_k = \mathbf{w}_k^T \mathbf{x}_k \tag{5.12}$$

$$\varepsilon_k = s_k - y_k = s_k - \mathbf{w}_k^T \mathbf{x}_k \tag{5.13}$$

$$\mathbf{w}_{k+1} = \mathbf{w}_k + 2\mu \mathbf{x}_k \epsilon_k \tag{5.14}$$

The fundamental angular frequency, ω_{0_k}, is updated using a modified LSM algorithm, with its own adaptive gain, μ_0

$$\omega_{0_{k+1}} = \omega_{0_k} + 2\mu_0 \varepsilon_k \sum_{r=1}^{n} r \left[a_{rk} \cos(r\omega_{0_k} k) - b_{rk} \sin(r\omega_{0_k} k) \right] \tag{5.15}$$

Input amplitude and phase are estimated by the adaptive weight vector $\mathbf{w}_k$, as in FLC, while ω_{0_k} estimates the input frequency. If $\mu_0 = 0$, the WFLC reduces to the FLC.

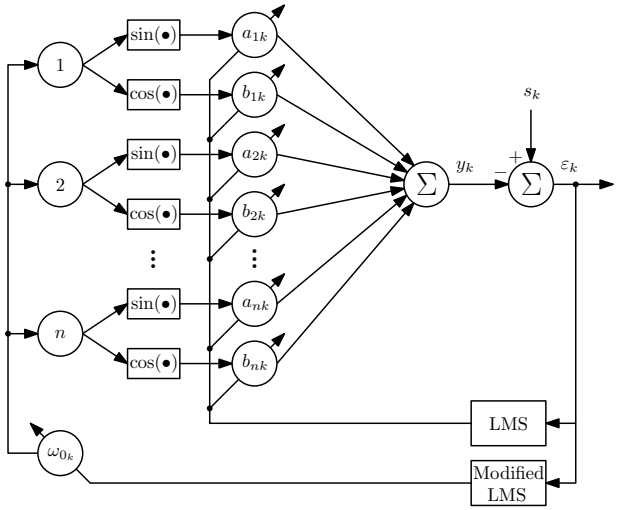

Figur 5.2: WFLC architecture

5.1.4 BMFLC

The band-limited multiple-FLC (BMFLC) [94, 96] is based on the concepts of the WFLC algorithm. The WFLC algorithm adapts to a single frequency present in the tremor signal, but for tremor signals modulated by two or more frequencies close in the spectral domain, the performance of the WFLC will degrade. In such cases, the frequency adaption process of the WFLC will never stabilize, and accurate estimation will never be attained. To overcome this weakness, the bandlimited multiple-FLC (BMFLC) can track multiple frequency components in the incoming signal. Instead of having one variable frequency w_{0_k} that adapts to the fundamental frequency of the tremor like with the WFLC, the BMFLC predefines a band of frequencies $[\omega_1 - \omega_n]$, and then divide the frequency band into n finite divisions, with distance Δw between them, as shown in Figure 5.4. In Figure 5.3 we can see that n-FLCs are combined to form the BMFLC, this algorithm is now capable of estimating a signal with multiple dominant frequencies. In [95], to compare the efficiency of the WFLC and BMFLC, they used a modulating sinusoidal signal with two frequencies (5.22), simulating a tremor signal. When the two frequencies in the signal where equal, the WFLC slightly outperformed the BMFLC, but when the frequency gap increase, the WFLC fails to adapt to the modulated signal. The BMFLC is not affected by the frequency gap. When setting the value of Δw to 0.1-0.5, estimation accuracy of 96-98% was obtained with the BMFLC.

$$y_k = \sum_{r=1}^{n} a_{rk} \sin(\omega_r k) + b_{rk} \cos(\omega_r k) \tag{5.16}$$

$$\mathbf{x}_k = \begin{bmatrix} [\sin(\omega_1 k) & \sin(\omega_2 k) & \cdots & \sin(\omega_n k)]^T \\ [\cos(\omega_1 k) & \cos(\omega_2 k) & \cdots & \cos(\omega_n k)]^T \end{bmatrix} \tag{5.17}$$

$$\mathbf{w}_k = \begin{bmatrix} [a_{1k} & a_{2k} & \cdots & a_{nk}]^T \\ [b_{1k} & b_{2k} & \cdots & b_{nk}]^T \end{bmatrix} \tag{5.18}$$

$$y_k = \mathbf{w}_k^T \mathbf{x}_k \tag{5.19}$$

$$\varepsilon_k = s_k - y_k \tag{5.20}$$

$$\mathbf{w}_{k+1} = \mathbf{w}_k + 2\mu \mathbf{x}_k \epsilon_k \tag{5.21}$$

$$s_k = 3.5 \sin(2\pi f_1 t) + 2.5 \cos(2\pi f_2 t) \tag{5.22}$$

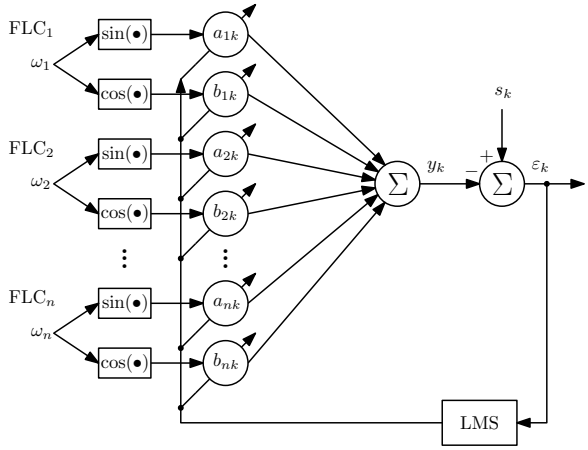

Figur 5.3: BMFLC architecture

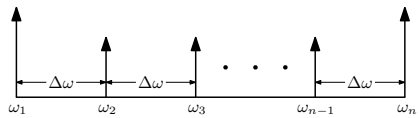

Figur 5.4: BMFLC frequency distribution

5.1.5 E-BMFLC

The Enhanced Band-limited Multiple Fourier Linear Combiner (E-BMFLC) filter [81, 86] is an improvement on the BMWFLC. The following model represents the hand movement of a patient with pathological hand tremor

$$m_k = m_{k-v} + m_{k-i} \tag{5.23}$$

In (5.23), m_k is the signal of the patients hand motion; m_{k-v} and m_{k-i} are the voluntary and involuntary components of the motion respectively. The main goal of the BMFLC was to estimate the involuntary motion m_{k-i} in real-time. The E-BMFLC have been developed to address two two major drawbacks of the BMFLC filter, inaccurate error calculation and infinite memory. The implementation of the E-BMFLC filter is divided into two phases of enhancement; *Phase* 1) *Harmonic Model Enrichment:* To deal with the incorrect error calculation, and *Phase* 2) *Memory manipulation*: Using a windowed memory instead of the conventional infinite memory.
Instead of using the truncated model that only considers the frequency of the tremor (m_{k-i}), $[\omega_1, \omega_n]$ seen in Fig 5.4, the complete frequency range of the hand motion (m_k),

$$[\omega_{min}, \omega_{max}] \tag{5.24}$$

is considered. The frequency window is divided into a number of divisions

$$n = \frac{\omega_{max} - \omega_{min}}{\Delta\omega} \tag{5.25}$$

and n is then the number of harmonics in for the Fourier combiner model of m_k. The following Fourier combiner is then used to model the complete hand motion m_k, where $\omega_1 = \omega_{min}$ and $\omega_n = \omega_{max}$.

$$\hat{m}_k = \sum_{r=1}^{n} a_{rk} \sin(\omega_r k) + b_{rk} \cos(\omega_r k) \tag{5.26}$$

Then $\mathbf{x}_k$ and $\mathbf{w}_k$ are defined

$$\mathbf{x}_k = \begin{bmatrix} [\sin(\omega_1 k) & \sin(\omega_2 k) & \cdots & \sin(\omega_n k)]^T \\ [\cos(\omega_1 k) & \cos(\omega_2 k) & \cdots & \cos(\omega_n k)]^T \end{bmatrix} \tag{5.27}$$

$$\mathbf{w}_k = \begin{bmatrix} [a_{1k} & a_{2k} & \cdots a_{nk} &]^T \\ [b_{1k} & b_{2k} & \cdots b_{nk} &]^T \end{bmatrix} \tag{5.28}$$

Using (5.40) and (5.41) the linear combiner can be written as

$$\hat{m}_k = \mathbf{w}_k^T \mathbf{x}_k \tag{5.29}$$

The error between the signal of the complete motion of the hand m_k and the estimated signal $\hat{m}_k$ is

$$\varepsilon_k = m_k - \hat{m}_k \tag{5.30}$$

and the recursive LMS algorithm used to update the weights of $\mathbf{w}_k$

$$\mathbf{w}_{k+1} = \rho \mathbf{w}_k + 2\mu \mathbf{x}_k \varepsilon_k \tag{5.31}$$

$$\rho = \sqrt[\delta]{\alpha} \tag{5.32}$$

$$\delta = \frac{1}{\Delta T} T_p \tag{5.33}$$

In (5.31), ρ defines the pole of discrete dynamics of the memory windowing for the filter in the Z-domain, considered to enhance the performance of the filter, especially for non-periodic signals [86]. Decreasing ρ increases the rate of forgetting past information. In (5.33), ΔT is the sampling time (in seconds), T_p is the width of the considered memory window (in seconds), and α is the minimum amplification gain considered within the window.

After the estimated motion $\hat{m}_k$ has been modeled, the estimate of the voluntary motion $\hat{m}_{k-v}$ and involuntary motion $\hat{m}_{k-i}$ can be extracted. To do this different band-limited windows of frequency can be considered to extract various frequency ranges. Using this technuiqe, the signal modeling and frequency truncation are decoupled, while in the formulation of BMFLC filter these two steps are fused. Two frequency ranges will be considered, $[\omega_a, \omega_b]$ and $[\omega_c, \omega_d]$, for voluntary and involuntary motion respectively. In order to extract $\hat{m}_{k-i}$ and $\hat{m}_{k-v}$, the calculated $\mathbf{w}_k$ and $\mathbf{x}_k$ should be truncated considering the frequency range of the voluntary and involuntary motion. The following definitions are made for this purpose

$$N_a = \frac{\omega_a - \omega_{min}}{\Delta\omega}, \quad N_b = \frac{\omega_b - \omega_{min}}{\Delta\omega} \tag{5.34}$$

$$N_c = \frac{\omega_c - \omega_{min}}{\Delta\omega}, \quad N_d = \frac{\omega_d - \omega_{min}}{\Delta\omega} \tag{5.35}$$

where ω_{min} is from (5.24), and $\Delta\omega$ is the same as in (5.45). The estimates for $\hat{m}_{k-i}$ and $\hat{m}_{k-v}$ can now be found with the following equations

$$\hat{m}_{k-v} = \mathbf{w}_{k-v}^T \mathbf{x}_{k-v} \tag{5.36}$$

$$\mathbf{x}_{k-v} = \begin{bmatrix} [\sin(\omega_{N_a} k) & \sin(\omega_{(N_a+1)} k) & \cdots & \sin(\omega_{N_b} k)]^T \\ [\cos(\omega_{N_a} k) & \cos(\omega_{(N_a+1)} k) & \cdots & \cos(\omega_{N_b} k)]^T \end{bmatrix} \tag{5.37}$$

$$\mathbf{w}_{k-v} = \begin{bmatrix} [a_{N_a} k & a_{(N_a+1)} k & \cdots & a_{N_b} k]^T \\ [b_{N_a} k & b_{(N_a+1)} k & \cdots & b_{N_b} k]^T \end{bmatrix} \tag{5.38}$$

$$\hat{m}_{k-i} = \mathbf{w}_{k-i}^T \mathbf{x}_{k-i} \tag{5.39}$$

$$\mathbf{x}_{k-i} = \begin{bmatrix} [\sin(\omega_{N_c} k) & \sin(\omega_{(N_c+1)} k) & \cdots & \sin(\omega_{N_d} k)]^T \\ [\cos(\omega_{N_c} k) & \cos(\omega_{(N_c+1)} k) & \cdots & \cos(\omega_{N_d} k)]^T \end{bmatrix} \tag{5.40}$$

$$\mathbf{w}_{k-i} = \begin{bmatrix} [a_{N_c} k & a_{(N_c+1)} k & \cdots & a_{N_d} k]^T \\ [b_{N_c} k & b_{(N_c+1)} k & \cdots & b_{N_d} k]^T \end{bmatrix} \tag{5.41}$$

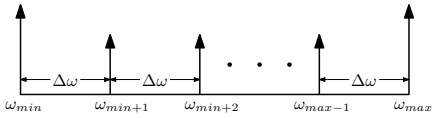

Figur 5.5: Complete frequency distribution of hand motion

5.2 BMWFLC

In this section, I will propose a new method for tracking multiple frequencies in a pathological tremor signal. The amplitude is not relevant to us since the dual parallel vibration absorber only needs the frequency to adapt, so we don't care about the accuracy of the amplitude estimation. The proposed filter is a combination of the E-BMFLC filter and the WFLC filter. Like the band-limited multiple-FLC (BMFLC) filter that consists of multiple-FLC, my idea is to extend this to a band-limited multiple-WFLC (BMWFLC) filter. In Figure 5.6 we can see the new filter architecture, we see that n-WFLC are combined to form the BMWFLC. The novelty here is that each frequency in the band now can adjust to the signal. To accomplish this we measure the magnitude of the Fourier coefficients of each WFLC in the BMWFLC, the WFLC with the largest magnitude contains the dominant frequency in the estimated signal. It is now possible to measure all the frequencies present in the estimated signal, and their strength with respect to each other.

5.2.1 Core equations

Each n-WFLC in the BMWFLC has its own frequency and learning rate, enabling each WFLC to adapt to the signal individually with its own speed. The learning rates are

$$\boldsymbol{\mu}_k = \begin{bmatrix} \mu_{1k} & \mu_{2_k} & \cdots & \mu_{n_k} \end{bmatrix} \tag{5.42}$$

and the angular frequencies for the WFLC in the filter are

$$\boldsymbol{\omega}_k = \begin{bmatrix} \omega_{1_k} & \omega_{2_k} & \cdots & \omega_{n_k} \end{bmatrix} \tag{5.43}$$

where k is the sampling instance. When $k = 0$ we get the size frequency window, where the frequencies have the distance Δw between them

$$[\omega_{1_0}, \omega_{n_0}] \tag{5.44}$$

The frequency window is divided into a number of divisions

$$n = \frac{\omega_{n_0} - \omega_{1_0}}{\Delta\omega} \tag{5.45}$$

and n is then the number of harmonics in for the Fourier combiner model of y_k.

$$y_k = \sum_{r=1}^{n} a_{rk} \sin(\omega_{r_k} k) + b_{rk} \cos(\omega_{r_k} k) \tag{5.46}$$

y_k will not be used as an output for this filter, since it will not be tuned to have an accurate estimate of the amplitude, only the frequencies (5.44) are of interest. Then $\mathbf{x}_k$ and $\mathbf{w}_k$ are defined

$$\mathbf{x}_k = \begin{bmatrix} [\sin(\omega_{1_k} k) & \sin(\omega_{2_k} k) & \cdots & \sin(\omega_{n_k} k)]^T \\ [\cos(\omega_{1_k} k) & \cos(\omega_{2_k} k) & \cdots & \cos(\omega_{n_k} k)]^T \end{bmatrix} \tag{5.47}$$

$$\mathbf{w}_k = \begin{bmatrix} [a_{1k} & a_{2k} & \cdots & a_{nk}]^T \\ [b_{1k} & b_{2k} & \cdots & b_{nk}]^T \end{bmatrix} \tag{5.48}$$

Using (5.47) and (5.48) the linear combiner can be written as

$$y_k = \mathbf{w}_k^T \mathbf{x}_k \tag{5.49}$$

and the error beween the signal of the complete motion of the hand and the estimated signal y_k is

$$\varepsilon_k = s_k - y_k \tag{5.50}$$

The recursive LMS algorithm used to update the weights of $\mathbf{w}_k$

$$\mathbf{w}_{k+1} = \rho \mathbf{w}_k + 2\mu_k \mathbf{x}_k \varepsilon_k \tag{5.51}$$

$$\rho = \sqrt[\delta]{\alpha} \tag{5.52}$$

$$\delta = \frac{1}{\Delta T} T_p \tag{5.53}$$

This is the *memory manipulation* from the E-BMFLC algorithm in section 5.1.5. It makes the filter forget past information, making it adapt faster when sudden changes occur in the signal s_k, E.g., a sudden change of frequency. Decreasing ρ increases the rate of forgetting past information. ΔT is the sampling time (in seconds), T_p is the width of the considered memory window (in seconds), and α is the minimum amplification gain considered within the window.

The fundamental angular frequencies $\boldsymbol{\mu}_k$, are updated using multiple modified LSM algorithms, one for each WFLC, each with its own adaptive gain $\boldsymbol{\omega}_k$

$$\omega_{r_{k+1}} = \omega_{r_k} + 2\varepsilon_k \mu_{rk} \left[a_{rk} \cos(r\omega_{r_k} k) - b_{rk} \sin(\omega_{r_k} k) \right], \qquad r = 1, 2, \ldots, n \tag{5.54}$$

Equation (5.54) is a special case of Equation (5.15) with one harmonic. Equation (5.54) uses the LMS algorithm to descend the performance surface to minimize the MSE (see section 2.3.3). If the learning rates $\boldsymbol{\mu}_k$, are too large all the frequencies will try to reach the frequencies with the largest magnitude in the magnitude spectrum, the global minimum on the performance surface. This is because the error ε_k looks at the error between the input signal s_k and the estimate of the entire signal y_k, so each WFLC in the BMWFLC wants to go for the dominant frequency in the signal. If the learning rates $\boldsymbol{\mu}_k$, is set small enough, each WFLC will get stuck in its local minimum, this is what we want, enabling each WFLC only converge towards the real frequency closest to it. When tracking multiple frequencies, the learning rate needs to be small, resulting in slow convergence, if only the frequency with the largest magnitude is being tracked, the learning rate can be set much higher since only the global minimum is of interest, resulting in faster convergence.

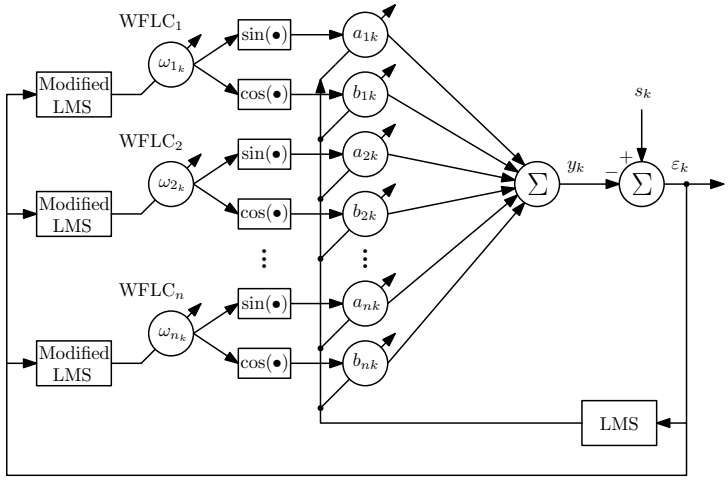

Figur 5.6: BMWFLC

5.2.2 Adaptive learning rate

One of the drawbacks with the FLC, WFLC and BMFLC algorithms is that the learning rate parameters μ and μ_0 needs fine tuning, and are sensitive to change in the amplitude of the input signal [97]. The two parameters also need to be tuned separately. Our primary goal is to dampen the tremor for people with PD and ET, but when the tremor is suppressed the amplitude of the signal will be decreased, and the sensitivity of the estimation will decrease. To solve this problem, we can use the amplitude of the input signal to adapt the learning rate. I have come up with a simple but elegant solution to this problem. We will use a queue data structure Q, which uses the first-in, first-out, or FIFO, policy. The queue will have a fixed length L, a good value for its length is to set it equal to the sampling rate of the signal, f_s.

Algorithm 1: Max amplitude window

Input: The measured signal; y_k
Input: Max length of queue; L
Output: The peak amplitude from the time slice; A_{peak}
Q.enqueue($abs(y_k)$);
if *(Q.length* $> L$*)* **then**
  Q.dequeue();
end
$A_{peak} = \max Q$

Algorithm 1 checks the L last samples from the tremor signal, and return the peak amplitude. This value can now be used to adapt the learning rates. If the length L is set to 100 and our sample rate of the signal is 100 Hz, the window will contain the tremor values for the past 1 second so that the learning rates can adapt relatively fast to any changes in the amplitude of the tremor. The following equations adapt the learning rates.

$$\mu_k = \frac{\kappa}{A_{peak}} \tag{5.55}$$

The value for the scaling parameter κ can be found by tuning, I found that a good starting value is 0.01. The equation to make μ_{nk} adaptive is

$$\mu_{rk} = \mu_k h + \mu_{rk}\beta e^{-\lambda t}, \qquad r = 1, 2, \ldots, n \tag{5.56}$$

For the first term h scales the learning rate u_{nk} with respect to the value of μ_k. The second term is adds exponential decay, making mu_{r_k} an exponential decaying learning rate. At time $t = 0$, $e^0 = 1$, and $\mu_{r_k} = \mu_k h + \mu_{r_k}\beta$. When $\lim_{t\to\infty}$ the term becomes 0, and $\mu_{nk} = \mu_k h$. What this does is to make the learning rate larger in the start and exponentially decaying to the desired and stable $\mu_{r_k} = \mu_k h$ form. μ_{r_k} should have a value that is $\mu_{r_k} << \mu_k$ for it to be stable [97], so for the scaling parameter h a good starting value is 0.00001. The parameter β is the value we want scale up the learnngrate at the start, a good value to start with is 50. λ (known as the decay constant) makes the learning rate decay faster when it increases i size. A good starting value for this constant is 0.2. The reason to use a exponential decaying learning rate is to make the estimation of the frequency go faster in the start, but for such high values, the filter would become unstable over time, so it decays to a stable value.

5.2.3 Magnitude spectrum - extracting frequencies

To find the frequencies in the input signal, we will look at the magnitudes of the Fourier components in the BMFLC, the magnitude of each FLC; the FLC with the highest magnitude should contain the dominant frequency in the estimated signal, which then is the estimate of the dominant frequency for the real signal. This is based on the concept of magnitude spectrum for a Fourier series, presented in 2.4.2.

$$M_{rk} = \sqrt{a_{rk}^2 + b_{rk}^2}, \qquad r = 1, 2, \ldots, n \tag{5.57}$$

$$\mathbf{M} = \begin{bmatrix} M_{1k} & M_{2k} & \cdots & M_{nk} \end{bmatrix} \tag{5.58}$$

The cool thing about this method is that we can use it to estimate multiple frequencies in the signal. To accomplish this, we look for the magnitudes that are peaks in the magnitude spectrum. By peak magnitude I mean that the magnitude of interest should be larger than the magnitude to its immediate left and right in the magnitude spectrum, $M_{r-1} < M_r > M_{r+1}$, an example can be seen in Figure 5.8a, where the two red markers are peaks in the spectrum. We want to be able to tell our algorithm how many peaks it should track in the spectrum, each peak it tracks is an estimate of a frequency, so we define a variable called ftt (frequencies to track). Instead of making all the FLC in the truncated Fourier series into WFLC, we can say that the ftt number of FLC with the largest magnitude of Fourier coefficients are allowed to become WFLC. When the learning rate is set to zero, $\mu_{rk} = 0$, it becomes an FLC, and its respective frequency ω_{r_k} lose its capability to adapt to the signal. When the BWMFLC starts to adapt to the signal, all the magnitudes of the FLC are tracked, and the fft number of FLC with the largest peak magnitudes in the magnitude spectrum become WFLC, by setting $\mu_{rk} > 0$. We define an array to store the

peak magnitudes and their position in the spectrum. M_{peak_1} is largest, M_{peak_2} second largest peaks and Pos_{p_1} and Pos_{p_2} are their position in the spectrum respectively. The magnitude peaks can now be used to compare how much power the different dominant frequencies have in respect to each other, this is not something I have implemented here, so this should be looked further at in future iterations of the BMWFLC filter.

$$\mathbf{M}_{peak} = \begin{bmatrix} [M_{p_1}, Pos_{p_1}] & [M_{p_2}, Pos_{p_2}] & \cdots & [M_{p_r}, Pos_{p_r}] \end{bmatrix} \tag{5.59}$$

Algorithm 2 shows how we can find the magnitude peaks, and return an array with all the peaks, it should be sorted the same way as (5.59).

Algorithm 2: Find peak magnitudes

Input: Magnitude spectrum; **M** (5.58)
Output: Peak magnitudes; $\mathbf{M}_{peak}$ (5.59)
for $i = 0; i < M.length; i = i + 1$ **do**
  if *i == 0* **then**
    if $M[i] > M[i+1]$ **then**
      $M_{peak}.append([M[i], i])$
    end
  else if $i < M.length$ **then**
    if $M[i] > M[i-1]$ *and* $M[i] > M[i+1]$ **then**
      $M_{peak}.append([M[i], i])$
    end
  else if $i == M.length$ **then**
    if $M[i] > M[i-1]$ **then**
      $M_{peak}.append([M[i], i])$
    end
  end
end
$M_{peak}.sort()$

It is now easy to get the estimate for the frequencies; we use the positions from (5.59), and the estimates will be the frequencies in (5.44) that corresponds to them. E.g if $Pos_{p_1} = 8$, the estimate for the frequency with the most power in the input signal will be ω_{8_k}. In Figure 5.7 we see the frequency window of the BMWFLC, the two arrows with red arrowheads represent the two dominant frequencies in the signal when $ftt = 2$, they can adapt to the signal by setting the learning rates, $\mu_{4k} > 0$ and $\mu_{7k} > 0$.

Algorithm 3: Adapt and return $\boldsymbol{\omega}_k$, the estimated frequencies

Input: Peak magnitudes sorted; $\mathbf{M}_{peak}$ (5.59)
Input: Number of frequencies to track; ftt
Input: Angular frequencies; $\boldsymbol{\omega}_k$ (5.43)
Input: Learning rates; $\boldsymbol{\mu}_k$ (5.42)
Output: Estimated frequencies; ef
ef = []
for $i = 0; i < ftt; i = i + 1$ **do**
    positionOfPeak= $M_{peak}[i][1]$
    adaptLearningRate($\boldsymbol{\mu}_k$[positionOfPeak]) //Equation (5.56)
    adaptAngularFrequency($\boldsymbol{\omega}_k$[positionOfPeak]) //Equation (5.54)
    ef.append($\boldsymbol{\omega}_k$[positionOfPeak])
end

Since the frequencies in $\boldsymbol{\omega}_k$ will move change over time, there should be a mechanism to reset the frequencies to their original values $\boldsymbol{\omega}_0$, if they no longer are present in the signal. An easy way to do this is to make a threshold variable, η, and if any of the magnitudes in $\mathbf{M}_k$ gets under this threshold, its respective frequency in $\boldsymbol{\omega}_k$ should reset to its original value $\boldsymbol{\omega}_0$.

$$\omega_{r_k} = \begin{cases} \omega_{r_0}, & \text{if } M_{rk} < \eta \\ \omega_{r_k}, & \text{otherwise} \end{cases} \qquad r = 1, 2, \ldots, n \tag{5.60}$$

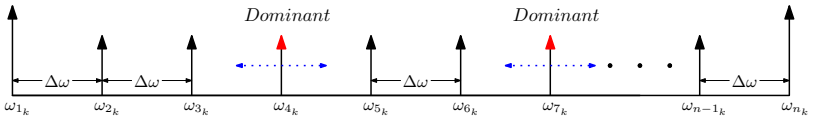

Figur 5.7: BWMFLC frequency distribution with two dominant frequency, ω_4 and ω_7.

Example 5.2.1.
To get a better understanding of how finding frequencies in the signal using the magnitude spectrum in the BMWFLC works, we will use the signal $s_k = \underbrace{4}_{A_1}\sin(2\pi\underbrace{4.2}_{f_1}t) + \underbrace{3}_{A_2}\cos(2\pi\underbrace{5}_{f_2}t)$ as input to our algorithm. We chose the band of [3Hz, 7Hz], with $\Delta f = 0.1$. In Figure 5.8a, each stem plotted is the magnitude of the Fourier coefficients of its respective FLC (WFLC for the peaks), after running the algorithm for 10 seconds. The two dominant frequencies have red markers, and it's now easy to see which frequencies are dominant.

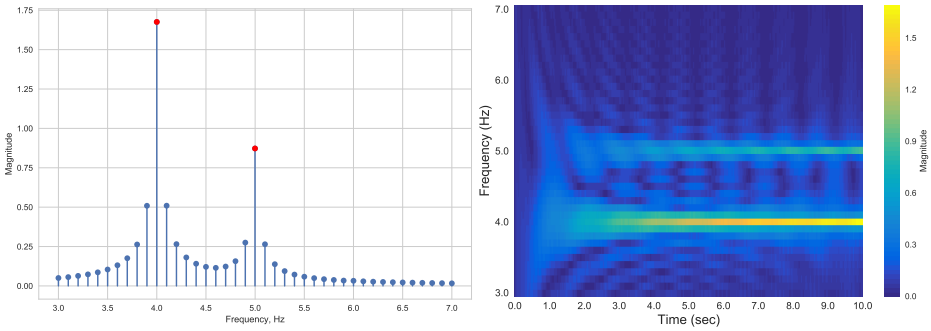

(a) **(b)**

Figur 5.8: (a) Magnitude of BMWFLC after 10 seconds running on simulated signal. (b) Heatmap of magnitude spectrum from the BMWFLC

5.2.4 Flowchart for BMWFLC algorithm

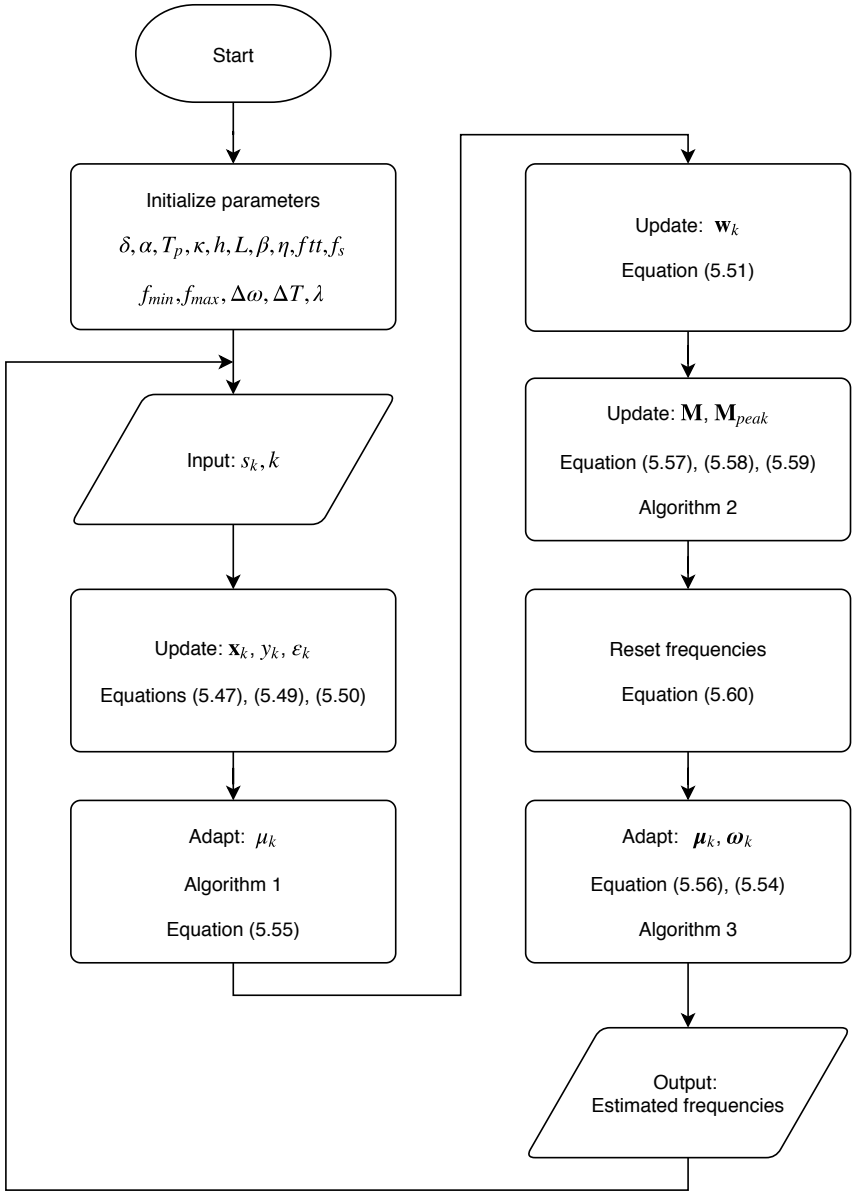

Figur 5.9: Flowchart for BMWFLC algorithm

Kapittel 6

Tremor data

6.1 Real dataset

The real dataset was downloaded from the website of Motus Bioengineering Inc., Benicia, CA [28]. The data was recorded with a biaxial gyroscope developed by Motus Bioengineering Inc., with a sampling rate of 100 Hz. The sensor responds to angular velocity and is set up to measure flexion-extension or the pronation-supination axis of the wrist. The recordings are of 1 DOF at a time, when both flexion-extension and the pronation-supination have been recorded simultaneously the recordings come in two separate files. This dataset has been used by several other researchers to test the performance of their pathological tremor estimators [80, 81, 83, 84, 87].

In Table 6.1 the data we are going to use is listed, there are more data in the original set, only recordings relevant for us have been chosen. All the patients in this dataset suffered from PD. In the type column in the table, P/S and F/E stands for pronation-supination and flexion-extension respectively. The + sign states which movement is positive in the recorded data, so P/S+ means pronation-supination with supination positive. All recordings in the same session where recorded simultaneously from the same patient.

Session	Recording	Placement	Placement	Duration (sec)	Type
1	1	P+/S	RH	10	Rest tremor
2	2	P+/S	RH	30	Rest tremor
	3	P+/S	LH	30	Rest tremor
3	4	P+/S	RH	10	Rest tremor
	5	F+/E	RH	10	Rest tremor
4	6	P/S+	LH	10	Rest tremor
	7	P+/S	RH	10	Rest tremor
5	8	P+/S	RH	30	Voluntary movement P/S
	9	P+/S	LH	30	Rest tremor
	10	F+/E	RH	30	Voluntary movement P/S
	11	F/E+	LH	30	Rest tremor
6	12	F+/E	RH	60	Postural tremor
	13	F/E+	LH	60	Postural tremor
7	14	P+/S	RH	30	Action tremor
	15	P+/S	LH	30	Action tremor

Tabell 6.1: Real dataset

6.2 Simulated data

To simulate the tremor signal we will use the model presented in [81, 86], Equation 5.23, and add additional white noise, n_k.

$$m_k = m_{k-v} + m_{k-i} + n_k \tag{6.1}$$

6.2.1 Involuntary movement

In theory, a tremor signal can be completely reconstructed by a Fourier series. For simplicity, a pseudo-tremor form can be constructed using just two sinusoids [28]. The involuntary movement m_{k-i} is simulated with a modulating sinusoidal signal with two frequencies, using the same form as Equation (5.22).

$$m_{k-i} = A_1 \sin(2\pi f_1 t) + A_2 \cos(2\pi f_2 t) \tag{6.2}$$

6.2.2 Voluntary movement

A tremor accompanied by voluntary movement is known as "actiontremor (section 2.1). An example of an action tremor from recording 15 in was plotted Figure 9.47, where the voluntary movement is the long slow-moving wave in the signal. The voluntary movement can be simulated using a single sinusoid, with the frequency in the range of 0-3 Hz.

$$m_{k-v} = A_3 \sin(2\pi f_3 t) \tag{6.3}$$

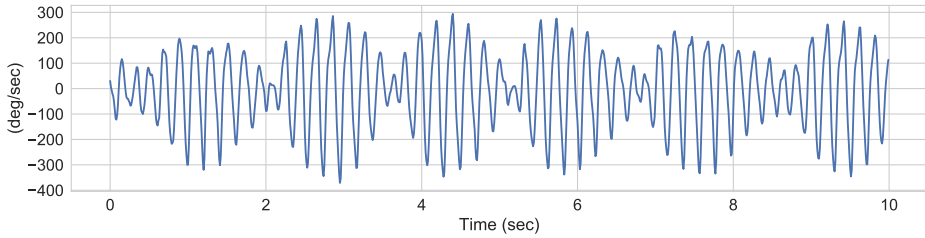

Figur 6.1: Recording number 1 from Table 6.1

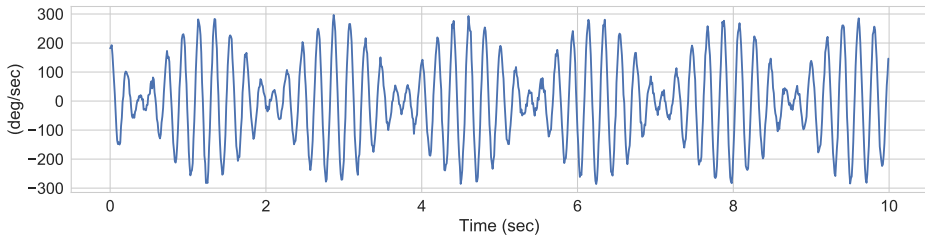

Figur 6.2: Simulated signal. $m_{k-i} = 128\sin(2\pi \cdot 4.6 \cdot t) + 153\cos(2\pi \cdot 5.2 \cdot t) + n_k$, with $\sigma_{n_k} = 10$

6.2.3 Noise

White noise is added to the signal to simulate noise from the gyroscope and the electrical circuit; the noise, n_k, is modeled using random samples from a normal (Gaussian) distribution [98] with zero mean and standard deviation σ_{n_k}.

Kapittel 7

Time-Frequency analysis

To evaluate the frequency estimation of the BMWFLC on the real data set we will use two time-frequency signal analysis tools; power spectral density (PSD) and spectrogram.

7.1 Power Spectral Density

PSD is used to obtain the distribution of power across frequencies. [99] PSD estimation, using the Welch-Barlett method [100, 101], is the most common type of analysis used for tremor signals [102], and this is the method of our choice. To make the plots the *scipy.signal.welch* module from the open-source software SciPy [103] is utilized. For most tremor signals, duration of 5-10 s is recommended for the signal window, and overlap of 50% is often used in practice [102]; based on this a Hanning window of 10 s and overlap of 50% is used for all the plots. Both linear and logarithmic power scales will be used; the linear scale shows a clear picture of which frequencies have the most power in the tremor, but information of the smaller peaks will be lost; the logarithmic scales shows information about the higher harmonics in the signal which are suppressed by the linear scale. [104] The linear scale is of most use to us since we want to find the frequencies with the most power; the logarithmic scale gives us more detail of the frequencies with lower power, making easier to see the harmonics of the high powered frequencies.

In Figure 7.1 we take the PSD of the signal shown in Figure 6.1. From Figure B.32a it's easy to see that there are two prominent peaks in the signal, at 4.6 Hz and 5.2 Hz, they are the two natural frequencies of this tremor, and the frequencies we want to estimate. From 7.1b we see that there are 2nd and 3d harmonics at 9.1 Hz and 14.3 Hz for the 4.6 Hz peak, and at 9.7 Hz and 15 Hz for the 5.2 Hz peak. In this particular tremor, the 2nd and 3rd harmonics have very little power compared to the 1st harmonic.

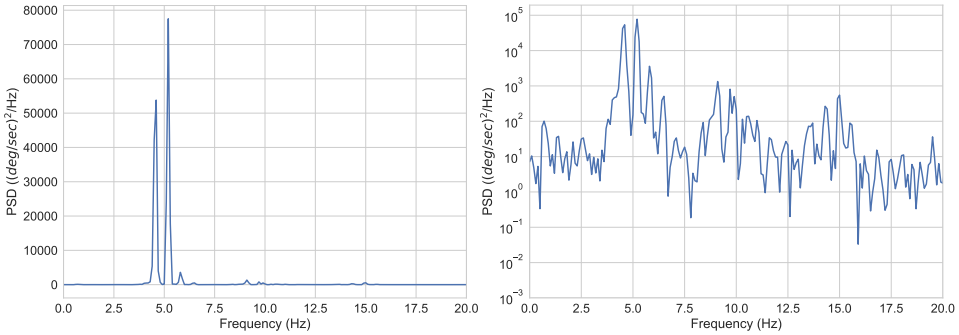

Figur 7.1: PSD with (a) linear and (b) logarithmic scaling of recording 1

7.2 Spectrogram

The spectrogram shows how the spectral density varies with time. Spectrograms are usually generated using short-time Fourier transform (STFT) [105]. To plot the spectrograms the *spectrogram* function from the Signal Processing Toolbox™[106] in MATLAB ®[107] is used, which uses STFT. For the plots, a Hanning window with a length of 20% of the sample data, and an overlap of 99% is used. In Figure 7.2 the spectrogram of recording 9 (Table 6.1) can be seen. From this figure, we can see that this tremor only has one natural frequency at approximately 5.3 Hz, and 2nd and 3rd harmonics at approximately 10.6 Hz and 15.8 Hz respectively. The two frequencies with the most power estimated by the BMWFLC are also plotted in the figure black and red dots for most and second most power respectively.

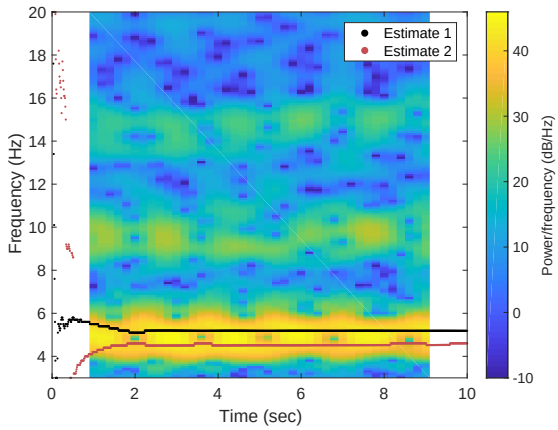

Figur 7.2: Spectrogram of recording 9 with Hanning window with length 20% of the sample data, and a overlap of 99%. Estimated frequencies by the BMWFLC are plotted with black and red markers for most and second most power respectively

Kapittel 8

Test rig setup

IIn collaboration with Estenstad [1] , we built a 1DOF test rig that simulates pathological hand tremor with flexion-extension movement.

The actuator used in the rig consisted of an I12T11 Compax3 Servo Drive [108] with a linear motor, type SMH 60601 [109], connected to a linear positioner. .The measurement setup consists of a microcontroller and two sensors, one for measuring the DVA, and one for the tremor on from the wrist. The microcontroller used was the Arduino Uno rev3 [110] microcontroller board based on the ATmega328P [111]. For the measuring of the tremor and the DVA two LSM6DS3 [112], which is an accelerometer and gyroscope sensor, was used. Accelerometers have traditionally been used for measuring tremor, but in [28] they argue that the gyroscope is a better choice compared to the accelerometer, because gyroscope sensors do not respond to changes in their orientation with respect to gravity, which the accelerometer does. Based on this we also chose to use a gyroscope to measure the tremor from our test rig; only activating the gyroscope in the LSM6DS3 sensor.

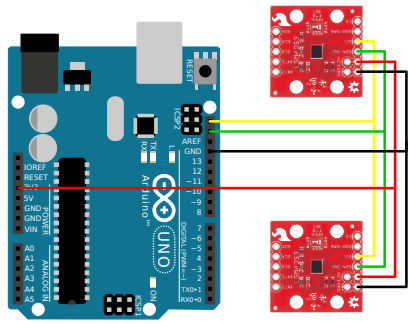

Figur 8.1: Wiring diagram for the Arduino Uno and the two LSM6DS3 sensors

My main responsibilities for the rig was the measurement setup, and the serial communication with the actuator to make it move. The controller software did not have the

functionality we needed, it was mostly for setting up the actuator, and the IO ports on the driver. We could not send a analog signal in, like i sinusoid and make the actuator follow it. The driver fortunately had the option to be controlled with serial communication from a computer. A separate windows application was developed with WPF C# [113] to handle the serial communication with the actuator, to send move commands and simulate the tremor. A screenshot from the application can be seen in Figure 8.3.

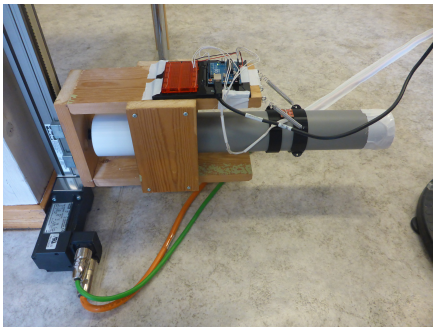

(a)

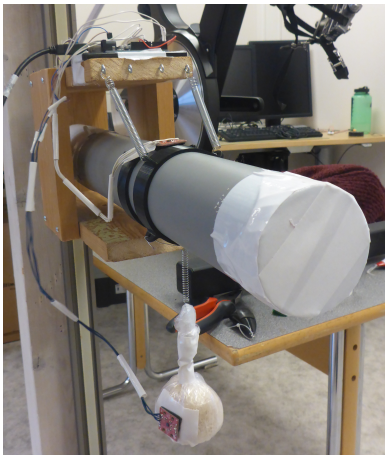

(b)

Figur 8.2: (a) Test rig (b) Test rig with DVA attached

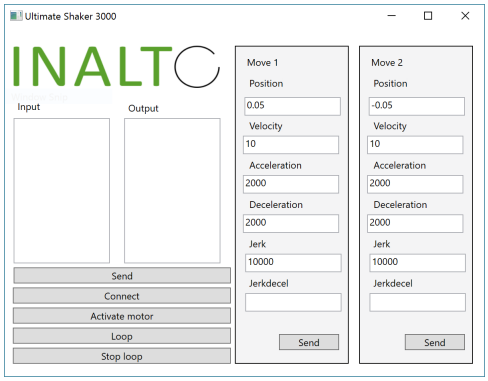

Figur 8.3: Application for controlling the actuator

The code for the application can be found at https://github.com/Bjarten/BMWFLC-filter. More details of the mechanical deigns of this the test rig can be found in Estenstad [1].

Kapittel 9

Results

Only the most interesting results from the real dataset are presented and discussed in section 9.3. The the remaining results can be found in Apendix B. The code used to implement ant test the filters can be found at https://github.com/Bjarten/BMWFLC-filter.

9.1 Simulated tremor data - Tuned filter

9.1.1 Initial filter settings

Here are the tuned filter parameters used for all the tests. Some tests will change some of the parameters to test their effect on the estimates. I do not claim that these are the optimal parameters for this filter, but as good as I have been able to tune them. The filter does need to be re-tuned if the sampling rate,f_s, is different than the one used here.

$\alpha = 0.67,\ \ T_p = 2,\ \ \kappa = 0.01,\ \ h = 0.0001,\ \ L = 200,\ \ \beta = 50,\ \ \eta = 0.4, f_{min} = 3\,Hz,\ \ f_{max} = 20\,Hz, \Delta\omega = 0.1,\ \ \Delta T = 0.01,\ \ \lambda = 0.2, f_s = 100\,Hz$

$ftt = 2$ for all signals besides simulated signal 6 where it is set to $ftt = 6$.

9.1.2 Simulated signal settings

Since $\Delta\omega = 0.1$, and the starting frequency is $f_{min} = 3Hz$, the starting frequencies in the BMWFLC will be 3.0 Hz, 3.1 Hz, 3.2 Hz, ..., 19.9 Hz, 20 Hz. To make it as hard as possible for the filter to estimate the frequencies, since this is a performance test, the values in the simulated signals end with x.x5, making the lie in between the frequencies in the filter. Only in simulated signal 2 does the frequencies end with x.x0 Hz, to see how it performs in the best case scenario. To simulate the tremor signal we use equation (6.1).

Simulated signal 1 - Rest tremor

$$A_1 = 128, \quad A_2 = 153, \quad A_3 = 0, \quad f_1 = 4.60, \quad f_2 = 5.20, \quad f_3 = 0, \quad \sigma_{n_k} = 10$$

Simulated signal 2 - Rest tremor

$$A_1 = 128, \quad A_2 = 153, \quad A_3 = 0, \quad f_1 = 4.65, \quad f_2 = 5.25, \quad f_3 = 0, \quad \sigma_{n_k} = 10$$

Simulated signal 3 - Action tremor

$$A_1 = 128, \quad A_2 = 153, \quad A_3 = 500, \quad f_1 = 4.65, \quad f_2 = 5.25, \quad f_3 = 0.6, \quad \sigma_{n_k} = 10$$

Simulated signal 4 - Varying amplitude

$$A_1(t) = \begin{cases} 300, & \text{for} \quad 0 \leq t < 5 \\ 500, & \text{for} \quad 5 \leq t < 20 \\ 20, & \text{for} \quad 20 \leq t < 30 \end{cases}, \quad A_2(t) = \begin{cases} 400, & \text{for} \quad 0 \leq t < 10 \\ 1000, & \text{for} \quad 10 \leq t < 20 \\ 10, & \text{for} \quad 20 \leq t < 30 \end{cases}, \quad A_3 = 0$$

$$f_1 = 4.65, \quad f_2 = 5.25, \quad f_3 = 0, \quad \sigma_{n_k} = 10$$

Simulated signal 5 - Varying frequency

$$f_1(t) = \begin{cases} 4.05, & \text{for} \quad 0 \leq t < 5 \\ 4.55, & \text{for} \quad 5 \leq t < 20 \\ 3.55, & \text{for} \quad 20 \leq t < 30 \end{cases}, \quad f_2(t) = \begin{cases} 5.05, & \text{for} \quad 0 \leq t < 10 \\ 5.55, & \text{for} \quad 10 \leq t < 20 \\ 5.05, & \text{for} \quad 20 \leq t < 30 \end{cases}, \quad f_3 = 0$$

$$A_1 = 300, \quad A_2 = 400, \quad A_3 = 0, \quad \sigma_{n_k} = 10$$

Simulated signal 6 - Multiple frequencies

$$\begin{aligned} m_k = & A_1 \sin(2\pi f_1 t) + A_2 \cos(2\pi f_2 t) + A_3 \sin(2\pi f_3 t) + \\ & A_4 \cos(2\pi f_4 t) + A_5 \sin(2\pi f_5 t) + A_6 \cos(2\pi f_6 t) + n_k \end{aligned} \tag{9.1}$$

$$A_1 = 100, \quad A_2 = 150, \quad A_3 = 200, \quad A_4 = 80, \quad A_5 = 310, \quad A_6 = 230,$$
$$f_1 = 4.05, \quad f_2 = 4.55, \quad f_3 = 5.85, \quad f_4 = 8.55, \quad f_5 = 10.25, \quad f_6 = 18.55, \quad \sigma_{n_k} = 10$$

9.1.3 Simulated signal 1 - Rest tremor

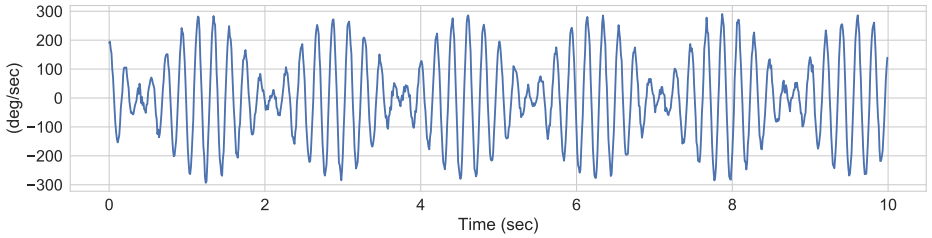

Figur 9.1: Simulated signal 2: Simulation of rest tremor

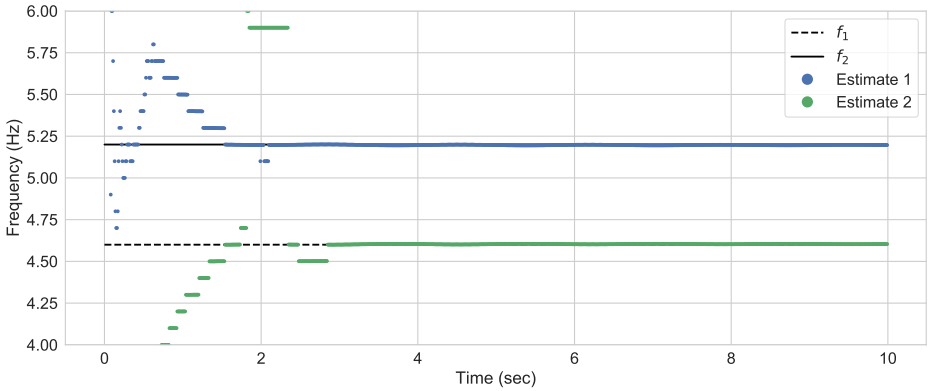

Figur 9.2: Estimated frequencies from simulated signal 1 using the BMWFLC filter

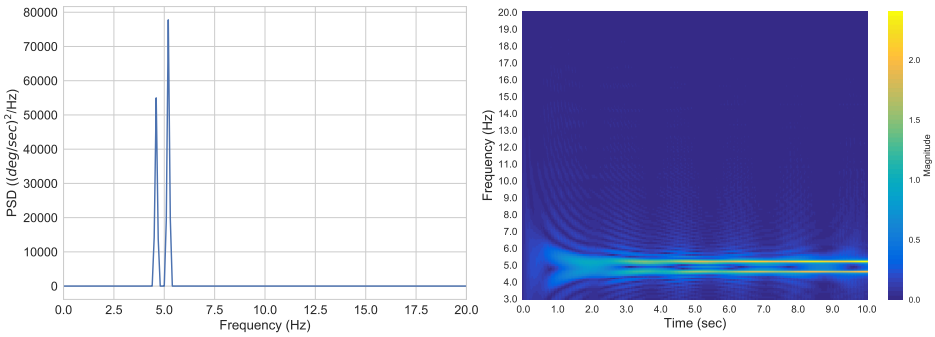

(a) **(b)**

Figur 9.3: (a) PSD with linear scaling. (b) Heatmap of magnitude spectrum from the BMWFLC filter. (Simulated signal 1)

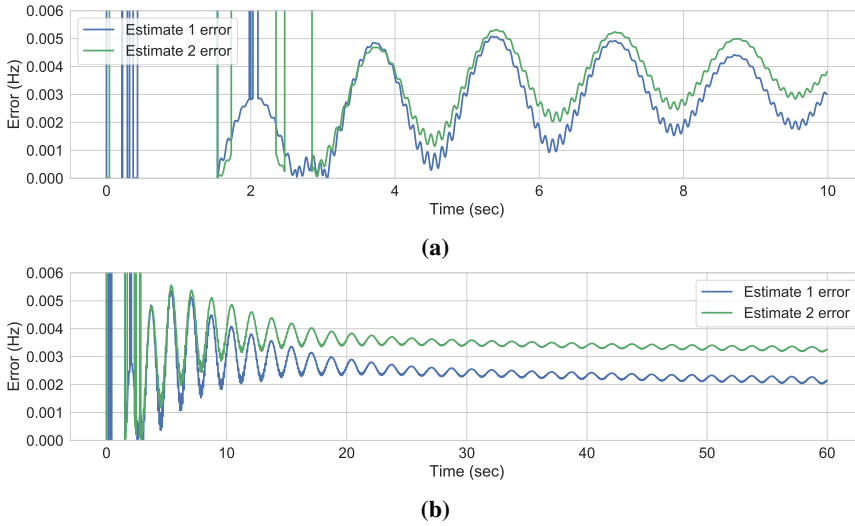

Figur 9.4: Error between real frequency and estimated frequency. (Simulated signal 1)

This simulation is done to test the BMWFLC filter performance on a rest tremor with two frequencies close in the frequency domain. Since this is a simulated signal we know what frequencies the signal is modulated by, $f_1 = 4.60$ and $f_2 = 5.20$, and the amplitudes, $A_1 = 128$ and $A_2 = 153$. This is a best-case scenario for the frequencies since they match perfectly with the frequency division in the filter. In Figure 9.2 the black dotted and solid lines are frequencies f_1 and f_2 respectively. In this plot, estimate 1 is the frequency with the largest amplitude, and estimate 2 second largest. We see that estimate 1 correctly classifies f_2 to have the highest amplitude after about 0.5 seconds and then starts to converge toward the frequency and stabilizes after 2.1 seconds. f_1 is also classified correctly by estimate 2 as having the second largest amplitude at about 0.5 seconds. The frequency estimate does a large jump at 1.9 seconds and settles down and is stable after 2.85 seconds. In Figure 9.3b we see how the magnitude spectra from the BMWFLC filter is adjusting with the signal. The peaks are getting thinner as the time goes by, meaning that the confidence in the estimated frequency is getting higher, the top of these two peaks are the estimated frequencies returned by the filter. From Figure 9.4a we can see the error from the estimates, and both have an error below 0.006 Hz when they stabilize, and in Figure 9.4b we observe that both estimates are slowly converging towards 0, but estimate 1 is converging faster than estimate 2. The reason for this difference is because the two WFLC that are estimating the frequencies uses the LMS algorithms to minimize the MSE between the estimated and real signal (5.54). So the WFLC that will minimize the error the most is the one that is most similar to the original signal. If the learning rate is set to high, both estimates will converge to f_2, both wanting to minimize the error the most.

9.1.4 Simulated signal 2 - Rest tremor

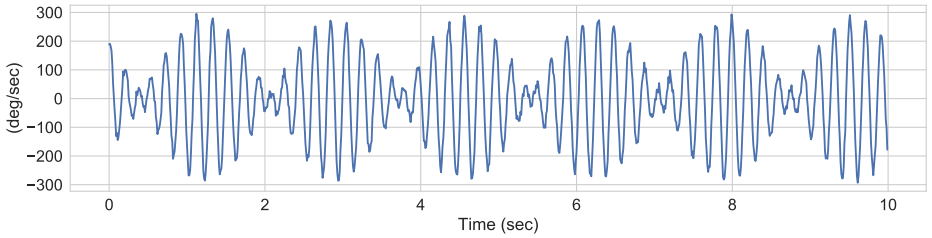

Figur 9.5: Simulated signal 2: Simulation of rest tremor

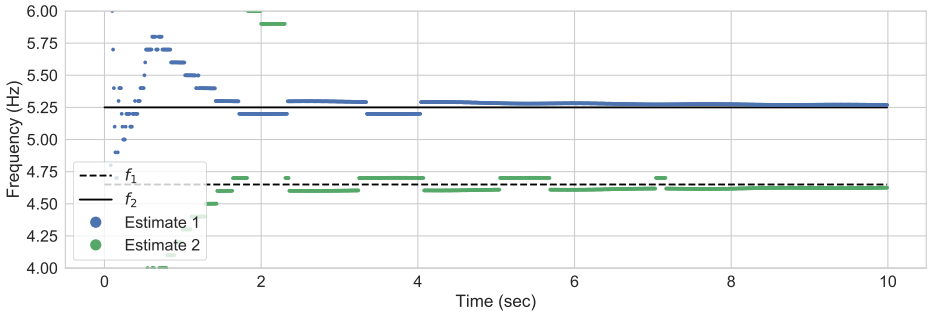

Figur 9.6: Estimated frequencies from simulated signal 2 using the BMWFLC filter

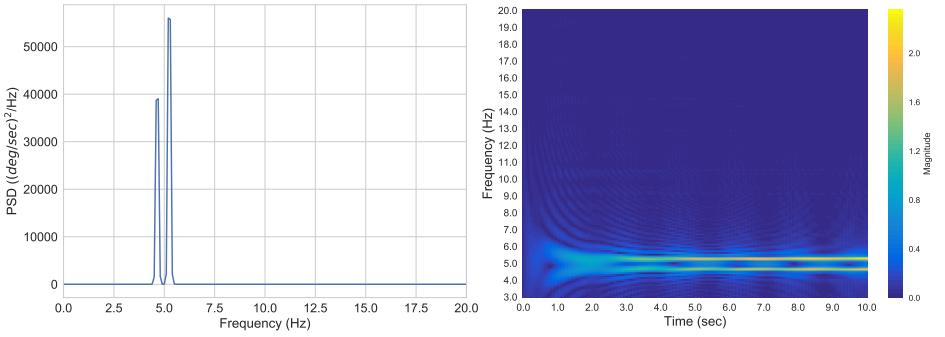

(a) **(b)**

Figur 9.7: (a) PSD with linear scaling. (b) Heatmap of magnitude spectrum from the BMWFLC filter. (Simulated signal 2)

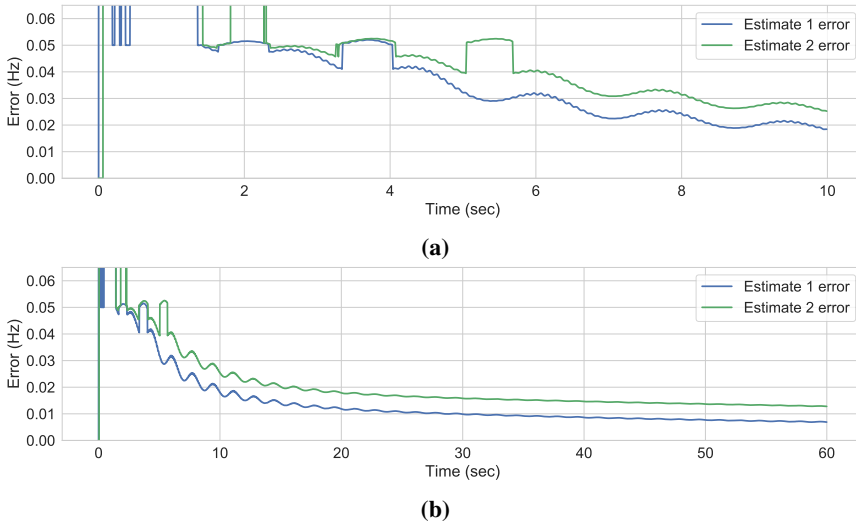

Figur 9.8: Error between real frequency and estimated frequency. (Simulated signal 2)

This signal is the same as signal 1 except for the frequencies that are $f_1 = 4.65$ and 5.25 Hz, making them a worst case scenario for the filter. If we look at estimation plots of signal 1 (Figure 9.2) and signal 2 (Figure 9.6), we see that they look similar, except that the estimations are oscillating around the real value in the signal, taking longer to settle down. This is because the filter can't decide which value is closer to the real value of the signal. If we look at estimate 2 in Figure 9.6, it is trying to reach 4.65 Hz, but the two closest frequencies in the filter are 4.6 and 4.7 Hz. So the two estimates start fightingeach other, both wanting to be the most accurate. In Figure 9.9 we see how this look when we plot the magnitude spectrum for the filter at 4 and 4.5 seconds. The red marker indicates the peak magnitudes, and only their respective WFLC have $\mu_{rk} > 0$, giving them the ability to adapt to the signal. The estimation error for frequency 1 after 10 and 60 seconds are 0.03 and 0.015 Hz respectively, and for frequency 2, 0.02 and 0.0065 Hz.

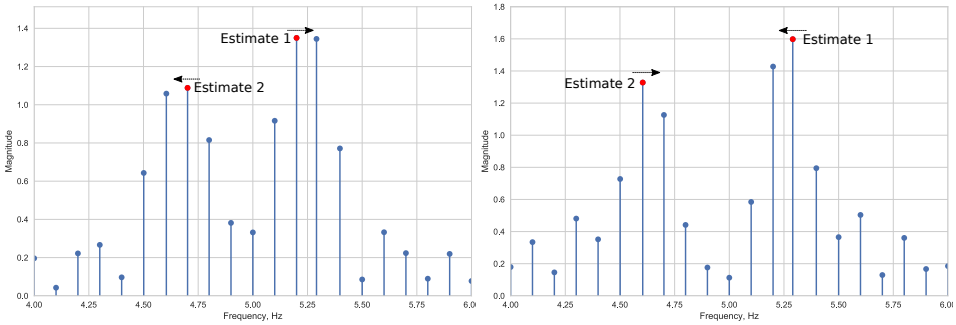

Figur 9.9: Magnitude spectrum at (a) 4 seconds and (b) 4.5 seconds

9.1.5 Simulated signal 3 - Action tremor

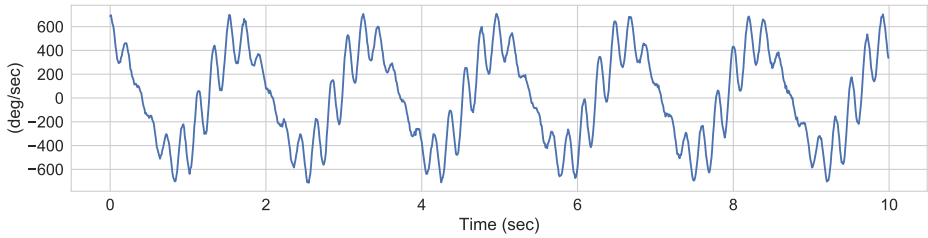

Figur 9.10: Simulated signal 3: Simulation of action tremor

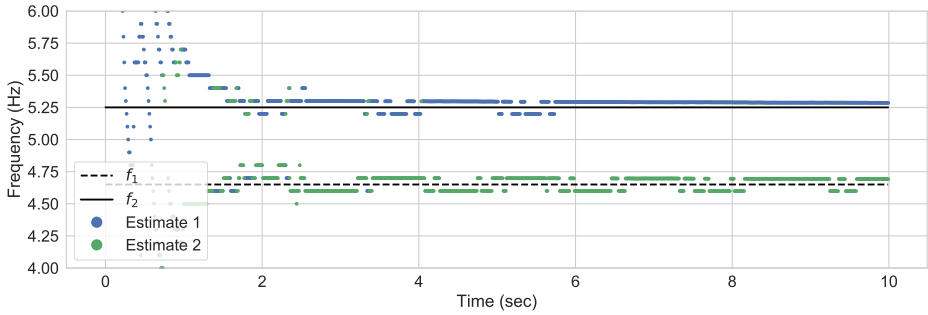

Figur 9.11: Estimated frequencies from simulated signal 3 using the BMWFLC filter

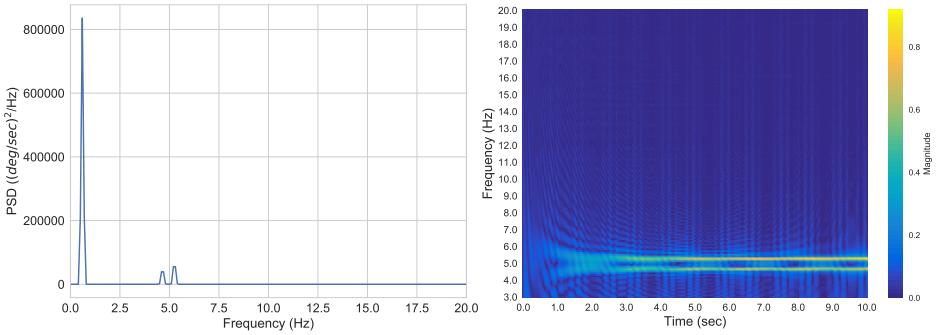

(a) **(b)**

Figur 9.12: (a) PSD with linear scaling. (b) Heatmap of magnitude spectrum from the BMWFLC filter. (Simulated signal 3)

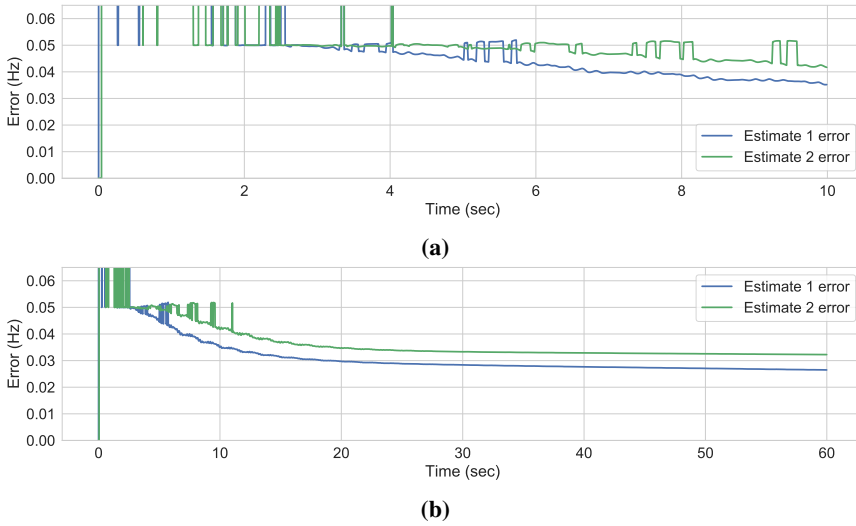

Figur 9.13: Error between real frequency and estimated frequency. (Simulated signal 3)

This signal is the same as signal 2, but with voluntary movement m_{k-v} with $A_3 = 500$ and $f_3 = 0.6$ Hz. Comparing the estimation plots of simulated signal 2 (Figure 9.6) and simulated signal 3 (Figure 9.11), we see that the estimation is a bit more scattered for signal 3 before the 2-second mark, and after 2 seconds the estimates oscillating quite a bit more around the true frequencies. From the error plots in Figure 9.13b and Figure 9.8b we see that estimate 1 for signal 3 has a much slower convergence rate than for signal 2, and after 60 seconds it is under 0.0035 Hz for signal 3 and for signal 2 its 0.035 Hz. The reason for this is the adaptive learning rate which scale the learning rates μ_k and μ_{rk} to the peak amplitude in the input signal, Equations (5.55) and (5.56). If the adaptive learning rate were turned off, the filter would become unstable because of the high values in the input signal s_k caused by the voluntary motion. with constant learning rates are done in section 9.2.2 and section 9.2.2. The filter does an excellent job of filtering out the voluntary motion.

9.1.6 Simulated signal 4 - Varying amplitude

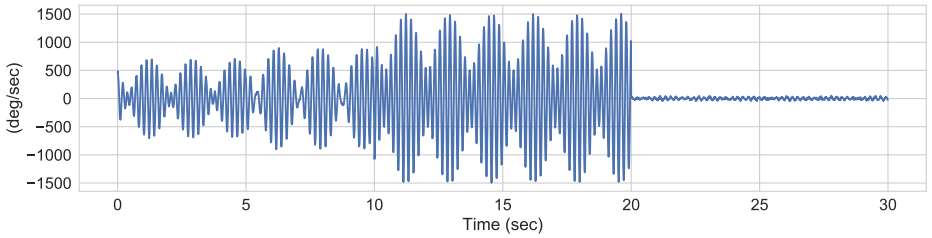

Figur 9.14: Simulated signal 4: Simulation of tremor with varying amplitude

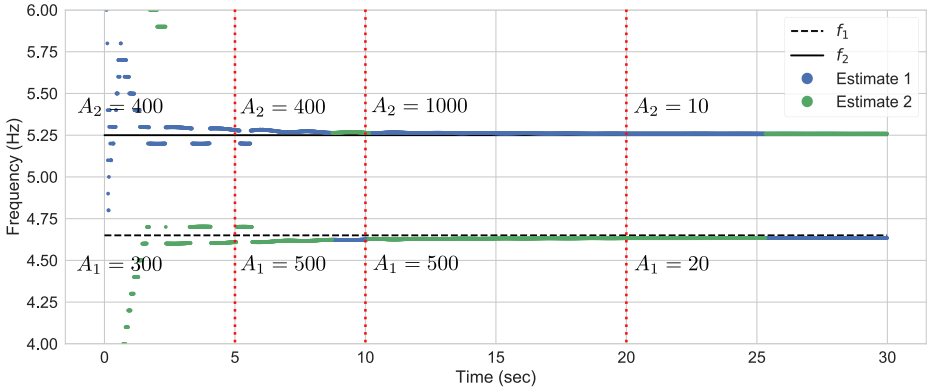

Figur 9.15: Estimated frequencies from simulated signal 4 using the BMWFLC filter

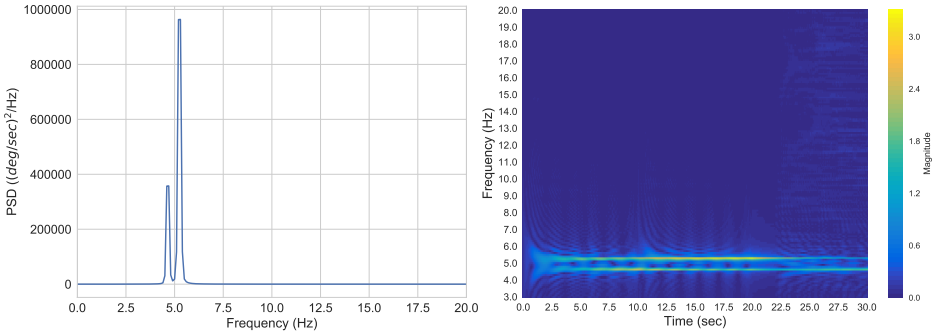

(a) **(b)**

Figur 9.16: (a) PSD with linear scaling. (b) Heatmap of magnitude spectrum from the BMWFLC filter. (Simulated signal 4)

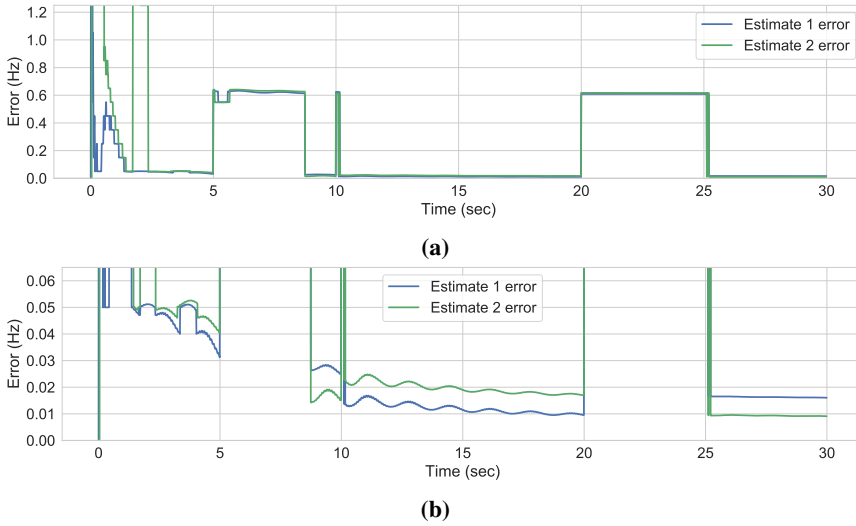

Figur 9.17: Error between real frequency and estimated frequency. (Simulated signal 4)

This is a test to see if the filter can correctly estimate which of the two frequencies have the highest amplitude when the amplitude make sudden changes. After the 5 second mark, the filter correctly switches the estimates at 8.65 seconds, 3.65 seconds after the amplitude step. On the second step at the 10-second mark, the amplitudes correctly switch places at 10.17 seconds, 0.17 seconds after the step. The reason for this fast response is because both the estimates had similar magnitudes in the magnitude spectrum since a switch just took place and the filter hadn't had much time to adapt to the new values. At the 20 second mark, the filter has had time to adapted to the new values, the step is quite big, and the new amplitudes lie close to each other. The estimates correctly switch at 25.25 seconds, 5.25 seconds after the step. There is also white noise added to the signal that may affect the estimation when the amplitudes are so low.

9.1.7 Simulated signal 5 - Varying frequency

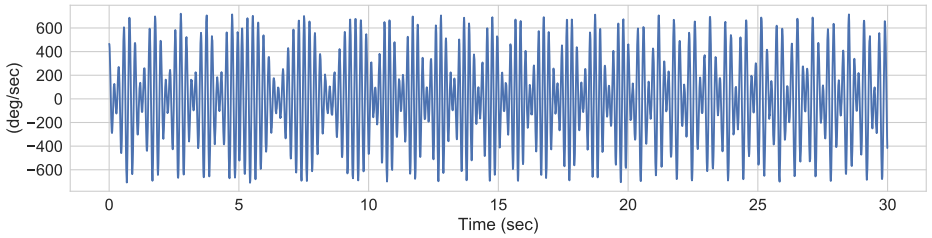

Figur 9.18: Simulated signal 5: Simulation of tremor with varying frequencies

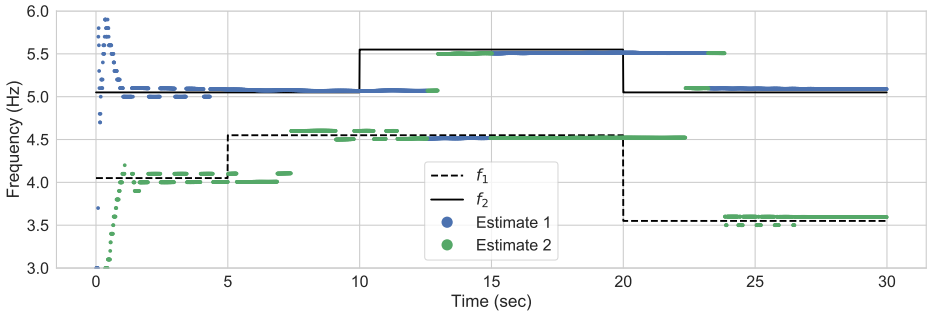

Figur 9.19: Estimated frequencies from simulated signal 5 using the BMWFLC filter

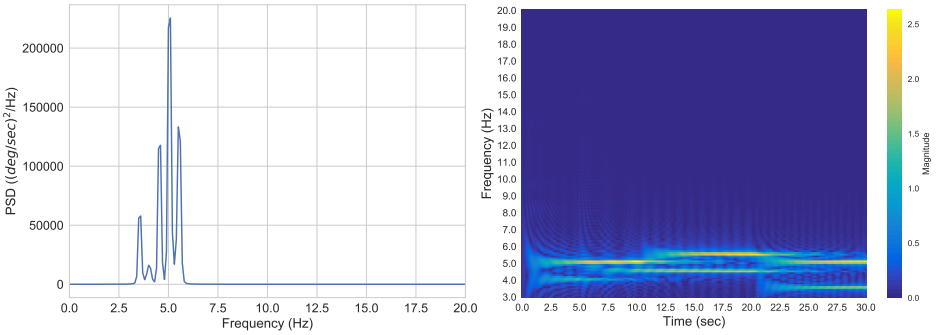

(a) **(b)**

Figur 9.20: (a) PSD with linear scaling. (b) Heatmap of magnitude spectrum from the BMWFLC filter. (Simulated signal 5)

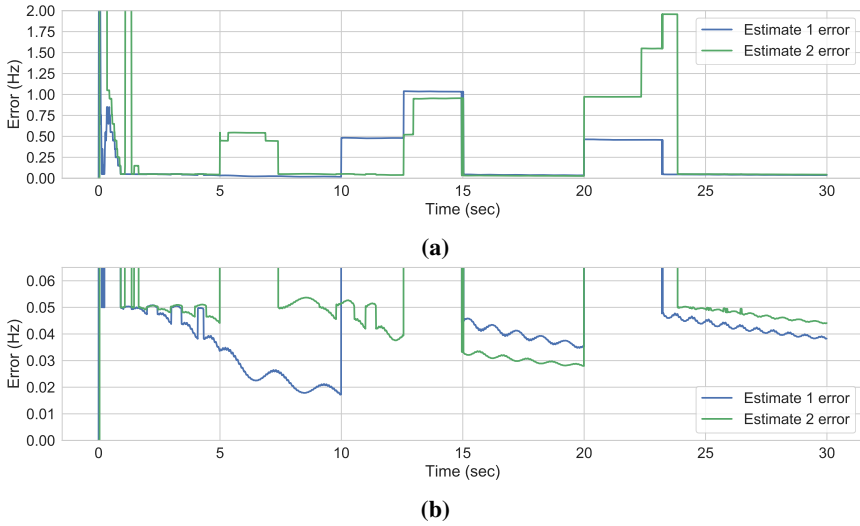

Figur 9.21: Error between real frequency and estimated frequency. (Simulated signal 5)

From Figure 9.19 we see the first frequency step at 5 seconds is when f_1 goes from 4.05 Hz to 4.55 Hz. The estimate 2 correctly follows the real frequency at 7.4 seconds, taking 2.4 seconds to respond to the change. The next step is at 10 seconds when f_2 goes from 5.05 Hz to 5.55 Hz, and the estimate follows at 13.06 seconds, 3.06 seconds after the step. At this point, f_1 is estimated to have the largest amplitude, which is wrong, but at 14.95 seconds this is corrected. The reason for the long response time for the second step is that the filter had a longer time to adapt to f_2 than f_1, and has a stronger memory of this signal. The next step is at 20 seconds where both frequencies change, f_1 from 4.55 to 3.55 Hz and f_2 from 5.55 to 5.05 Hz. At 22.35 seconds, estimate 1 is still at the old frequency of f_2 and estimate 2 is estimating the new frequency of f_2 after the step, the new frequency of f_1 is then found by estimate 2 at 23.84 seconds.

From these results we see that when the filter has had some time to adapt to a signal, it takes longer time for it to change when there is a sudden change in frequency.

9.1.8 Simulated signal 6 - Multiple frequencies

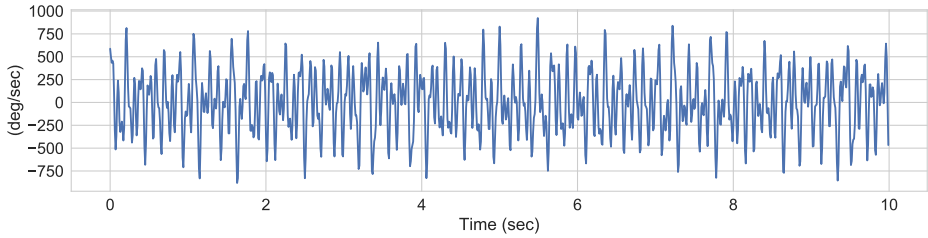

Figur 9.22: Simulated signal 6: Simulation of tremor with 6 frequencies

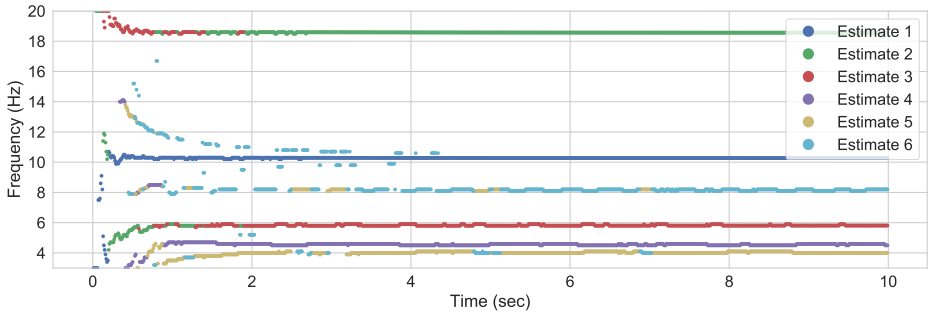

Figur 9.23: Estimated frequencies from simulated signal 6 using the BMWFLC filter

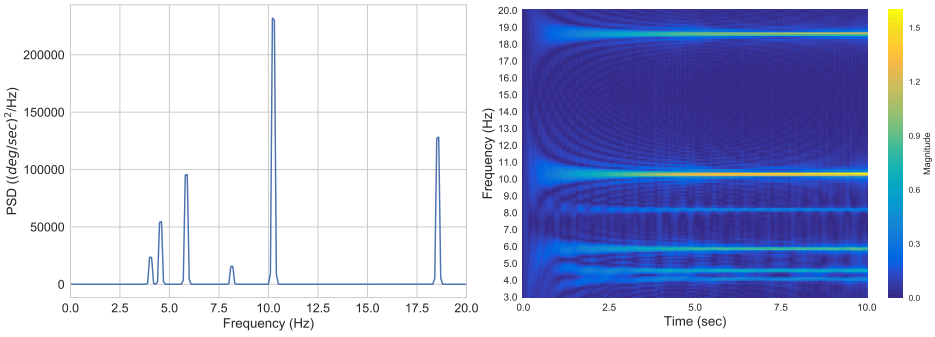

(a) **(b)**

Figur 9.24: (a) PSD with linear scaling. (b) Heatmap of magnitude spectrum from the BMWFLC filter. (Simulated signal 6)

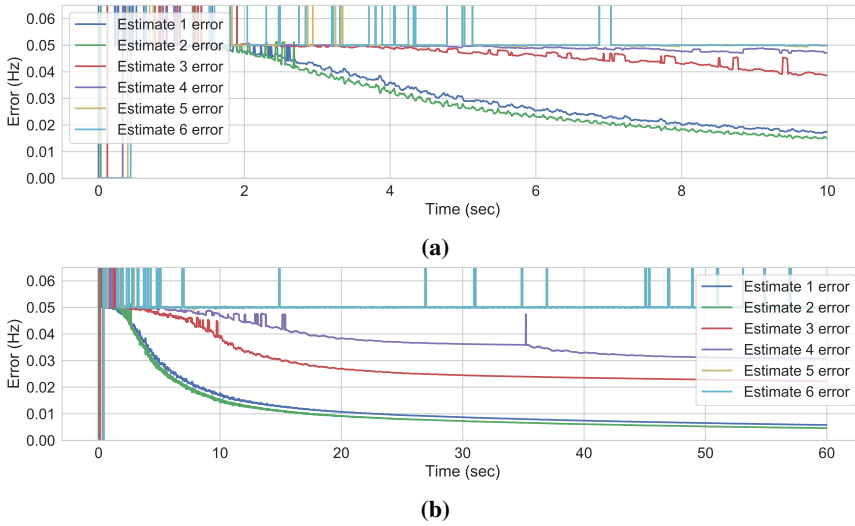

Figur 9.25: Error between real frequency and estimated frequency. (Simulated signal 6)

For this test, a signal with six different frequencies and amplitudes is sent into the filter. The filter handles this well as seen in Figure 9.23, after 2 seconds most of the frequencies and amplitudes are correctly estimated. It has some problem deciding which one of $f_1 = 4.05$ Hz, $A_1 = 80$,and $f_4 = 8.55$, $A_4 = 80$, has the smallest amplitude, estimate 5 and 6. And occasionally switches them, but this happens rarely. From the error plots in Figure 9.25, we see that the frequencies with the largest amplitudes minimize the error fastest, this is the same effect that was observed and discussed in section 9.1.3. These results show that the filter has no problems detecting and estimating multiple frequencies in a signal, and their amplitude with respect to each other. The filter not designed to estimate the amplitude of the signal, but using the magnitude spectrum (Figure 9.24b) the power of each frequency can be compared against each other. E.g. how much higher is the amplitude in estimate 1 compared to estimate 2. This is not implemented in the algorithm now, but shouldn't be hard to add if this feature is desired.

9.2 Testing different filter settings

9.2.1 Simulated signal 2 with $\mu_k = 0$

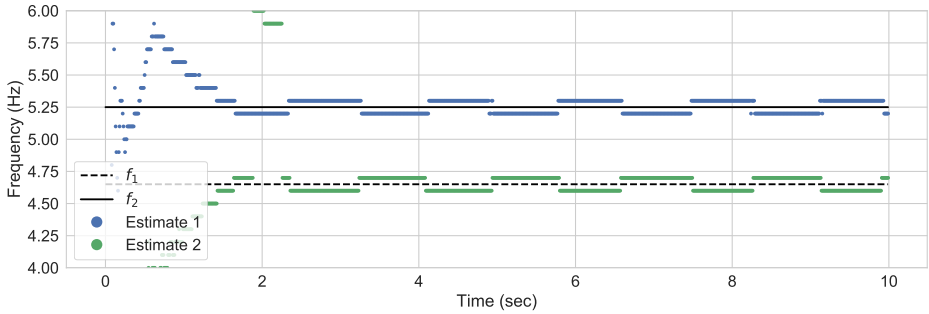

Figur 9.26: Estimated frequencies from simulated signal 2 using the BMWFLC filter with $\mu_k = 0$

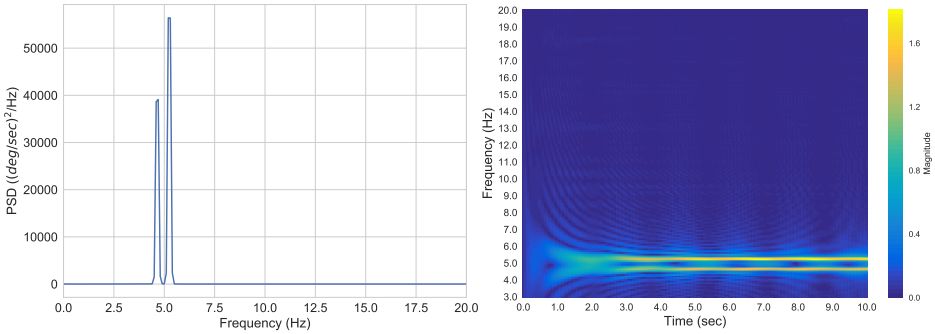

(a) **(b)**

Figur 9.27: (a) PSD with linear scaling. (b) Heatmap of magnitude spectrum from the BMWFLC filter. (Simulated signal 2). With $\mu_k = 0$

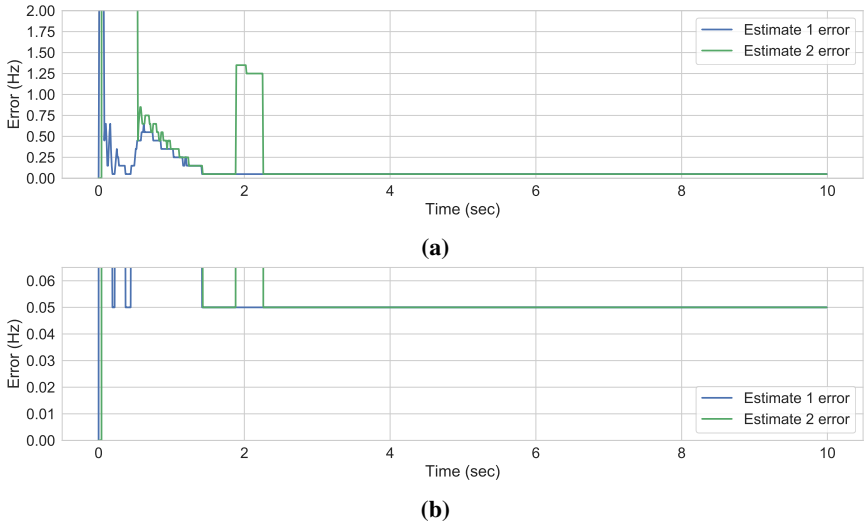

Figur 9.28: Error between real frequency and estimated frequency. (Simulated signal 2)

By setting all the learning rates in $\boldsymbol{\mu}_k$ (5.42) to 0, the BMWFLC loses its ability to adapt the frequencies $\boldsymbol{\omega}_k$ (5.43) to the signal. From the error plots in Figure 9.28 we see that the error stops at 0.05 Hz and doesn't go below this. Just what we expected since the filter can't minimize the error for the frequencies when the learning rate is 0. In Figure 9.26 we see that the estimates are oscillating around the true frequencies, both of the estimates are an equal distance from the real frequency, so the filter can't decide which is best. This was not a problem when $\mu_{rk} > 0$, which was the case in section 9.1.4.

9.2.2 Simulated signal 4 with μ_k and $\boldsymbol{\mu}_k$ constant

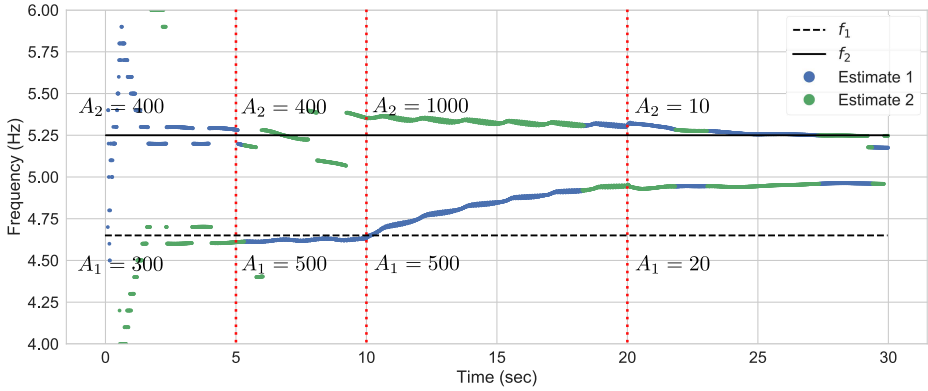

Figur 9.29: Estimated frequencies from simulated signal 4 using the BMWFLC filter with μ_k and $\boldsymbol{\mu}_k$ constant

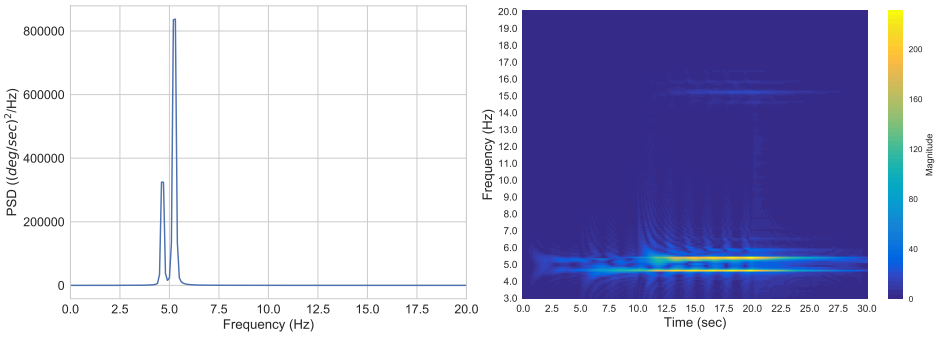

(a) **(b)**

Figur 9.30: (a) PSD with linear scaling. (b) Heatmap of magnitude spectrum from the BMWFLC filter. (Simulated signal 4). With μ_k and $\boldsymbol{\mu}_k$ constant

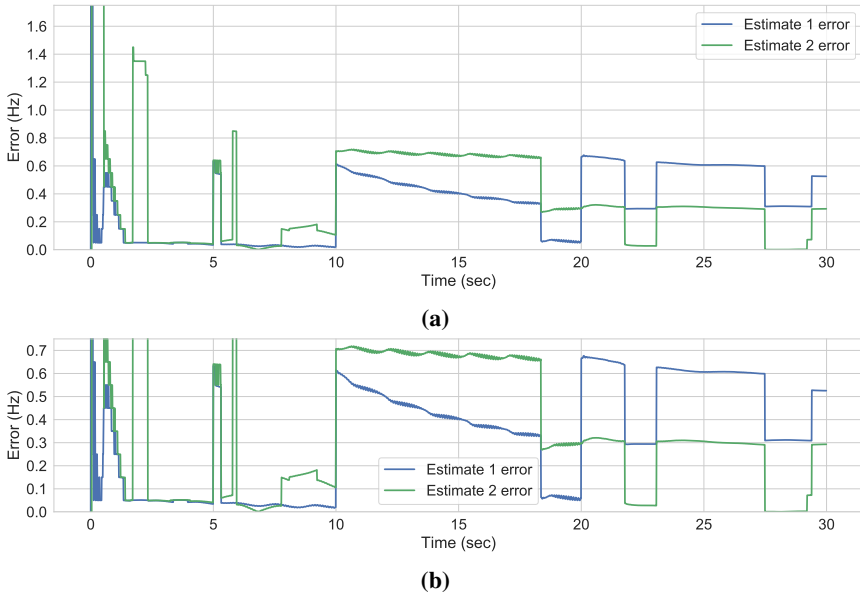

Figur 9.31: Error between real frequency and estimated frequency. (Simulated signal 4)

The learning rates are set to $\mu_k = 0.001$ and $\boldsymbol{\mu}_k = 0.00000001$, turning off the adaptive learning rate (Adaptive learning rate in section 5.2.2). From Figure 9.29 we see that before the first step in amplitude at the 5-second mark, the estimates behave similarly to what they did in Figure 9.15 when the adaptive learning rate was on. After the first amplitude step when A_1 goes from 300 to 500, we see that both estimates start to converge towards f_1. The reason for this is that the error between ε_k (5.49) gets larger because of the increased size of s_k , which in return affects the LMS term in Equation (5.51) and (5.54), making the estimated gradient descend the MSE performance surface faster. This knocks the estimate 2 out of its local minima, and it starts towards the global minima which are f_1 where the amplitude is largest. The same happens at the 10-second mark when f_2 has the largest amplitude, and both estimates start converging towards f_1. The adaptive learning rate has been implemented to keep the estimates stable no matter what amplitude in the input signal is, and the effect when this is turned on can be seen in section 9.1.6, and the other test scenarios, since this is the only test where it's turned off. This is an important feature for the filter, since pathological tremor can vary in amplitude, and voluntary motion can add large amplitudes to the input signal. The filter will also adapt when the amplitude in the input gets smaller; this is especially important since this filter is designed for tremor suppression applications, making it sensitive even though the tremor is being suppressed.

9.3 Real tremor data - Tuned filter

9.3.1 Recording 1 - Rest tremor

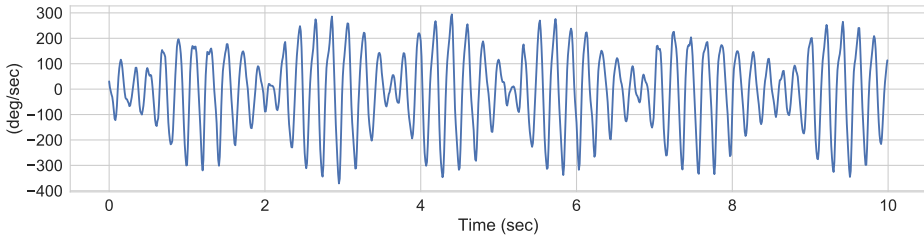

Figur 9.32: Recording 1 from session 1. Orientation: P+/S. Placement: RH

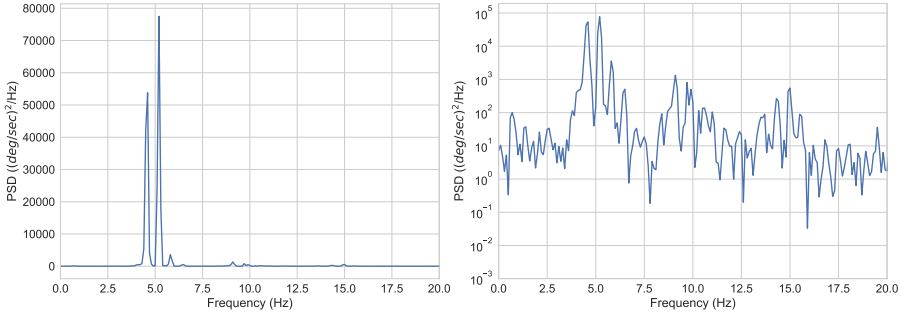

(a) **(b)**

Figur 9.33: PSD with (a) linear and (b) logarithmic scaling. (Recording 1)

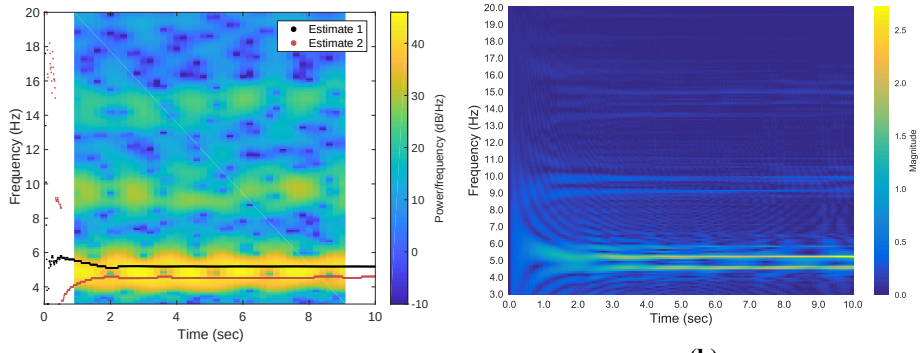

(a) **(b)**

Figur 9.34: (a) Spectrogram of signal with estimated frequencies and (b) Heatmap of the magnitude spectrum from the BMWFLC filter. (Recording 1)

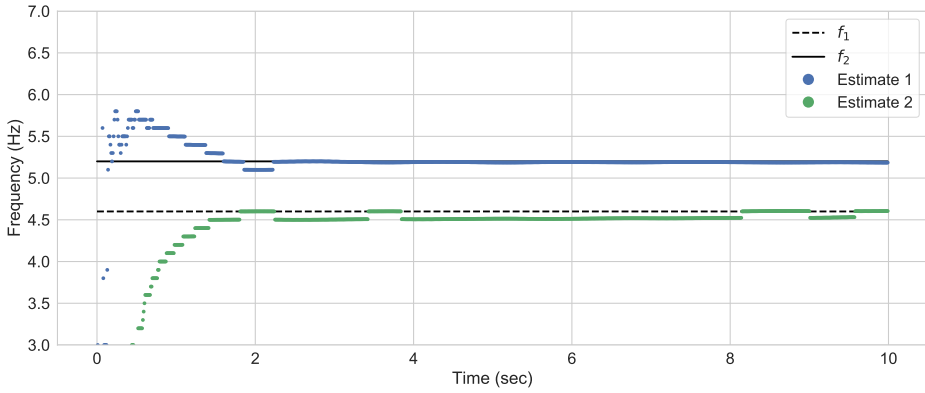

Figur 9.35: Estimated frequencies from recording 1. f_1 and f_2 are also estimates in this figure

In Figure 9.35 $f_1 = 5.2$ Hz and $f_2 = 4.6$ Hz are the peaks from the PSD plots in Figure 9.33, these also estimate the frequencies, since this is a real signal, we cant know what the actual frequency components are. We also see in Figure 9.33b that the peak at 5.2 Hz is sharper than the one at 4.6 Hz, meaning its a better estimate. The one at 4.6 Hz is flatter and is rising on the 4.5 Hz as well. This is reflected well in the estimates in Figure 9.35, where estimate 1 is stable at 5.2 Hz and estimate 2 switches between 4.6 and 4.5 Hz. These are an excellent result, and performance seems to be equal to the simulations of the signal in section 9.1.3 and 9.1.3. It even seems to perform better as the jump in the frequency in estimate 2 after 2 seconds that was present in both simulations are now gone. Error plots will not be plotted for the real signals since we don't know the real value of the frequencies in the signal. Only for this recording will there be a plot like in Figure 9.35, since this was a particularly stable tremor, for the rest, the accuracy of the estimation should be read out of the spectrogram plot Figure 9.34a, and from the PSD plots 9.33.

9.3.2 Recording 6 - Rest tremor

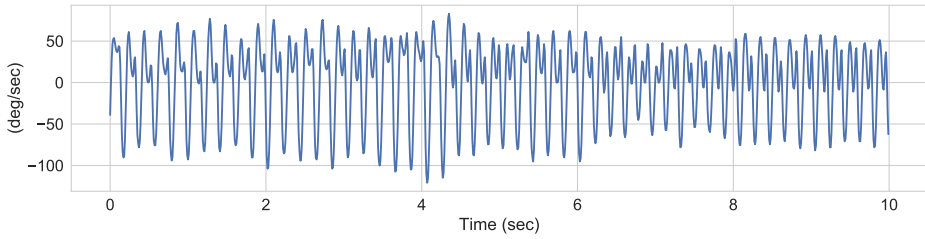

Figur 9.36: Recording 6 from session 4. Orientation: P/S+. Placement: LH

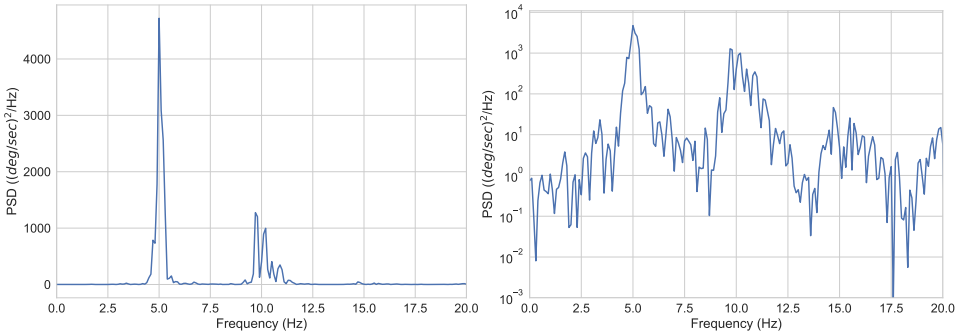

(a) **(b)**

Figur 9.37: PSD with (a) linear and (b) logarithmic scaling. (Recording 6)

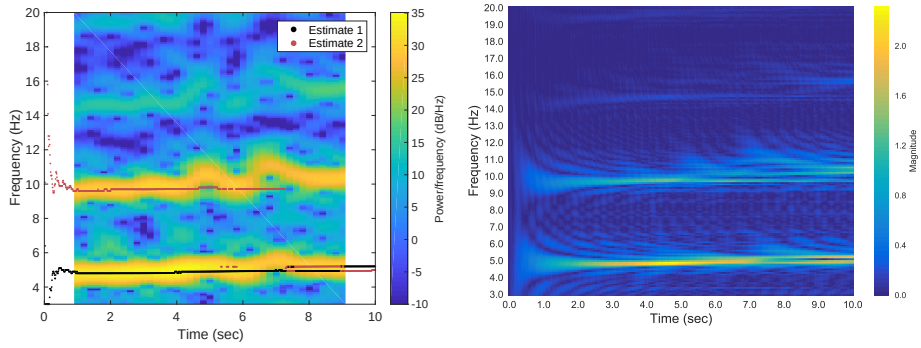

(a) **(b)**

Figur 9.38: (a) Spectrogram of signal with estimated frequencies and (b) Heatmap of the magnitude spectrum from the BMWFLC filter. (Recording 6)

In this tremor, we can see that there is one fundamental frequency around 5 Hz and a strong 2nd harmonic that drifts around 10 Hz. From the spectrogram in Figure 9.38a we see that estimate two loses the 2nd harmonics at 7.3 seconds after the tremor does a sudden frequency jump. If we look at the heat map of the magnitude spectrum in Figure 9.38b the magnitudes split into two peaks after the frequency jump that took place around 7 seconds, and both frequencies are estimated to be here. The magnitude spectrum will take some time to adapt to the signal after the sudden jump. A fix to this problem could be to divide the BMWFLC filter into sections the same way as the E-BMFLC filter presented is section 5.1.5, can be used to extract the voluntary, m_{k-v}, and involuntary signal, m_{k-v}, from the total estimate of the signal m_k. So instead of extracting the voluntary and involuntary motion, we could extract the signal containing fundamental frequency, which would lie in the range 3-7 Hz for PD, and the signal containing the harmonics in the range 7-20 Hz. Now, these two could run as separate BMWFLC filters without adding much computational cost. This has not been tested as the idea came late in the process after inspecting the results from the filter on the real data, this could be implemented in future work and should be an elegant solution to the problem.

For now, we can try to get an estimate of the 2nd without losing it by setting $ftt = 3$ and see if it helps.

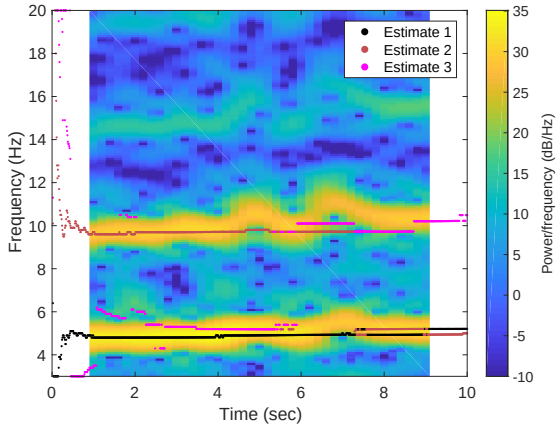

Figur 9.39: Spectrogram of signal 6 with $ftt = 3$

This worked, now the 2nd frequency was tracked all the way, but there still lacks some logic to deal with this properly, and should be looked further into in the future.

9.3.3 Recording 12 - Postural tremor

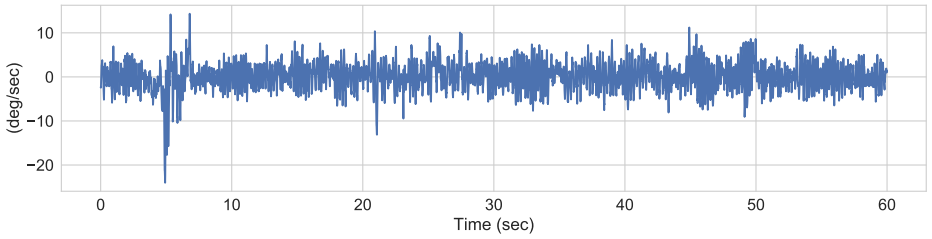

Figur 9.40: Recording 12 from session 6. Orientation: F+/E. Placement: RH

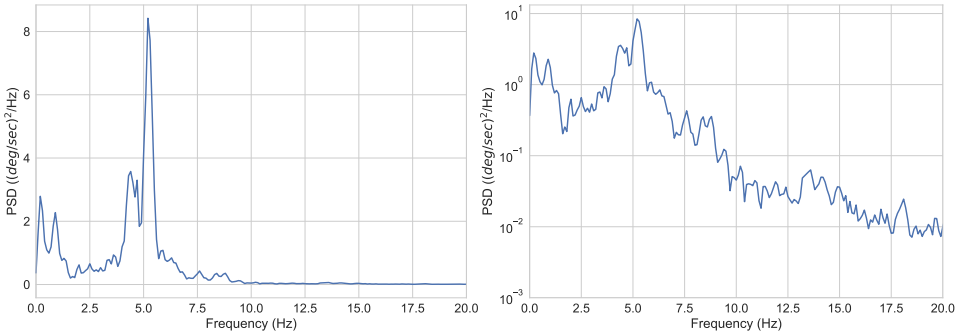

(a) **(b)**

Figur 9.41: PSD with (a) linear and (b) logarithmic scaling. (Recording 12)

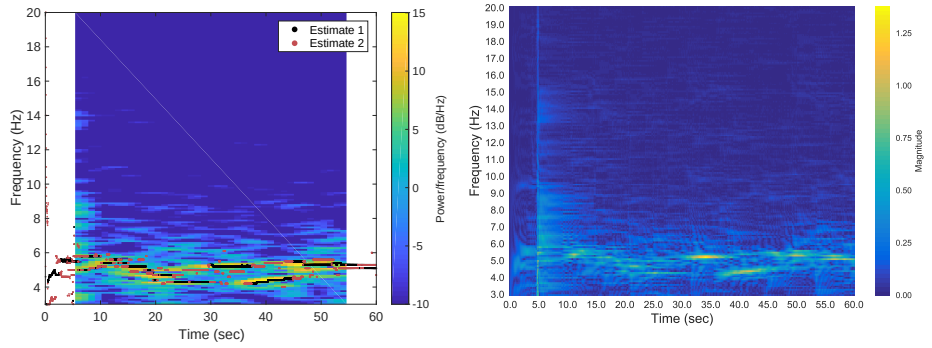

(a) **(b)**

Figur 9.42: (a) Spectrogram of signal with estimated frequencies and (b) Heatmap of the magnitude spectrum from the BMWFLC filter. (Recording 12)

This is a recording of a postural tremor, and from the spectrogram 9.42b we see that it's highly labile.

Overall the estimation seems too do quite well, and we can clearly see the resemblance between the spectrogram and the heatmap of the magnitude spectrum in Figure 9.42.

9.3.4 Recording 15 - Action tremor

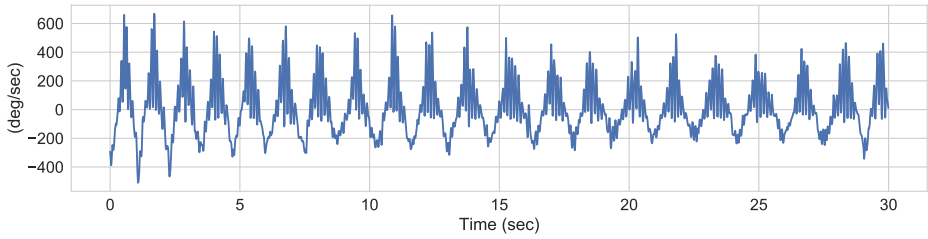

Figur 9.43: Recording 15 from session 7. Orientation: P+/S. Placement: LH

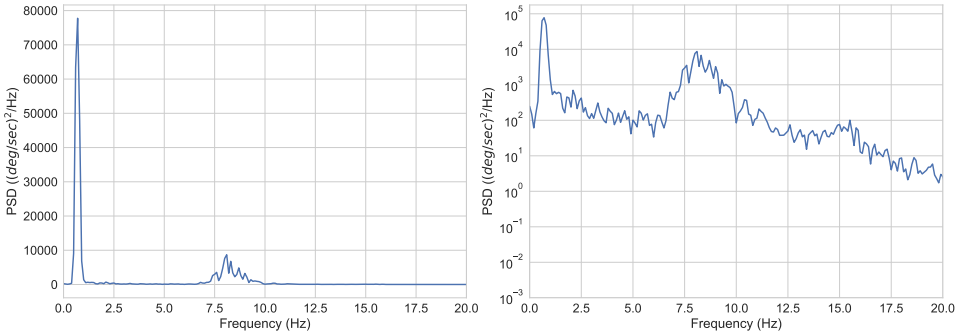

(a) **(b)**

Figur 9.44: PSD with (a) linear and (b) logarithmic scaling. (Recording 15)

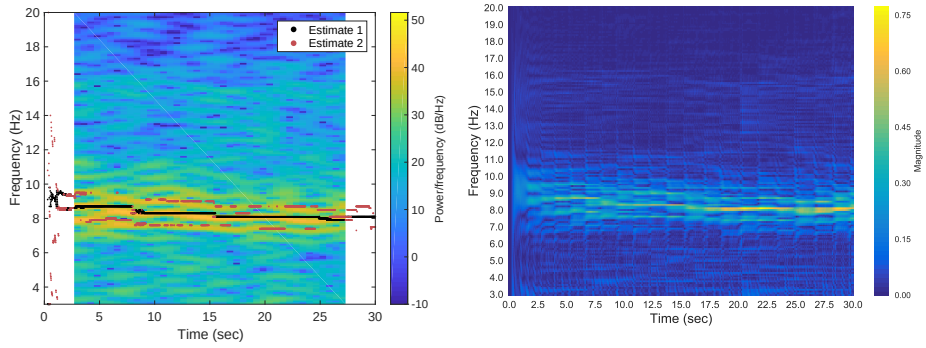

(a) **(b)**

Figur 9.45: (a) Spectrogram of signal with estimated frequencies and (b) Heatmap of the magnitude spectrum from the BMWFLC filter. (Recording 15)

From the spectrogram in Figure 9.45a we see that the tremor starts at about 8.7 Hz and then slowly moves towards 8.1 Hz. Estimate 1 tracks the main frequency nicely as it is descending. There seems to be multiple frequencies percent around the main one, and estimates 2 tries its best too lock onto one of them, but they are rather unstable. The voluntary motion is filtered out, but it ads some noise to the magnitude spectrum Figure 9.45b, as can be seen by vertical ripples going through the spectrum.

The overall performance of the filter on the simulated data was really good.

9.4 Real-time test with DVA system

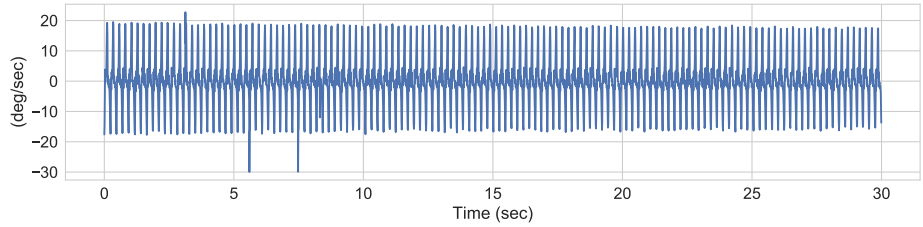

Figur 9.46: Recording from test rig 30 seconds

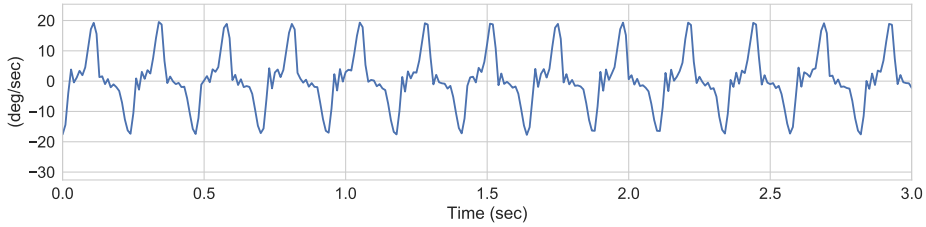

Figur 9.47: Recording from test rig zoomed in

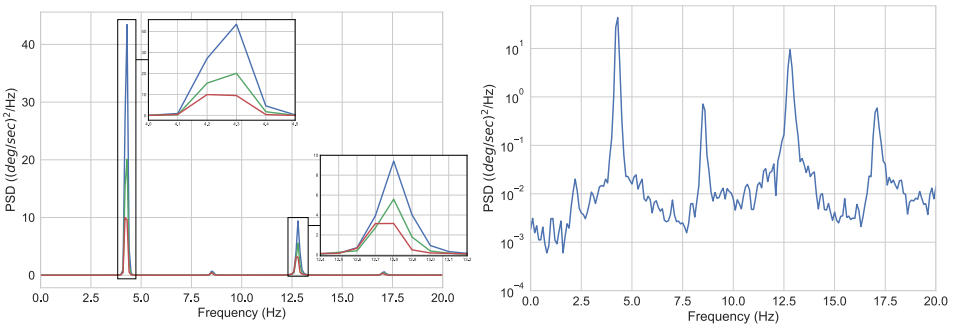

(a) **(b)**

Figur 9.48: (a) Linear PSD of simulated tremor from test rig. Plots of the arm with nothing, weight and DVA attached; blue, green and red line repectivly. (b) Logarithmic plot of tremor with nothing attached

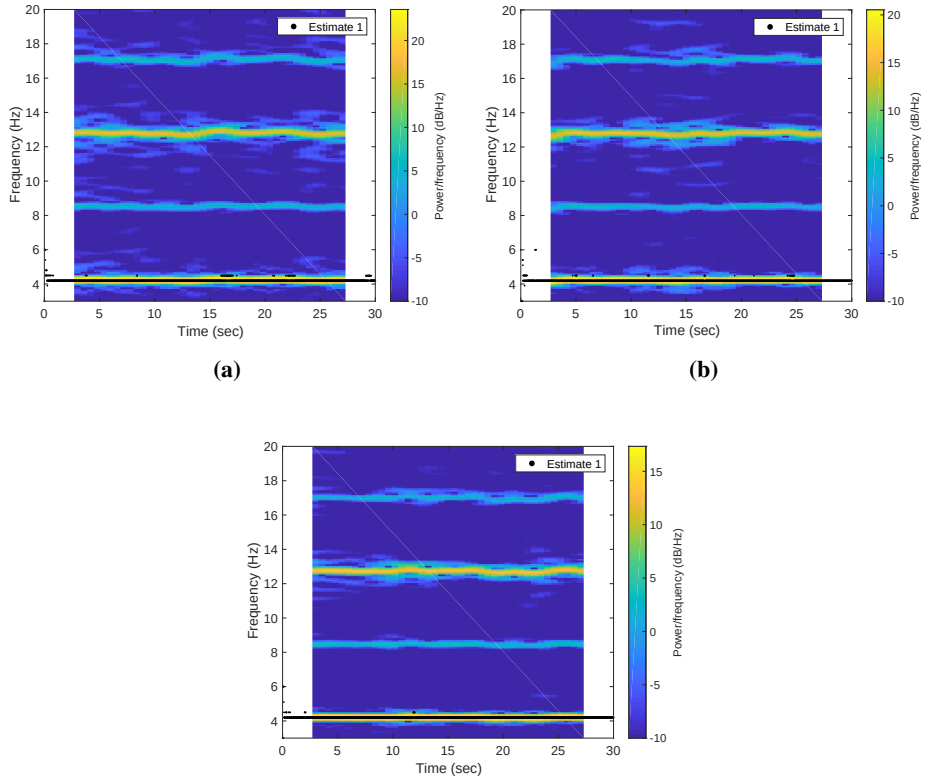

(a) **(b)**

(c) Spectrogram of the arm with (a) nothing, (b) weight and (c) DVA attached

Estenstad [1] made a test procedure to test a 1DOF DVA on the arm. We ran the arm at different frequencies to test out DVAs with different spring constants and mass to measuring their damping effect. For each test one recording was done with nothing attached to the arm, only the mass and then the spring and mass which is the DVA, 27 test in total. The best result achieved 93,25% damping with a DVA connected. The tremor presented here had a dampening effect of 75,89% with the DVA connected. In Figure 9.48a we see the different PSD plots for the tremor with nothing, only the mas, and the DVA attached.

These are the settings for the real time test $\alpha = 0.67,\ T_p = 10,\ \kappa = 0.01,\ h = 0.001,\ L = 100,\ \beta = 50,\ , f_{min} = 3\,Hz,\ f_{max} = 7\,Hz, \Delta\omega = 0.3,\ \Delta T = 0.01,\ \lambda = 0.2, f_s = 100\,Hz$
This was the best resolution I could get with the filter and still making it run in real time. The filter spans from 3 to 7 Hz with with $\Delta\omega = 0.3$. As we can see from the spectrogram plot in Figure 9.49a, the estimate has no problem finding the real frequency in the signal. Unfortunately the first harmonics lies outside our frequency window and was not estimated. An solution to this problem can be to use a stronger microcontroller. The one we use was a 8-bit controller, an upgrade to 16-bit or 32-bit should significantly increase the

window size. Optimizing the code should also give better results. Unfortunately I didn't have time left to start on this process. The algorithm have shown great results in simulations on the desktop computer, and it run smoothly on the microcontroller, although not with the ideal resolution. Since a 8-bit controller is rather weak, i have no doubt that an hardware upgrade will fix the problem.

9.5 Summary

Summary of key findings from the results.

9.5.1 Rest tremor

In section 9.1.3 the filter is tested on a simulated rest tremor signal with two frequencies close in the frequency domain. The estimate of the frequency with the largest and second largest amplitude has a stable estimate after 2.1 and 2.85 seconds respectively, booth with an error under 0.006 Hz, with the error slowly converging towards zero. The frequency that had the largest and smallest amplitude was correctly estimated in under 0.5 seconds. This was a best case scenario where the frequencies in the tremor matched perfectly with the frequency division in the BMWFLC. In section 9.1.4 the same rest tremor signal was tested again, this time the frequencies did not match the frequency division in the BMWFLC, but with the worst case scenario. The estimates had about the same settling time, with an error for the frequency with larges amplitude after 10 and 60 seconds being 0.02 and 0.0065 Hz respectively, and for the one with the smallest 0.03 and 0.015 Hz.

In section 9.3.1 the filter is tested on the real tremor signal the two previous signals where modeled after, a rest tremor with two frequencies close in the frequency domain. The results where excellent, and the performance seems on par with the results from the simulated signals. The next rest tremor signal does not contain two fundamental frequencies, just one with a strong 2nd harmonic (9.3.2). The 1st harmonic is tracked without any problems, but the 2nd harmonic loses its tracking when the frequency does a sudden jump. To get an estimate of the 2nd harmonic throughout the signal, the number of frequencies to track for the filter is adjusted from 2 to 3, this solves the problem somewhat. A more elegant solution is suggested and can be implemented if this becomes a problem in the future.

The results for the simulated rest tremor are really good, the filter adapted to the signal fast and the error of the estimates where low. The results for the real data are also really good, a minor tracking problem occurs when the frequency makes sudden changes, and a solution to this is suggested.

9.5.2 Action tremor

in 9.1.5 the filter is tested on a simulated action tremor. The estimates behave similar as they did for the rest tremor but error converge slower towards zero. After 60 seconds the the error for estimate 1 for the action tremor was 0.035 Hz, and for the rest tremor 0.0065 Hz . This is because of the large amplitude on the inputs signal caused by the voluntary movement, adapting the learning rate to keep the estimates stable. In section 9.2.2 a signal with varying amplitude is tested with constant learning rate, the adaptive feature turned off, the result is unstable estimates.

In section 9.3.4 the filter is tested on a real signal containing action tremor. From the spectrogram we see that there is only one frequency that is stable, and multiple other scattered around it. The stable frequency starts at 8.7 Hz and then slowly moves towards 8.1 Hz. Estimate 1 tracks the main frequency nicely as it is descending.

The results on both the simulated and real action tremor are good, and the voluntary movement is filter away nicely. The error rate converge slower because of the high amplitude in the signal, but should adapt to a faster rate again when the voluntary movement stops.

9.5.3 Postural tremor

In section 9.3.3 we the filter on a recording of postural tremor. From the spectrogram we see that it's highly labile. Overall the estimation seems too do quite well, but it's hard to evaluate due to the nature of the tremor.

9.5.4 Stress tests

In section 9.1.8 a signal with six different frequencies and amplitudes is sent into the filter. These results show that the filter has no problems detecting and estimating multiple frequencies in a signal, and their amplitude with respect to each other.

In section 9.1.6 a simulated signal with two frequencies with varying amplitude is used to see if the filter can correctly estimate which of the two frequencies have the highest amplitude when the amplitude make sudden changes. All the amplitudes are correctly estimated, but it takes different amounts of time deepening on how long the filter had to adapt signal before a new amplitude step. If the filter has had a long time to adapt, it will take longer time for it to adapt to a sudden change of amplitude.

In section 9.1.7 a simulated signal with two varying frequencies is used to see of the filter adapts.From the results we see that when the filter has had some time to adapt to a signal, it takes longer time for it to when there is a sudden change of frequency. Normal tremor doesn't contain sudden jumps in frequency like this, it will change slowly over time, so if there are small burst of change it will be filtered out. If the signal changes all the time like in the postural tremor, the filter doesn't have time to adapt to the signal over a longer period, since it's constantly changing, and therefore the estimation can keep up.

9.5.5 Real-time test with DVA system

The algorithm ran in real-time, but not with the ideal resolution. The fundamental frequency was tracked with no problems, but the 2nd harmonics was outside of the frequency window and could not be tracked. The 8-bit microcontroller we used is rather weak, and I have no doubt that an hardware upgrade will fix the problem. An upgrade to a 16-bit or 32-bit controller should significantly increase the window size and resolution. Optimizing the code could also give better results.

Kapittel 10

Discussion and conclusion

The presented problem forms the basis of this project, and this thesis is built around the following problem:
How to reduce tremors in the upper limb with a mechanical solution in a non-embarrassing way?

In cooperation with Estenstad [1] a design for a vibration absorber for reducing pathological hand tremor was developed. The system is semi-active, and was chosen for its potentially great tremor absorption, while still being small enough to be non-embarrassing. The design consists of a dual vibration absorber that can tune into two frequencies in the hand tremor. The main objective in this thesis has been the development of a filter that can estimate multiple frequencies in pathological tremor for the purpose of tuning the dual vibration absorber to the hand tremor in real time. The Band-limited Multiple Weighted Fourier Linear Combiner (BMWFLC) was developed for this purpose, and additionally it can estimate the amplitude of the frequencies with respect to each other.

Multiple tests with real and simulated tremor data carried out to validate its performance. For a best case scenario where the frequencies in simulated rest tremor matched perfectly with the frequency division in the BMWFLC, the estimate of the frequency with the largest and second largest amplitude had a stable estimate after 2.1 and 2.85 seconds respectively, booth with an error under 0.006 Hz with the error slowly converging towards zero. For the worst case scenario when the frequencies did not match the frequency division in the BMWFLC, the estimates had about the same settling time, with an error for the estimates under 0.053 Hz, slowly converging toward zero. Which frequency that had the largest and smallest amplitude was correctly estimated in under 0.5 seconds for both worst and best case scenario. When the filter is tested on real data of rest tremor the results are excellent, the performance seems on par with the results from the simulated signals, though there are some problems for rest tremor signal with unstable 2nd harmonic, but its a minor problem and solutions are suggest to fix it. The filter is also tested on real data of postural tremor, which is highly labile. The overall the estimation seems too do quite well, but it's hard to evaluate due to the nature of the tremor.

The filter is also stress tested with simulated signals with varying amplitude, frequency

and a signal containing six fundamental frequencies. The filter have good performance on all the test. One important feature of the filter is that it can adapt to sudden changes in amplitude of the input signal, keeping stable if it amplitude gets to high, and increasing sensitivity when the amplitude is low. Especially the latter one is important since we are designing a tremor suppressor, the estimator should be able to work well when the amplitude is lower due to damping. There will also be many sudden peaks in amplitude every time the hand makes voluntary movements.

The algorithm was implemented on a 8-bit microcontroller, and tested on a 1DOF test rig that simulate pathological hand tremor with flexion extension movement. The algorithm ran in real-time, but not with the ideal resolution. The fundamental frequency was tracked, but the 2nd harmonics was outside of the frequency window and could not be tracked. The 8-bit microcontroller we used is rather weak, and a hardware upgrade should fix the problem. A 16-bit or 32-bit microcontroller will significantly increase the window size and resolution of the filter. Optimizing the code could also give better results.

The tremor estimator developed meets requirements for the semi-active dual vibration absorber, it can estimate multiple frequencies in pathological tremor for and the algorithm can run in real-time, and the work toward testing it with a semi-active dual parallel vibration absorber can start. To my knowledge from the literature search, this is the only frequency estimator for pathological tremor estimation that can estimate frequencies that are close in the frequency domain and the first with the capability to estimate over two frequencies simultaneously.

Kapittel 11

Further work

The main future goal is to keep on working towards the semi-active dual vibration absorber. There is still some work left on the mechanical front before the prototype will be finished Estenstad [1], in the mean time there is still a some work to be done to make the estimates from the filter better. Here are some suggestion of things that can be done:

1. Implement the BMWLFC filter on a better microcontroller to see how much the performance improves. A 16-bit or 32-bit microcontroller should significantly increase the window size and resolution of the filter.
2. To improve tracking of harmonics; Divide the BMWFLC filter into sections the same way as the E-BMFLC filter presented is section 5.1.5, can be used to extract the voluntary, m_{k-v}, and involuntary signal, m_{k-i}, from the total estimate of the signal m_k. Instead of extracting the voluntary and involuntary motion, we could extract the signal containing fundamental frequency, which would lie in the range 3-7 Hz for PD, and the signal containing the harmonics in the range 7-20 Hz. Now, these two could run as separate BMWFLC filters without adding much computational cost.
3. Create a new algorithm to extract the frequencies from the magnitude spectrum in the BMWFLC filter then the one presented in section 5.2.3, and/or find new ways to utilize the data in the magnitude spectrum.
4. Expand the algorithm to estimate frequency for 3DOF. If the dominant frequencies in different axes are not the same, the valid dominant frequency in the axis with the highest peak power is defined as the dominant frequency of all axes. [114]
5. Though the BMWFLC filter is mainly developed for frequency estimation, and not a tremor estimator that estimates the input signal s_k, the filter may get good a estimate of y_k if the filter is set up in the right way. I suggest that a comparison with E-BMFLC filter [81, 86] can be done to evaluate the estimation performance.
6. Implement and test the algorithm with a prototype of the semi-active dual vibration absorber.

Bibliografi

[1] Ida Estenstad. Design and validation of a wearable device for upper limb tremor suppression. Thesis, 2018.

[2] Abdul Qayyum Rana and Kelvin L. Chou. *Essential tremor in clinical practice*. 2015. ISBN 3-319-14598-3.

[3] Liftware steady, 2018. URL `https://www.liftware.com/steady/`.

[4] Sarah Gebai, Mohammad Hammoud, Ali Hallal, and Ali Al Shaer. Involuntary tremor controlled using mechanical means: Involunatry hand tremor. In *Advances in Biomedical Engineering (ICABME), 2017 Fourth International Conference on*, pages 1–4. IEEE, 2017.

[5] Readi-steadi® anti-tremor orthotic glove system, year = 2018, url = "https://www.readi-steadi.com/", urldate = [Online; accessed 06.06.2018].

[6] Gyroglove, 2018. URL `https://gyrogear.co/gyroglove`.

[7] Gregor K Wenning, Stefan Kiechl, Klaus Seppi, Joerg Müller, Birgit Högl, Michael Saletu, Gregor Rungger, Arno Gasperi, Johann Willeit, and Werner Poewe. Prevalence of movement disorders in men and women aged 50–89 years (bruneck study cohort): a population-based study. *The lancet neurology*, 4(12):815–820, 2005.

[8] S Moghal, AH Rajput, C D'Arcy, and R Rajput. Prevalence of movement disorders in elderly community residents. *Neuroepidemiology*, 13(4):175–178, 1994.

[9] Skjelvinger - essensiell tremor, 2016. URL `https://legehandboka.no/handboken/kliniske-kapitler/nevrologi/tilstander-og-sykdommer/bevegelsesforstyrrelser/essensiell-tremor/`.

[10] Parkinsons sykdom (ps), 2016. URL `https://legehandboka.no/handboken/kliniske-kapitler/nevrologi/tilstander-og-sykdommer/bevegelsesforstyrrelser/parkinsons-sykdom/`.

[11] Elan D Louis and Joaquim J Ferreira. How common is the most common adult movement disorder? update on the worldwide prevalence of essential tremor. *Movement Disorders*, 25(5):534–541, 2010.

[12] Constance Hammond, Hagai Bergman, and Peter Brown. Pathological synchronization in parkinson's disease: networks, models and treatments. *Trends in Neurosciences*, 30(7):357 – 364, 2007. ISSN 0166-2236. doi: https://doi.org/10.1016/j.tins.2007.05.004. URL http://www.sciencedirect.com/science/article/pii/S0166223607001233. July INMED/TINS special issue—Physiogenic and pathogenic oscillations: the beauty and the beast.

[13] Joan K. Monin, Jesús Gutierrez, Sarah Kellner, Sarah Morgan, Kathleen Collins, Brittany Rohl, Fanny Migliore, Stephanie Cosentino, Edward Huey, Elan D. Louis, and Julian Benito-Leon. Psychological suffering in essential tremor: A study of patients and those who are close to them. *Tremor and Other Hyperkinetic Movements*, 7, 2017. doi: 10.7916/D8Q53WF0. URL https://tremorjournal.org/index.php/tremor/article/download/526/pdf.

[14] Duane A. Lundervold, Patrick A. Ament, and Peter Holt. Social anxiety, tremor severity, and tremor disability: A search for clinically relevant measures. *Psychiatry Journal*, 2013, 2013. ISSN 2314-4327. doi: 10.1155/2013/257459. URL http://downloads.hindawi.com/journals/psychiatry/2013/257459.pdf.

[15] Vrutangkumar V Shah, Sachin Goyal, and Harish J Palanthandalam-Madapusi. A possible explanation of how high-frequency deep brain stimulation suppresses low-frequency tremors in parkinson's disease. *IEEE Transactions on Neural Systems and Rehabilitation Engineering*, 25(12):2498–2508, 2017.

[16] Mathias Toft, Bård Lilleeng, Jon Ramm-Pettersen, Geir Ketil Røste, Lena Pedersen, Inger Marie Skogseid, and Espen Dietrichs. Behandling av bevegelsesforstyrrelser med dyp hjernestimulering, 2008. URL https://tidsskriftet.no/2008/09/tema-bevegelsesforstyrrelser/behandling-av-bevegelsesforstyrrelser-med-dyp-hjernestimulering.

[17] Paul Krack, Raul Martinez-Fernandez, Marta Alamo, and Jose A Obeso. Current applications and limitations of surgical treatments for movement disorders. *Movement Disorders*, 32(1):36–52, 2017.

[18] M Bang Henriksen, EL Johnsen, N Sunde, A Vase, MC Gjelstrup, and K Østergaard. Surviving 10 years with deep brain stimulation for parkinson's disease–a follow-up of 79 patients. *European journal of neurology*, 23(1):53–61, 2016.

[19] Johannes C Rothlind, Michele K York, Kim Carlson, Ping Luo, William J Marks, Frances M Weaver, Matthew Stern, Kenneth Follett, and Domenic Reda. Neuropsychological changes following deep brain stimulation surgery for parkinson's disease: comparisons of treatment at pallidal and subthalamic targets versus best medical therapy. *J Neurol Neurosurg Psychiatry*, 86(6):622–629, 2015.

[20] Günther Deuschl, Jan Raethjen, Helge Hellriegel, and Rodger Elble. Treatment of patients with essential tremor. *The Lancet Neurology*, 10(2):148–161, 2011.

[21] Joseph Jankovic and L Giselle Aguilar. Current approaches to the treatment of parkinson's disease. *Neuropsychiatric disease and treatment*, 4(4):743, 2008.

[22] Olivier Rascol, David J Brooks, Amos D Korczyn, Peter P De Deyn, Carl E Clarke, and Anthony E Lang. A five-year study of the incidence of dyskinesia in patients with early parkinson's disease who were treated with ropinirole or levodopa. *New England Journal of Medicine*, 342(20):1484–1491, 2000.

[23] E Rocon, JM Belda-Lois, JJ Sanchez-Lacuesta, and JL Pons. Pathological tremor management: Modelling, compensatory technology and evaluation. *Technology and Disability*, 16(1):3–18, 2004.

[24] Stanley Fahn, Joseph Jankovic, and Mark Hallet. *Principles and Practice of Movement Disorders*. 2011.

[25] Joseph Jankovic and Eduardo Tolosa. *Parkinson's Disease and Movement Disorders*. 2015. ISBN 1-4963-1763-7.

[26] Bhomraj Thanvi, Nelson Lo, and Tom Robinson. Essential tremor: the most common movement disorder in older people. *Age and Ageing*, 35(4):344–349, 2006. ISSN 0002-0729. doi: 10.1093/ageing/afj072.

[27] R. J. Elble. Essential tremor frequency decreases with time. *Neurology*, 55(10): 1547–1551. ISSN 00283878. doi: 10.1212/WNL.55.10.1547.

[28] George N Reeke, Roman R Poznanski, Kenneth A Lindsay, Jay R Rosenberg, and Olaf Sporns. *Modeling in the neurosciences: from biological systems to neuromimetic robotics*. CRC Press, 2005. Data can are avalible at the website: http://motusbioengineering.com/sample-test-results-2.htm.

[29] M. Gresty and D. Buckwell. Spectral analysis of tremor: understanding the results. *Journal of Neurology, Neurosurgery & Psychiatry*, 53(11):976, 1990. ISSN 0022-3050,00223050. doi: 10.1136/jnnp.53.11.976.

[30] Steven Smith. *Digital Signal Processing: A Practical Guide for Engineers and Scientists*. Elsevier Science, Burlingtion, 2003. ISBN 978-0-7506-7444-7.

[31] G N Reeke, Roman Poznanski, Kenneth Lindsay, Jay Rosenberg, and Olaf Sporns. *Modeling in the Neurosciences: From Biological Systems to Neuromimetic Robotics*. Taylor and Francis Group, Boca Raton, 2nd ed. edition, 2005. ISBN 978-0-415-32868-5.

[32] Yue Zhou, Mary E Jenkins, Michael D Naish, and Ana Luisa Trejos. The measurement and analysis of parkinsonian hand tremor. In *Biomedical and Health Informatics (BHI), 2016 IEEE-EMBS International Conference on*, pages 414–417. IEEE, 2016.

[33] Sarah Gebai, Mohammad Hammoud, Ali Hallal, and Hassan Khachfe. Tremor reduction at the palm of a parkinson's patient using dynamic vibration absorber. *Bioengineering*, 3(3):18, 2016. ISSN 2306-5354. URL http://www.mdpi.com/2306-5354/3/3/18.

[34] André Preumont and Peter Bain. *Twelve Lectures on Structural Dynamics*. 2013.

[35] Felix Weber. Optimal semi-active vibration absorber for harmonic excitation based on controlled semi-active damper. *Smart Materials and Structures*, 23(9):095033, 2014.

[36] Bernard Widrow and Samuel S.D. Stearns. Adaptive signal processing. *Englewood Cliffs, NJ, Prentice-Hall, Inc*, 1:491, 1985.

[37] Tildon H. Glisson. *Fourier Series*, pages 583–608. Springer Netherlands, Dordrecht, 2011. ISBN 978-90-481-9443-8. doi: 10.1007/978-90-481-9443-8_16. URL https://doi.org/10.1007/978-90-481-9443-8_16.

[38] *Appendix D: Trigonometric Fourier Series*, pages 641–644. Wiley-Blackwell, 2014. ISBN 9781118844373. doi: 10.1002/9781118844373.app4. URL https://onlinelibrary.wiley.com/doi/abs/10.1002/9781118844373.app4.

[39] Apurba Das. *Fourier Series*, pages 23–50. Springer Berlin Heidelberg, Berlin, Heidelberg, 2012. ISBN 978-3-642-28818-0. doi: 10.1007/978-3-642-28818-0_2. URL https://doi.org/10.1007/978-3-642-28818-0_2.

[40] Charan Langton. *The intuitive guide to Fourier analysis & spectral estimation with MATLAB*, pages 5–38. MountCastle Academic, San Ramon, Calif, 2017. ISBN 0913063266.

[41] R. A. R. C. Gopura, D. S. V. Bandara, Kazuo Kiguchi, and G. K. I. Mann. Developments in hardware systems of active upper-limb exoskeleton robots: A review. *Robotics and Autonomous Systems*, 75:203–220, 2016. ISSN 0921-8890. doi: https://doi.org/10.1016/j.robot.2015.10.001. URL http://www.sciencedirect.com/science/article/pii/S0921889015002274.

[42] Eduardo Rocon, Mario Manto, Jose Pons, Stephane Camut, and Juan Manuel Belda. Mechanical suppression of essential tremor. *The Cerebellum*, 6(1):73, 2007. ISSN 1473-4230. doi: 10.1080/14734220601103037. URL https://doi.org/10.1080/14734220601103037https://link.springer.com/content/pdf/10.1080%2F14734220601103037.pdf.

[43] Eduardo Rocon and José L. Pons. *Upper Limb Exoskeleton for Tremor Suppression: Physical HR Interaction*, pages 67–98. Springer Berlin Heidelberg, Berlin, Heidelberg, 2011. ISBN 978-3-642-17659-3. doi: 10.1007/978-3-642-17659-3_4. URL https://doi.org/10.1007/978-3-642-17659-3_4https://link.springer.com/content/pdf/10.1007%2F978-3-642-17659-3_4.pdf.

[44] Gil Herrnstadt and Carlo Menon. Voluntary-driven elbow orthosis with speed-controlled tremor suppression. *Frontiers in Bioengineering and Biotechnology*, 4(29), 2016. ISSN 2296-4185. doi: 10.3389/fbioe.2016.00029. URL https://www.frontiersin.org/article/10.3389/fbioe.2016.00029.

[45] D. Huen, J. Liu, and B. Lo. An integrated wearable robot for tremor suppression with context aware sensing. In *2016 IEEE 13th International Conference on Wearable and Implantable Body Sensor Networks (BSN)*, pages 312–317. doi: 10.1109/BSN.2016.7516280. URL http://ieeexplore.ieee.org/document/7516280/.

[46] Behzad Taheri. *Real-Time Pathological Tremor Identification and Suppression in Human Arm via Active Orthotic Devices*. 2013.

[47] S. Dosen, S. Muceli, J. L. Dideriksen, J. P. Romero, E. Rocon, J. Pons, and D. Farina. Online tremor suppression using electromyography and low-level electrical stimulation. *IEEE Transactions on Neural Systems and Rehabilitation Engineering*, 23(3):385–395, 2015. doi: 10.1109/TNSRE.2014.2328296. URL https://www.scopus.com/inward/record.uri?eid=2-s2.0-84929309739&doi=10.1109%2fTNSRE.2014.2328296&partnerID=40&md5=298d57fecd99d95ca0399f1baa62e763http://ieeexplore.ieee.org/document/6856155/.

[48] Onanong Jitkritsadakul, Chusak Thanawattano, Chanawat Anan, and Roongroj Bhidayasiri. Exploring the effect of electrical muscle stimulation as a novel treatment of intractable tremor in parkinson's disease. *Journal of the Neurological Sciences*, 358(1):146–152, 2015. ISSN 0022-510X. doi: https://doi.org/10.1016/j.jns.2015.08.1527. URL http://www.sciencedirect.com/science/article/pii/S0022510X15020237.

[49] Cristiano De Marchis, Thiago Santos Monteiro, Cristina Simon-Martinez, Silvia Conforto, and Alireza Gharabaghi. Multi-contact functional electrical stimulation for hand opening: electrophysiologically driven identification of the optimal stimulation site. *Journal of NeuroEngineering and Rehabilitation*, 13(1):22, 2016. ISSN 1743-0003. doi: 10.1186/s12984-016-0129-6. URL https://doi.org/10.1186/s12984-016-0129-6https://jneuroengrehab.biomedcentral.com/track/pdf/10.1186/s12984-016-0129-6?site=jneuroengrehab.biomedcentral.com.

[50] JAE-HOON HEO, YURI KWON, HYEONG-MIN JEON, DO-YOUNG KWON, CHAN-NYEONG LEE, KEON-WOO PARK, MARIO MANTO, JI-WON KIM, and GWANG-MOON EOM. Suppression of action tremor by sensory electrical stimulation in patients with essential tremor. *Journal of Mechanics in Medicine and Biology*, 16(08):1640026, 2016. doi: 10.1142/s0219519416400261. URL http://www.worldscientific.com/doi/abs/10.1142/S0219519416400261http://www.worldscientific.com/doi/pdfplus/10.1142/S0219519416400261.

[51] W. Xin, Y. Gao, S. Wang, and J. Zhao. A programmable electrical stimulator for suppressing pathological tremor. In *2016 12th World Congress on Intelligent Control and Automation (WCICA)*, pages 1669–1674. doi: 10.1109/WCICA.2016.7578413. URL http://ieeexplore.ieee.org/document/7578413/.

[52] F. L. Xu, M. Z. Hao, S. Q. Xu, Z. X. Hu, Q. Xiao, and N. Lan. Development of a closed-loop system for tremor suppression in patients with parkinson's disease. In *2016 38th Annual International Conference of the IEEE Engineering in Medicine and Biology Society (EMBC)*, pages 1782–1785. ISBN 1557-170X. doi: 10.1109/EMBC.2016.7591063. URL http://ieeexplore.ieee.org/document/7591063/.

[53] Jakob L. Dideriksen, Christopher M. Laine, Strahinja Dosen, Silvia Muceli, Eduardo Rocon, José L. Pons, Julian Benito-Leon, and Dario Farina. Electrical stimulation of afferent pathways for the suppression of pathological tremor. *Frontiers in Neuroscience*, 11(178), 2017. ISSN 1662-453X. doi: 10.3389/fnins.2017.00178. URL https://www.frontiersin.org/article/10.3389/fnins.2017.00178.

[54] Onanong Jitkritsadakul, Chusak Thanawattano, Chanawat Anan, and Roongroj Bhidayasiri. Tremor's glove-an innovative electrical muscle stimulation therapy for intractable tremor in parkinson's disease: A randomized sham-controlled trial. *Journal of the Neurological Sciences*, 381:331–340, 2017. ISSN 0022-510X. doi: https://doi.org/10.1016/j.jns.2017.08.3246. URL http://www.sciencedirect.com/science/article/pii/S0022510X17337437.

[55] E. Rocon, J. A. Gallego, L. Barrios, A. R. Victoria, J. Ibánez, D. Farina, F. Negro, J. L. Dideriksen, S. Conforto, T. D' Alessio, G. Severini, J. M. Belda-Lois, L. Z. Popovic, G. Grimaldi, M. Manto, and J. L. Pons. Multimodal bci-mediated fes suppression of pathological tremor. In *2010 Annual International Conference of the IEEE Engineering in Medicine and Biology*, pages 3337–3340. ISBN 1094-687X. doi: 10.1109/IEMBS.2010.5627914. URL http://ieeexplore.ieee.org/document/5627914/.

[56] J. A. Gallego, E. Rocon, J. Ibáñez, J. L. Dideriksen, A. D. Koutsou, R. Paradiso, M. B. Popovic, J. M. Belda-Lois, F. Gianfelici, D. Farina, D. B. Popovic, M. Manto, T. D' Alessio, and J. L. Pons. A soft wearable robot for tremor assessment and suppression. In *2011 IEEE International Conference on Robotics and Automation*, pages 2249–2254, . ISBN 1050-4729. doi: 10.1109/ICRA.2011.5979639. URL http://ieeexplore.ieee.org/document/5979639/.

[57] F. Widjaja, C. Y. Shee, W. L. Au, P. Poignet, and W. T. Ang. Using electromechanical delay for real-time anti-phase tremor attenuation system using functional electrical stimulation. In *2011 IEEE International Conference on Robotics and Automation*, pages 3694–3699. ISBN 1050-4729. doi: 10.1109/ICRA.2011.5979865. URL http://ieeexplore.ieee.org/document/5979865/.

[58] Dingguo Zhang, Philippe Poignet, Ferdinan Widjaja, and Wei Tech Ang. Neural oscillator based control for pathological tremor suppression via functional electrical stimulation. *Control Engineering Practice*, 19(1):74–88, 2011. ISSN 0967-0661. doi: https://doi.org/10.1016/j.conengprac.2010.08.009. URL http://www.sciencedirect.com/science/article/pii/S0967066110001991.

[59] J. A. Gallego, E. Rocon, J. M. Belda-Lois, A. D. Koutsou, S. Mena, A. Castillo, and J. L. Pons. Design and validation of a neuroprosthesis for the treatment of upper limb tremor. In *2013 35th Annual International Conference of the IEEE Engineering in Medicine and Biology Society (EMBC)*, pages 3606–3609, . ISBN 1094-687X. doi: 10.1109/EMBC.2013.6610323. URL http://ieeexplore.ieee.org/document/6610323/.

[60] Juan Álvaro Gallego, Eduardo Rocon, Juan Manuel Belda-Lois, and José Luis Pons. A neuroprosthesis for tremor management through the control of muscle co-contraction. *Journal of NeuroEngineering and Rehabilitation*, 10(1):36, 2013. ISSN 1743-0003. doi: 10.1186/1743-0003-10-36. URL https://doi.org/10.1186/1743-0003-10-36https://jneuroengrehab.biomedcentral.com/track/pdf/10.1186/1743-0003-10-36?site=jneuroengrehab.biomedcentral.com.

[61] Antônio Padilha Lanari Bó, Christine Azevedo-Coste, Christian Geny, Philippe Poignet, and Charles Fattal. On the use of fixed-intensity functional electrical stimulation for attenuating essential tremor. *Artificial Organs*, 38(11):984–991, 2014. ISSN 1525-1594. doi: 10.1111/aor.12261. URL http://dx.doi.org/10.1111/aor.12261http://onlinelibrary.wiley.com/store/10.1111/aor.12261/asset/aor12261.pdf?v=1&t=jcadx5db&s=bfea3ed44f023b384f80c27b89a155128aeb23f6.

[62] Engin H. Copur, Chris T. Freeman, Bing Chu, and Dina S. Laila. System identification for fes-based tremor suppression. *European Journal of Control*, 27:45–59, 2016. ISSN 0947-3580. doi: https://doi.org/10.1016/j.ejcon.2015.12.003. URL http://www.sciencedirect.com/science/article/pii/S0947358015001314.

[63] M. Z. Hao, S. Q. Xu, Z. X. Hu, F. L. Xu, C. X. M. Niu, Q. Xiao, and N. Lan. Inhibition of parkinsonian tremor with cutaneous afferent evoked by transcutaneous electrical nerve stimulation. *Journal of NeuroEngineering and Rehabilitation*, 14(1), 2017. doi: 10.1186/s12984-017-0286-2. URL https://www.scopus.com/inward/record.uri?eid=2-s2.0-85024125371&doi=10.1186%2fs12984-017-0286-2&partnerID=40&md5=f8dd9b1817188e79453552e96ae63444https://jneuroengrehab.biomedcentral.com/track/pdf/10.1186/s12984-017-0286-2?site=jneuroengrehab.biomedcentral.com.

[64] Liftware, 2018. URL https://www.liftware.com/.

[65] Peter Feys, Werner F Helsen, Sabine Verschueren, Stephan P Swinnen, Isabel Klok, Ann Lavrysen, Bart Nuttin, Pierre Ketelaer, and Xuguang Liu. Online movement control in multiple sclerosis patients with tremor: effects of tendon vibration. *Movement disorders*, 21(8):1148–1153, 2006.

[66] Project emma, year = 2018, url = "https://www.microsoft.com/en-us/research/project/project-emma/", urldate = [Online; accessed 06.06.2018].

[67] Arc pen, 2018. URL `https://www.hwansoojeon.com/arc`.

[68] Pushkar Deshpande. *Tremor suppression with shape memory alloy vibration absorber*. Thesis, 2016.

[69] CJ Teixeira, E Bicho, LA Rocha, and MF Gago. A self-tunable dynamic vibration absorber: Parkinson's disease's tremor suppression. In *Bioengineering (ENBENG), 2013 IEEE 3rd Portuguese Meeting in*, pages 1–6. IEEE, 2013.

[70] Eran Buki, Reuven Katz, Miriam Zacksenhouse, and Ilana Schlesinger. Vib-bracelet: a passive absorber for attenuating forearm tremor. *Medical & Biological Engineering & Computing*, 2017. ISSN 1741-0444. doi: 10.1007/s11517-017-1742-7. URL `https://doi.org/10.1007/s11517-017-1742-7https://link.springer.com/content/pdf/10.1007%2Fs11517-017-1742-7.pdfhttps://link.springer.com/article/10.1007%2Fs11517-017-1742-7`.

[71] Sarah Gebai, Mohammad Hammoud, Ali Hallal, and Ali AL Shaer. Structural control and biomechanical tremor suppression: Comparison between different types of passive absorber. *Journal of Vibration and Control*, page 1077546316689200, 2016.

[72] Sarah Gebai, Mohamad Hammoud, Ali Hallal, Ali Al Shaer, and Hassan Khachfe. Passive vibration absorber for tremor in hand of parkinsonian patients: Tuned vibration absorber for rest tremor. In *Advances in Computational Tools for Engineering Applications (ACTEA), 2016 3rd International Conference on*, pages 162–167. IEEE, 2016.

[73] Sarah Gebai, Mohamad Hammoud, Ali Hallal, Ali AL Shaer, and Hassan Khachfe. Biomechanical treatment for rest tremor of parkinson's patient. In *Multidisciplinary Conference on Engineering Technology (IMCET), IEEE International*, pages 32–36. IEEE, 2016.

[74] Sarah Gebai, Mohammad Hammoud, Ali Hallal, and Hassan Khachfe. Tremor reduction at the palm of a parkinson's patient using dynamic vibration absorber. *Bioengineering*, 3(3):18, 2016.

[75] Sarah Gebai and Mohamad Hammoud. Reduction of parkinsonism disorder symptoms using passive dual absorbers. In *Biomedical Engineering (MECBME), 2016 3rd Middle East Conference on*, pages 88–91. IEEE, 2016.

[76] Sarah Gebai and Mohamad Hammoud. Parkinson's disease treatment as seen from a mechanical point of view. *Advances in Parkinson's Disease*, 5(04):97, 2016.

[77] Rory J O'Connor and Manohar U Kini. Non-pharmacological and non-surgical interventions for tremor: a systematic review. *Parkinsonism & related disorders*, 17 (7):509–515, 2011.

[78] R Langton Hewer, RAY COOPER, and M HILARY MORGAN. An investigation into the value of treating intention tremor by weighting the affected limb. *Brain*, 95 (3):579–590, 1972.

[79] Jessica Hall. Mit engineers create glove that mitigates hand tremors from parkinson's, 2016. URL `https://www.extremetech.com/extreme/221368-mit-engineers-create-glove-that-mitigates-hand-tremors-from-mailing_id=1549287&mailing=whatsnewnow&mailingID=28AD39B732DCD774470935A1CABEBF3A`.

[80] Soroosh Shahtalebi, Arash Mohammadi, Seyed Farokh Atashzar, and Rajni V Patel. Wake: Wavelet decomposition coupled with adaptive kalman filtering for pathological tremor extraction. *arXiv preprint arXiv:1711.06815*, 2017.

[81] Vahid Khorasani Ghassab, Arash Mohammadi, Seyed Farokh Atashzar, and Rajni V Patel. Dynamic estimation strategy for e-bmflc filters in analyzing pathological hand tremors, year = 2017, type = Journal Article.

[82] Yue Zhou, Mary E Jenkins, Michael D Naish, and Ana Luisa Trejos. Design and validation of a high-order weighted-frequency fourier linear combiner-based kalman filter for parkinsonian tremor estimation. In *Engineering in Medicine and Biology Society (EMBC), 2016 IEEE 38th Annual International Conference of the*, pages 5893–5896. IEEE, 2016.

[83] Feiyun Xiao, Yongsheng Gao, Shengxin Wang, and Jie Zhao. Prediction of pathological tremor using adaptive multiple oscillators linear combiner. *Biomedical Signal Processing and Control*, 27:77–86, 2016.

[84] Shengxin Wang, Yongsheng Gao, Yanhe Zhu, and Jie Zhao. Estimation of pathological tremor from recorded signals based on adaptive sliding fast fourier transform. *Advances in Mechanical Engineering*, 8(6):1687814016654872, 2016.

[85] Shengxin Wang, Yongsheng Gao, Feiyun Xiao, Xizhe Zang, Yanhe Zhu, and Jie Zhao. Estimation of tremor parameters and extraction tremor from recorded signals for tremor suppression. In *Robotics and Automation (ICRA), 2016 IEEE International Conference on*, pages 3717–3722. IEEE, 2016.

[86] S. F. Atashzar, M. Shahbazi, O. Samotus, M. Tavakoli, M. S. Jog, and R. V. Patel. Characterization of upper-limb pathological tremors: Application to design of an augmented haptic rehabilitation system. *IEEE Journal of Selected Topics in Signal Processing*, 10(5):888–903, 2016. ISSN 1932-4553. doi: 10.1109/JSTSP.2016.2530632. URL `http://ieeexplore.ieee.org/document/7407298/`.

[87] Shengxin Wang, Yongsheng Gao, Jie Zhao, and Hegao Cai. Adaptive sliding band-limited multiple fourier linear combiner for estimation of pathological tremor. *Biomedical Signal Processing and Control*, 10:260–274, 2014.

[88] Amir Hosein Zamanian and Edmond Richer. Adaptive disturbance rejection controller for pathological tremor suppression with permanent magnet linear motor. In *ASME 2017 Dynamic Systems and Control Conference*, pages V001T37A003–V001T37A003. American Society of Mechanical Engineers, 2017.

[89] Behzad Taheri, David Case, and Edmond Richer. Adaptive suppression of severe pathological tremor by torque estimation method. *IEEE/ASME Transactions on Mechatronics*, 20(2):717–727, 2015.

[90] Juan Alvaro Gallego, E Rocon, and Jens Luis Pons. Estimation of instantaneous tremor parameters for fes-based tremor suppression. In *Robotics and Automation (ICRA), 2010 IEEE International Conference on*, pages 2922–2927. IEEE, 2010.

[91] Juan A Gallego, Eduardo Rocon, Javier O Roa, Juan C Moreno, and José L Pons. Real-time estimation of pathological tremor parameters from gyroscope data. *Sensors*, 10(3):2129–2149, 2010.

[92] Christopher A Vaz and Nitish V Thakor. Adaptive fourier estimation of time-varying evoked potentials. *IEEE Transactions on Biomedical Engineering*, 36(4): 448–455, 1989. ISSN 0018-9294. doi: 10.1109/10.18751.

[93] C. N. Riviere, R. S. Rader, and N. V. Thakor. Adaptive cancelling of physiological tremor for improved precision in microsurgery. *IEEE Transactions on Biomedical Engineering*, 45(7):839–846, 1998. ISSN 0018-9294. doi: 10.1109/10.686791. URL `http://ieeexplore.ieee.org/document/686791/`.

[94] K. C. Veluvolu, U. X. Tan, W. T. Latt, C. Y. Shee, and W. T. Ang. Bandlimited multiple fourier linear combiner for real-time tremor compensation. In *2007 29th Annual International Conference of the IEEE Engineering in Medicine and Biology Society*, pages 2847–2850. ISBN 1094-687X. doi: 10.1109/IEMBS.2007.4352922. URL `http://ieeexplore.ieee.org/document/4352922/`.

[95] KC Veluvolu and WT Ang. Estimation and filtering of physiological tremor for real-time compensation in surgical robotics applications. *The International Journal of Medical Robotics and Computer Assisted Surgery*, 6(3):334–342, 2010.

[96] Kalyana Chakravarthy Veluvolu, U-X Tan, Win Tun Latt, Cheng Yap Shee, and Wei Tech Ang. Adaptive filtering of physiological tremor for real-time compensation. In *Robotics and Biomimetics, 2008. ROBIO 2008. IEEE International Conference on*, pages 524–529. IEEE, 2009.

[97] Lana Z Popović, Tomislav B Šekara, and Mirjana B Popović. Adaptive band-pass filter (abpf) for tremor extraction from inertial sensor data. *Computer methods and programs in biomedicine*, 99(3):298–305, 2010.

[98] P. Mohana Shankar. *Concepts of Probability and Statistics*, pages 9–212. Springer International Publishing, Cham, 2017. ISBN 978-3-319-53198-4. doi: 10.1007/978-3-319-53198-4_2. URL `https://doi.org/10.1007/978-3-319-53198-4_2`.

[99] Manto Mario, Grimaldi Giuliana, Lorivel Thomas, Farina Dario, Popovic Lana, Conforto Silvia, D'Alessio Tommaso, Belda-Lois Juan-Manuel, Pons Jose-Luis, and Rocon Eduardo. Bioinformatic approaches used in modelling human tremor. *Current Bioinformatics*, 4(2):154–172, 2009.

[100] Peter Welch. The use of fast fourier transform for the estimation of power spectra: a method based on time averaging over short, modified periodograms. *IEEE Transactions on audio and electroacoustics*, 15(2):70–73, 1967.

[101] Maurice S Bartlett. Periodogram analysis and continuous spectra. *Biometrika*, 37 (1/2):1–16, 1950.

[102] James McNames. *Signal Processing*, pages 371–389. Springer New York, New York, NY, 2013. ISBN 978-1-4614-4027-7. doi: 10.1007/978-1-4614-4027-7_20. URL https://doi.org/10.1007/978-1-4614-4027-7_20.

[103] Eric Jones, Travis Oliphant, Pearu Peterson, et al. SciPy: Open source scientific tools for Python, 2001–. URL http://www.scipy.org/. [Online; accessed 30.04.2018].

[104] J Timmer, M Lauk, and G Deuschl. Quantitative analysis of tremor time series. *Electroencephalography and Clinical Neurophysiology/Electromyography and Motor Control*, 101(5):461–468, 1996.

[105] K. Deergha Rao and M.N.S. Swamy. *Spectral Analysis of Signals*, pages 721–751. Springer Singapore, Singapore, 2018. ISBN 978-981-10-8081-4. doi: 10.1007/978-981-10-8081-4_12. URL https://doi.org/10.1007/978-981-10-8081-4_12.

[106] MATLAB Signal Processing Toolbox. Matlab signal processing toolbox, version 7.5, (r2017b), 2017.

[107] MATLAB. *version 7.10.0 (R2017b)*. The MathWorks Inc., Natick, Massachusetts, 2010.

[108] Operating instructions compax3 i11t11, 2010. URL http://divapps.parker.com/divapps/eme/EME/Literature_List/Dokumentationen/C3I11T11%20eng.pdf.

[109] Smh / smb series, 2016. URL https://www.parker.com/literature/Electromechanical%20Europe/Literature/192_061013_SMB_SMH_Motoren.pdf.

[110] Arduino uno rev3, 2018. URL https://store.arduino.cc/arduino-uno-rev3.

[111] Atmega328p, 2018. URL https://www.microchip.com/wwwproducts/en/ATmega328P.

[112] Lsm6ds3, 2018. URL http://www.st.com/en/mems-and-sensors/lsm6ds3.html.

[113] Windows presentation foundation, 2018.

[114] Houde Dai, Pengyue Zhang, and Tim C Lueth. Quantitative assessment of parkinsonian tremor based on an inertial measurement unit. *Sensors*, 15(10):25055–25071, 2015.

Appendices

Tillegg A

Schematic for Arduino and LSM6DS3

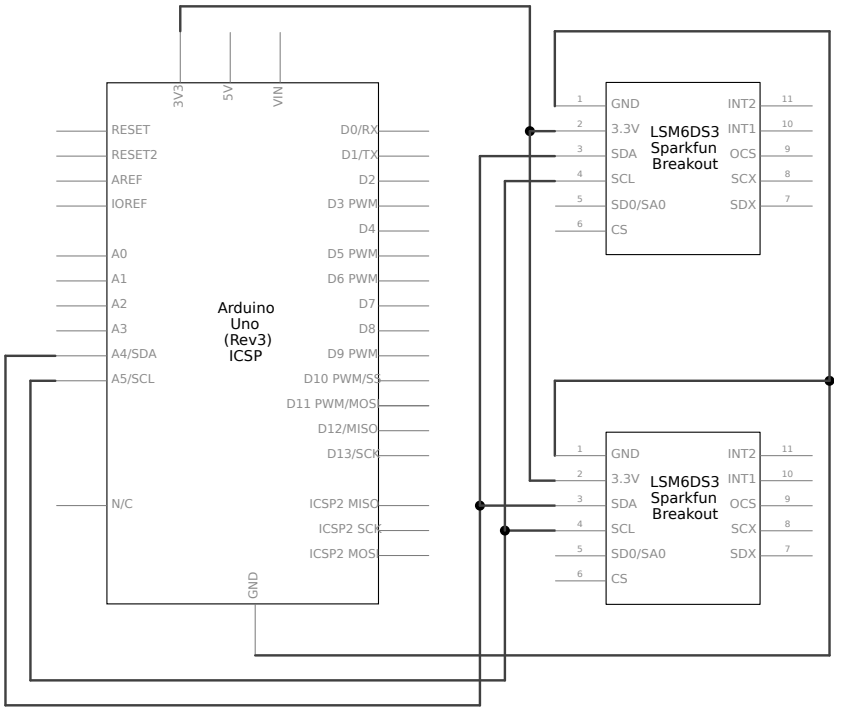

Figur A.1: Connection between the two LSM6DS3 and the Arduino Uno

Tillegg B

Real tremor data - Tuned filter

B.1 Recording 2 - Rest tremor

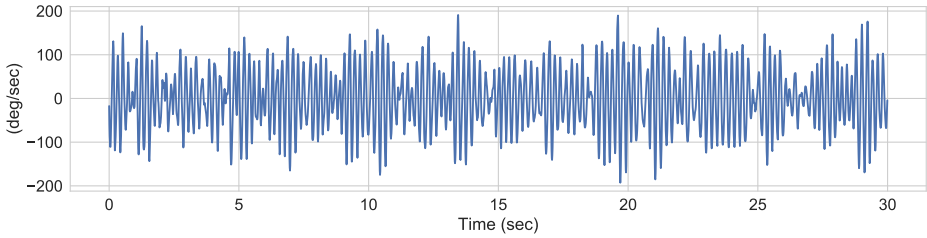

Figur B.1: Recording 2 from session 2. Orientation: P+/S. Placement: RH

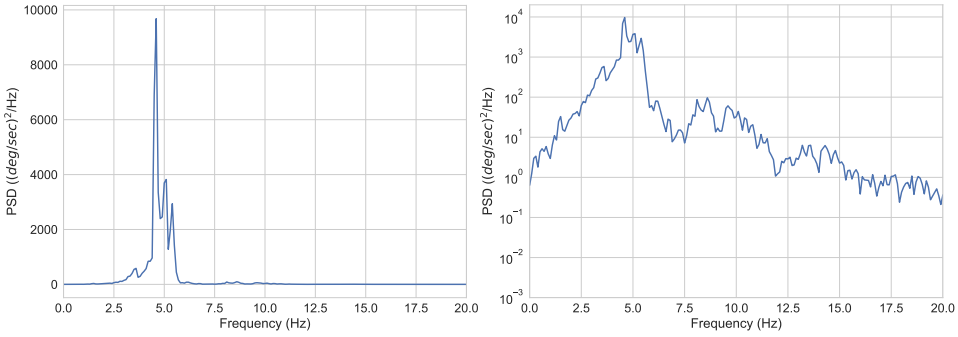

(a) **(b)**

Figur B.2: PSD with (a) linear and (b) logarithmic scaling. (Recording 2)

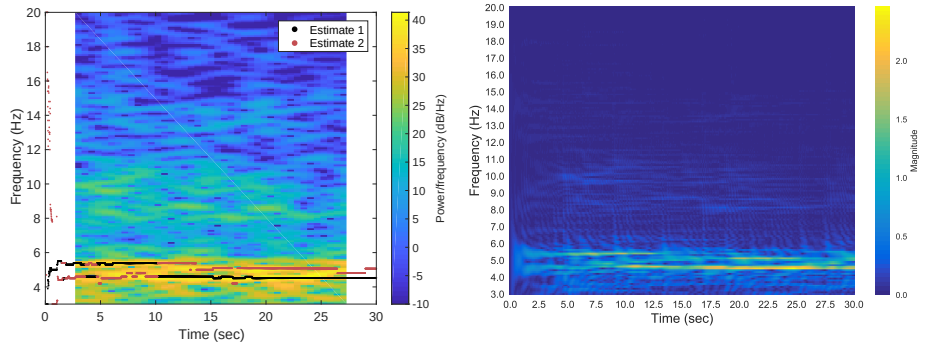

(a) **(b)**

Figur B.3: (a) Spectrogram of signal with estimated frequencies and (b) Heatmap of the magnitude spectrum from the BMWFLC filter. (Recording 2)

B.2 Recording 3 - Rest tremor

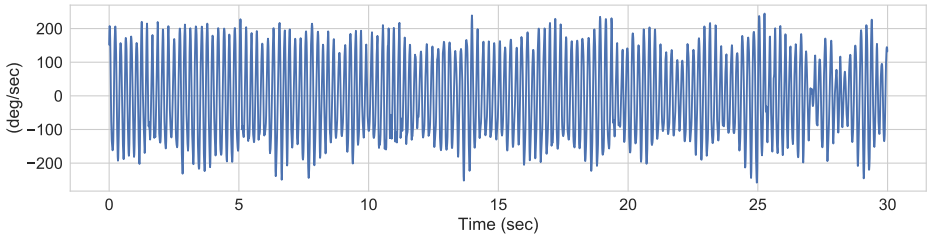

Figur B.4: Recording 3 from session 2. Orientation: P+/S. Placement: LH

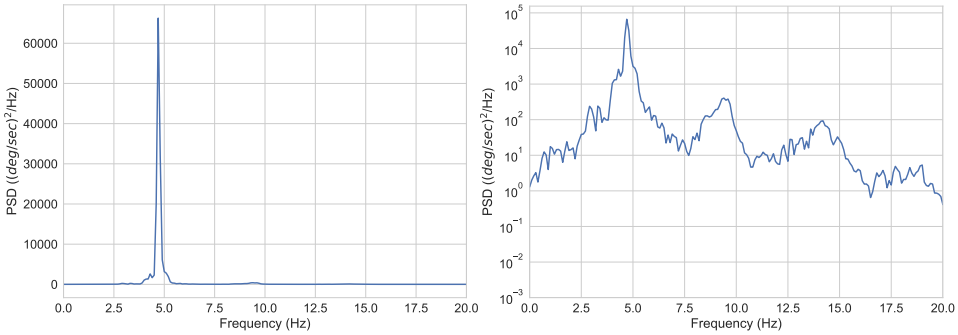

(a) **(b)**

Figur B.5: PSD with (a) linear and (b) logarithmic scaling. (Recording 3)

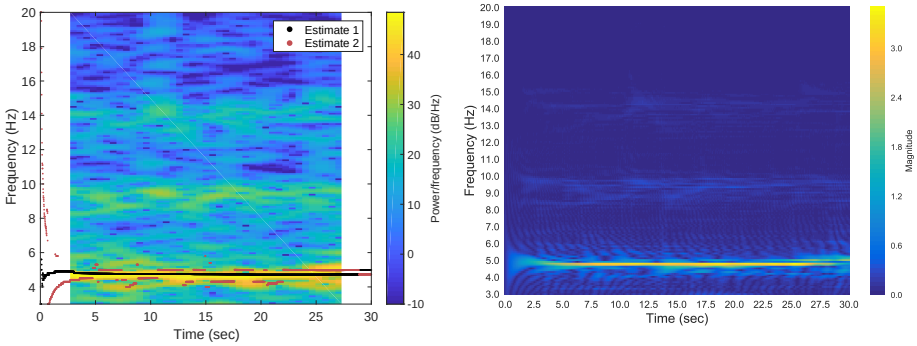

(a) **(b)**

Figur B.6: (a) Spectrogram of signal with estimated frequencies and (b) Heatmap of the magnitude spectrum from the BMWFLC filter. (Recording 3)

B.3 Recording 4 - Rest tremor

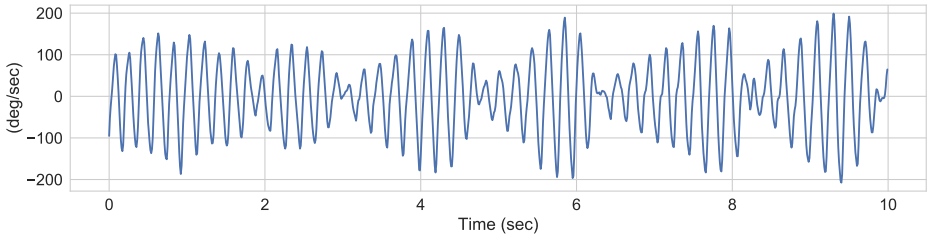

Figur B.7: Recording 4 from session 3. Orientation: P+/S. Placement: RH

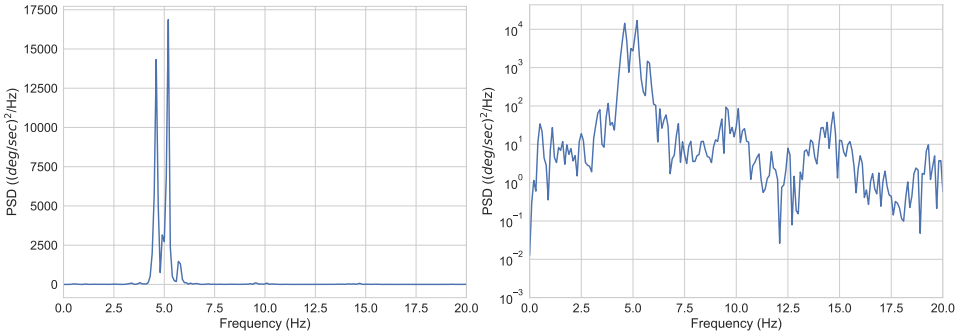

(a) **(b)**

Figur B.8: PSD with (a) linear and (b) logarithmic scaling. (Recording 4)

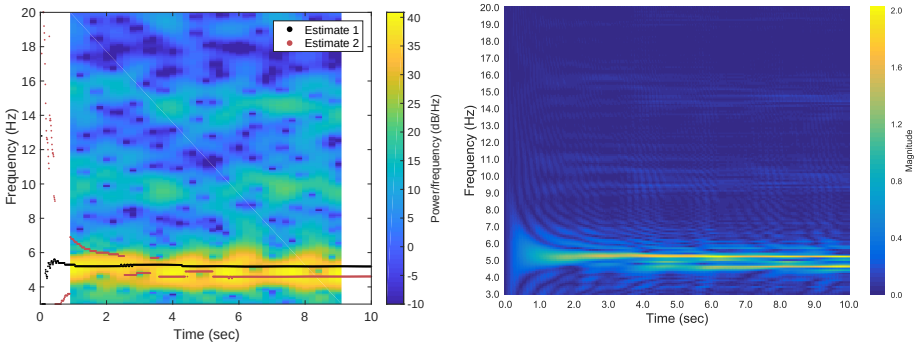

(a) **(b)**

Figur B.9: (a) Spectrogram of signal with estimated frequencies and (b) Heatmap of the magnitude spectrum from the BMWFLC filter. (Recording 4)

B.4 Recording 5 - Rest tremor

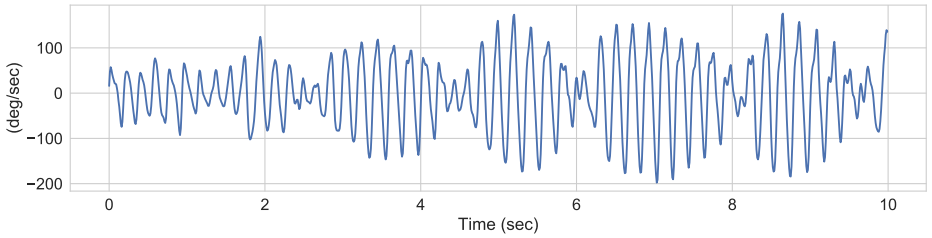

Figur B.10: Recording 5 from session 3. Orientation: F+/E. Placement: RH

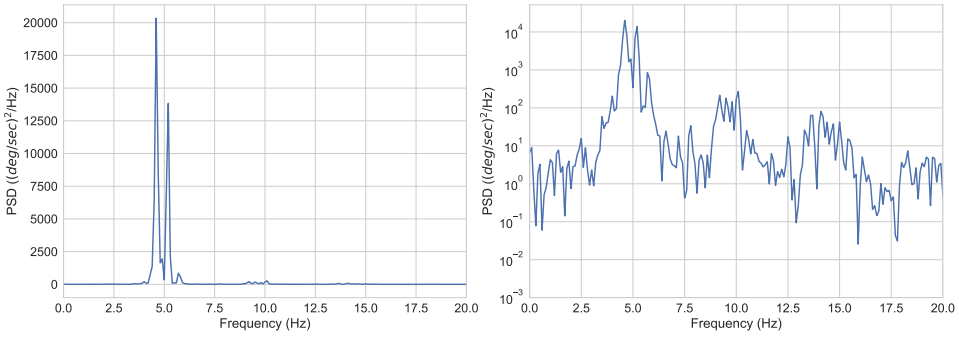

(a) **(b)**

Figur B.11: PSD with (a) linear and (b) logarithmic scaling. (Recording 5)

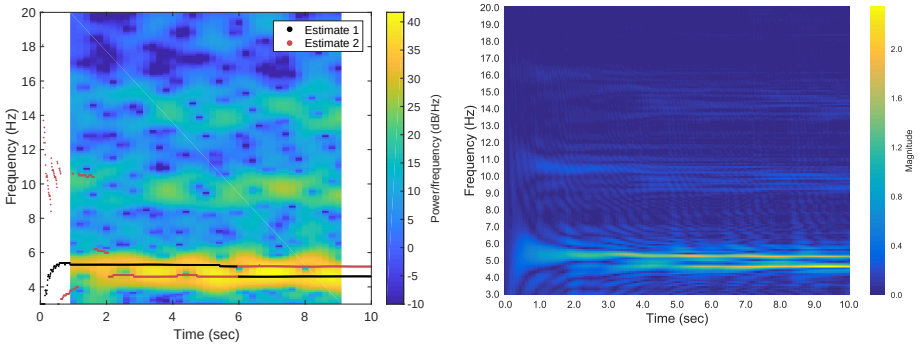

(a) **(b)**

Figur B.12: (a) Spectrogram of signal with estimated frequencies and (b) Heatmap of the magnitude spectrum from the BMWFLC filter. (Recording 5)

B.5 Recording 7 - Rest tremor

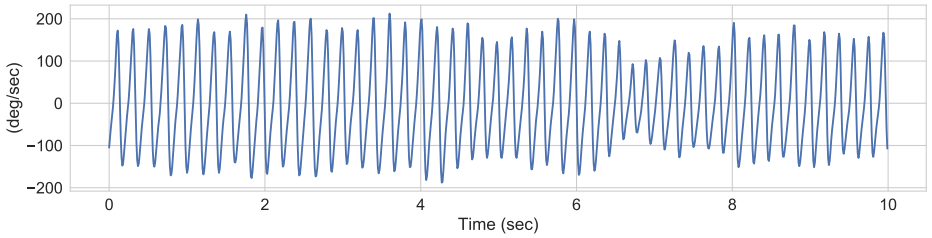

Figur B.13: Recording 7 from session 4. Orientation: P+/S. Placement: RH

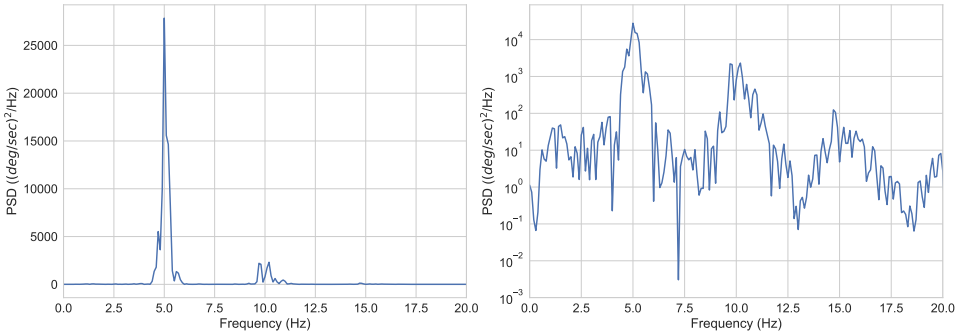

(a) **(b)**

Figur B.14: PSD with (a) linear and (b) logarithmic scaling. (Recording 7)

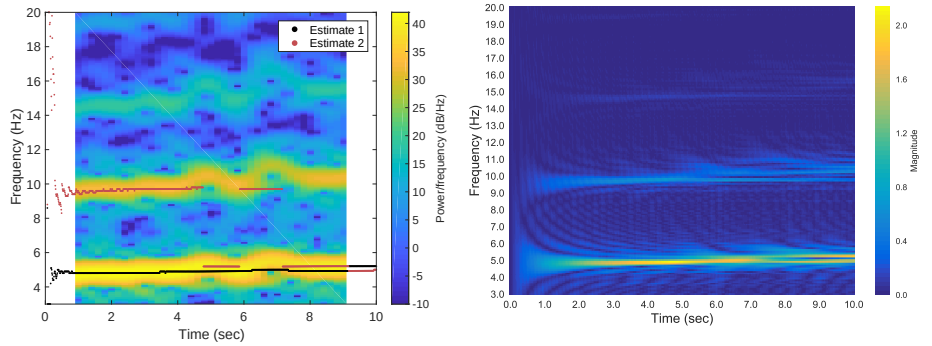

(a) **(b)**

Figur B.15: (a) Spectrogram of signal with estimated frequencies and (b) Heatmap of the magnitude spectrum from the BMWFLC filter. (Recording 7)

B.6 Recording 8 - Voluntary movement

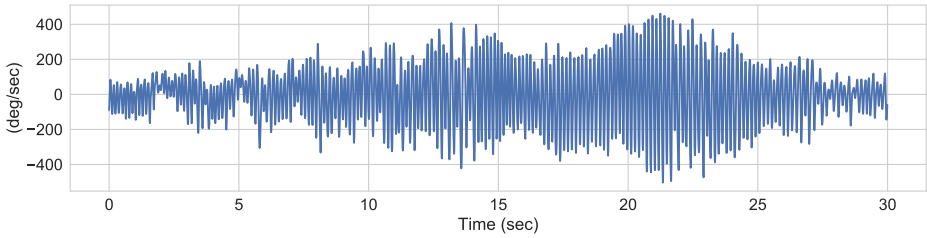

Figur B.16: Recording 8 from session 5. Orientation: P+/S. Placement: RH

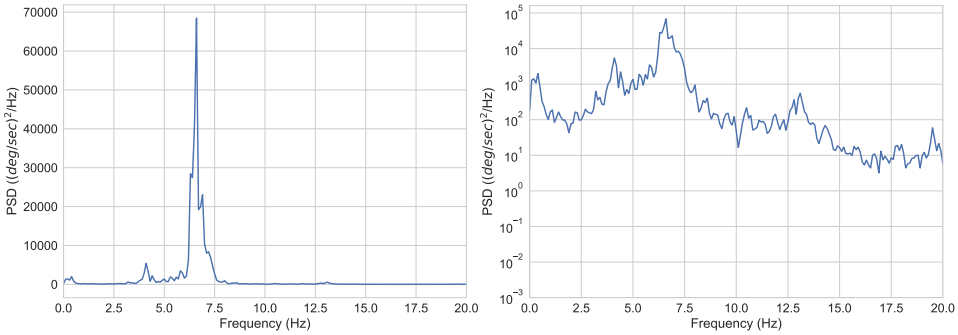

(a) **(b)**

Figur B.17: PSD with (a) linear and (b) logarithmic scaling. (Recording 8)

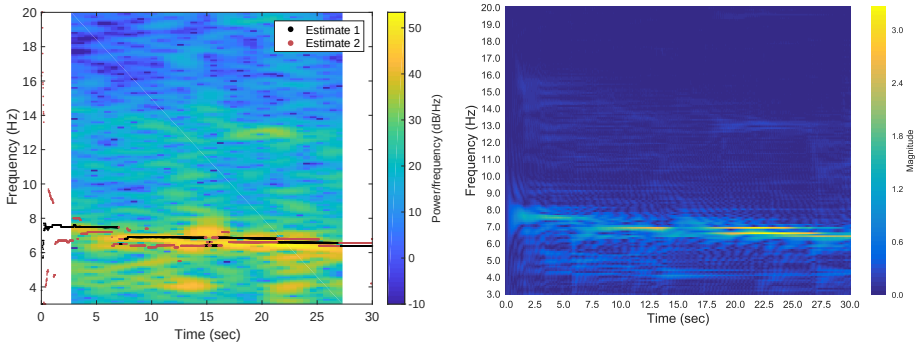

(a) **(b)**

Figur B.18: (a) Spectrogram of signal with estimated frequencies and (b) Heatmap of the magnitude spectrum from the BMWFLC filter. (Recording 8)

B.7 Recording 9 - Rest tremor

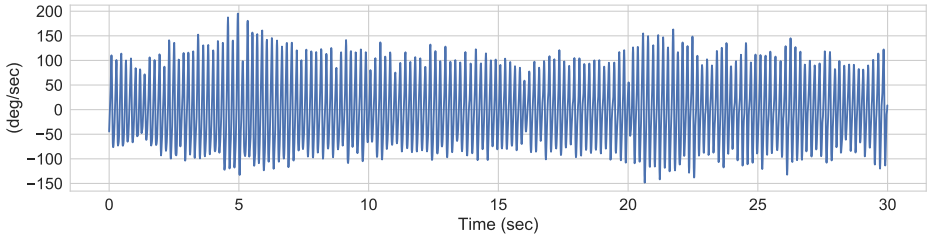

Figur B.19: Recording 9 from session 5. Orientation: P+/S. Placement: LH

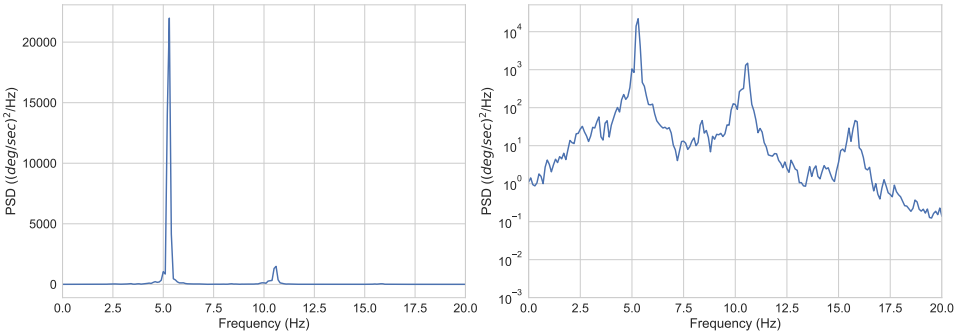

(a) **(b)**

Figur B.20: PSD with (a) linear and (b) logarithmic scaling. (Recording 9)

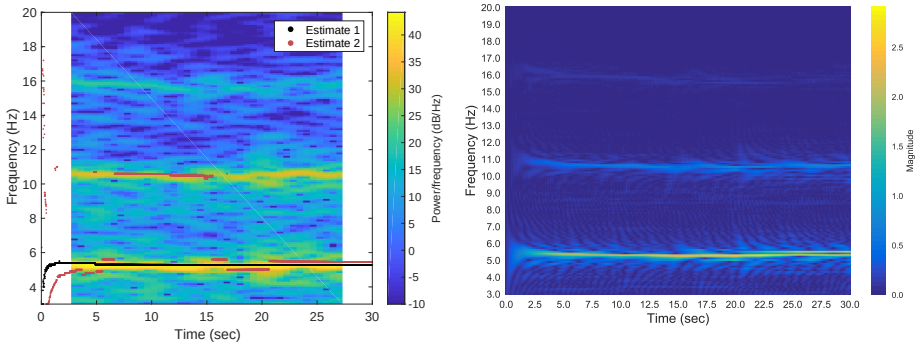

(a) **(b)**

Figur B.21: (a) Spectrogram of signal with estimated frequencies and (b) Heatmap of the magnitude spectrum from the BMWFLC filter. (Recording 9)

B.8 Recording 10 - Voluntary movement

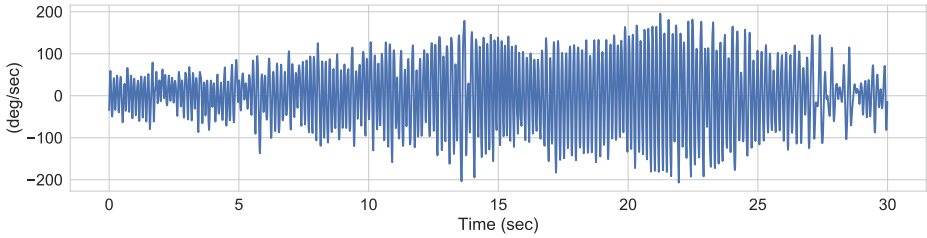

Figur B.22: Recording 10 from session 5. Orientation: F+/E. Placement: RH

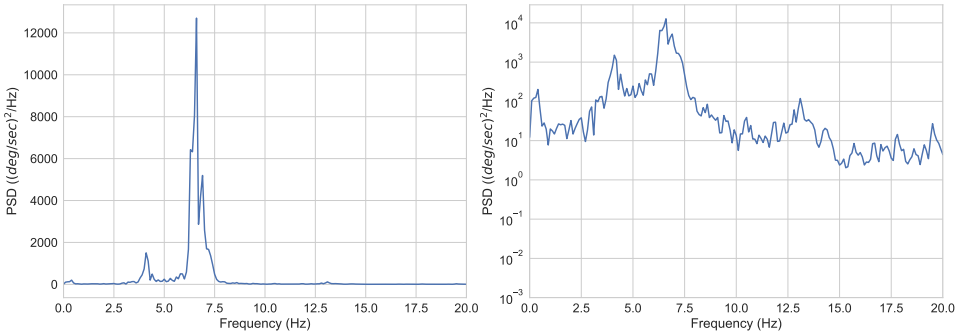

(a) **(b)**

Figur B.23: PSD with (a) linear and (b) logarithmic scaling. (Recording 10)

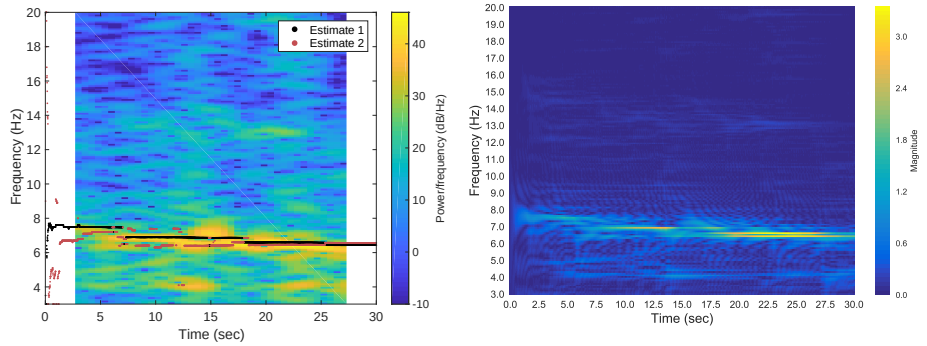

(a) **(b)**

Figur B.24: (a) Spectrogram of signal with estimated frequencies and (b) Heatmap of the magnitude spectrum from the BMWFLC filter. (Recording 10)

B.9 Recording 11 - Rest tremor

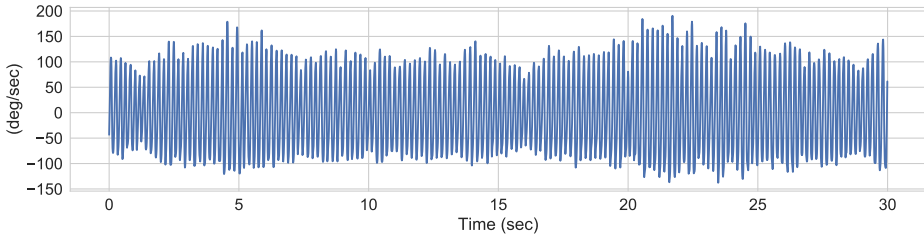

Figur B.25: Recording 11 from session 5. Orientation: F/E+. Placement: LH

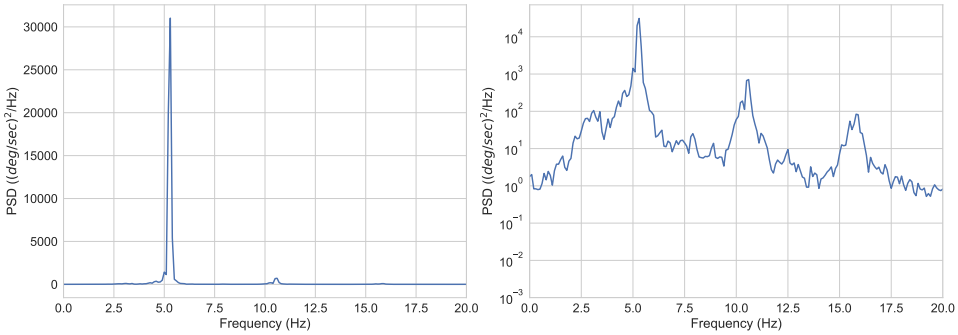

(a) **(b)**

Figur B.26: PSD with (a) linear and (b) logarithmic scaling. (Recording 11)

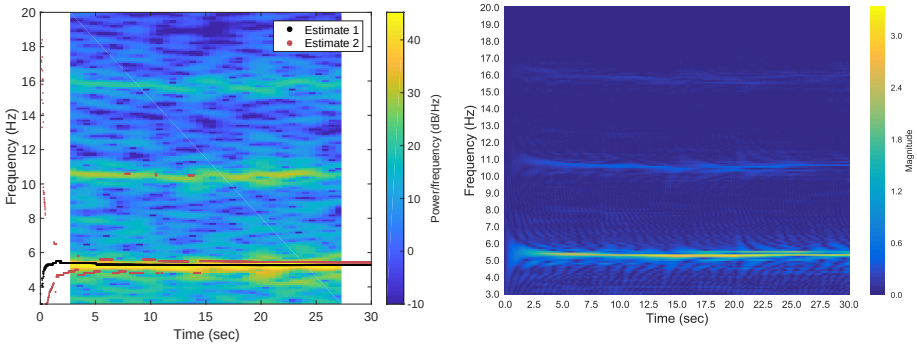

(a) **(b)**

Figur B.27: (a) Spectrogram of signal with estimated frequencies and (b) Heatmap of the magnitude spectrum from the BMWFLC filter. (Recording 11)

B.10 Recording 13 - Postural tremor

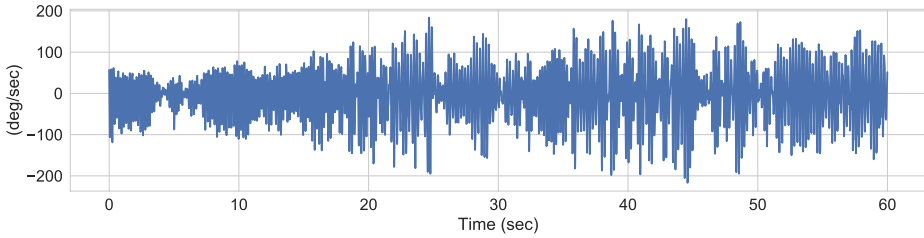

Figur B.28: Recording 13 from session 6. Orientation: F/E+. Placement: LH

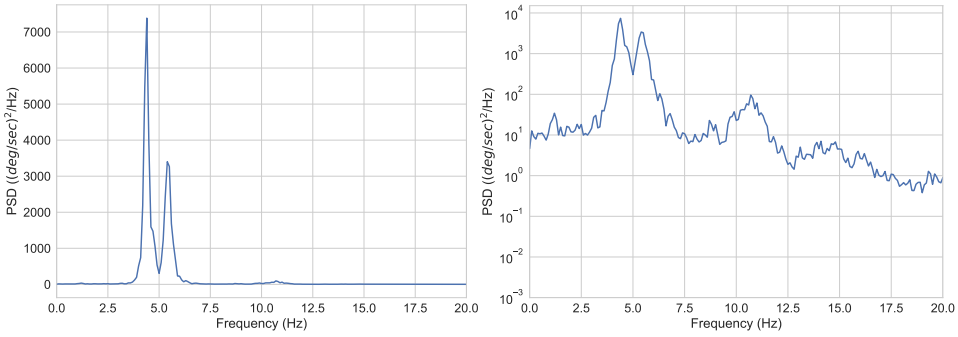

(a) **(b)**

Figur B.29: PSD with (a) linear and (b) logarithmic scaling. (Recording 13)

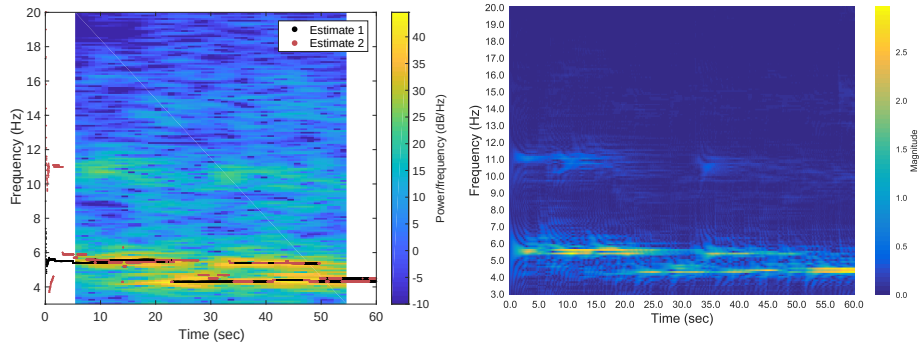

(a) **(b)**

Figur B.30: (a) Spectrogram of signal with estimated frequencies and (b) Heatmap of the magnitude spectrum from the BMWFLC filter. (Recording 13)

B.11 Recording 14 - Action tremor

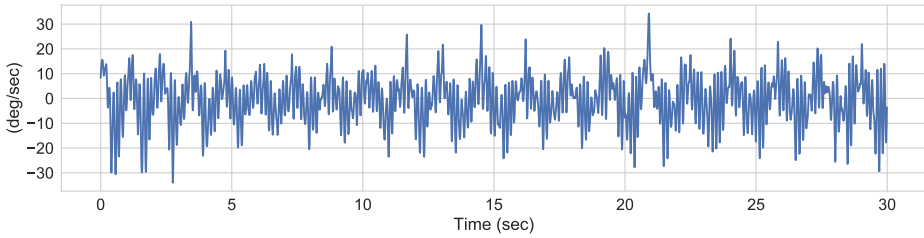

Figur B.31: Recording 14 from session 7. Orientation: P+/S. Placement: RH

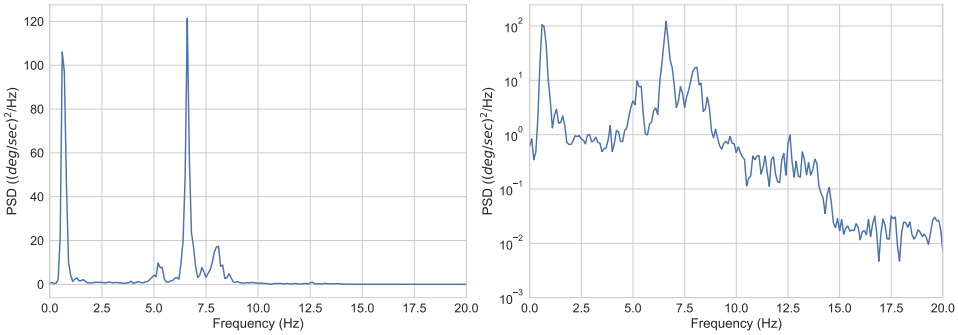

(a) **(b)**

Figur B.32: PSD with (a) linear and (b) logarithmic scaling. (Recording 14)

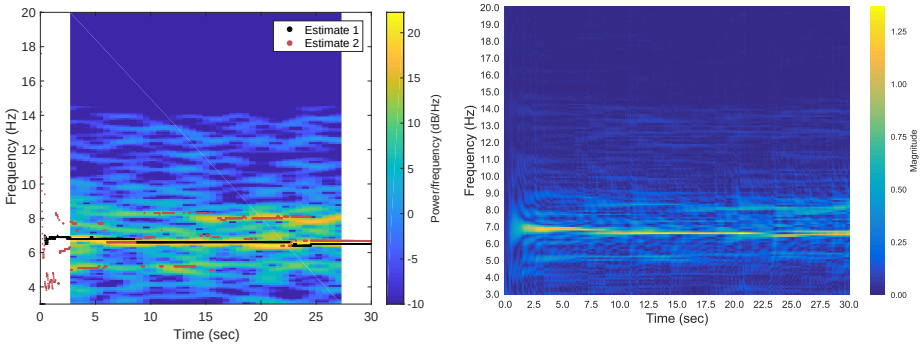

(a) **(b)**

Figur B.33: (a) Spectrogram of signal with estimated frequencies and (b) Heatmap of the magnitude spectrum from the BMWFLC filter. (Recording 14)